Using Molecular, Cellular and Bioengineering Approaches Towards Understanding Muscle Stem Cell Biology

by

Joanna Palade

A Dissertation Presented in Partial Fulfillment
of the Requirements for the Degree
Doctor of Philosophy

Approved April 2020 by the
Graduate Supervisory Committee:

Norma Wilson-Rawls, Chair
Kenro Kusumi
Jason Newbern
Jeffrey Rawls
Sarah Stabenfeldt

ARIZONA STATE UNIVERSITY

May 2020

ABSTRACT

Satellite cells are adult muscle stem cells that activate, proliferate, and differentiate into myofibers upon muscle damage. Satellite cells can be cultured and manipulated *in vitro*, and thus represent an accessible model for studying skeletal muscle biology, and a potential source of autologous stem cells for regenerative medicine. This work summarizes efforts to further understanding of satellite cell biology, using novel model organisms, bioengineering, and molecular and cellular approaches. Lizards are evolutionarily the closest vertebrates to humans that regenerate entire appendages. An analysis of lizard myoprogenitor cell transcriptome determined they were most transcriptionally similar to mammalian satellite cells. Further examination showed that among genes with the highest level of expression in lizard satellite cells were an increased number of regulators of chondrogenesis. In micromass culture, lizard satellite cells formed nodules that expressed chondrogenic regulatory genes, thus demonstrating increased musculoskeletal plasticity. However, to exploit satellite cells for therapeutics, development of an *ex vivo* culture is necessary. This work investigates whether substrates composed of extracellular matrix (ECM) proteins, as either coatings or hydrogels, can support expansion of this population whilst maintaining their myogenic potency. Stiffer substrates are necessary for *in vitro* proliferation and differentiation of satellite cells, while the ECM composition was not significantly important. Additionally, satellite cells on hydrogels entered a quiescent state that could be reversed when the cells were subsequently cultured on Matrigel. Proliferation and gene expression data further indicated that C2C12 cells are not a good proxy for satellite cells. To further understand how different signaling pathways control satellite cell behavior, an investigation of the Notch inhibitor protein Numb was carried out. *Numb*

deficient satellite cells fail to activate, proliferate and participate in muscle repair. Examination of Numb isoform expression in satellite cells and embryonic tissues revealed that while developing limb bud, neural tube, and heart express the long and short isoforms of NUMB, satellite cells predominantly express the short isoforms. A preliminary immunoprecipitation- proteomics experiment suggested that the roles of NUMB in satellite cells are related to cell cycle modulation, cytoskeleton dynamics, and regulation of transcription factors necessary for satellite cell function.

ACKNOWLEDGEMENTS

I want to thank my committee members for their help, support and guidance over the past 6 years. I would like to thank my advisor, Dr. Wilson-Rawls, for mentoring me and for being heavily invested in my growth both as a person and as a scientist, Dr. Rawls for teaching me how to interpret data and approach science in a practical and insightful way, and Dr. Kusumi for challenging me to think outside the box and always keep the big picture in mind. I want to thank Dr. Newbern for his constructive comments on my research projects, and help during my comprehensive exams, and Dr. Stabenfeldt for being a wonderful collaborator, and for the great advice.

I want to thank the fellow graduate students that made the lab an exciting, welcoming, and fun place to work: Alissa Lynch, who went through the graduate school journey side by side with me, and is my best friend; Alex Andre, on whom I can always count for support, whether personal in nature or concerning an experiment, and Cindy Xu, my close collaborator and friend whose work ethic and talent have inspired me throughout the years. I also want to mention Dr. Kasuen Kotagama, Tanner Lamb, Dr. Megan Rowton, Amanda Mulia, Dr. Elizabeth Hutchins, John Cornelius, our undergraduate volunteers Alexis Boschi and Bailey Gefroh, who all supported me during my graduate career in many different ways.

I am grateful for the GPSA and SOLS travel awards, the Harry Lowell Swift Scholarship for Advancing Human Health, and the Graduate College Completion award for providing additional financial support.

Lastly, I want to thank my close family and friends, as I could not have achieved this without their unwavering love and encouragement.

TABLE OF CONTENTS

Page

LIST OF TABLES

Table Page

LIST OF FIGURES

Figure Page

CHAPTER 1

INTRODUCTION

Satellite cells in skeletal muscle regeneration

While adult skeletal muscle regeneration involves a dynamic and well-orchestrated interplay between a myriad of cell types, signaling factors, extracellular matrix (ECM) proteins, and the myofibers themselves, satellite cells play a central role in this process, as they are indispensable for repair. Satellite cells, or muscle stem cells, which make up a minority of the total myonuclei in muscle (2-4%), are the predominant source of new myofibers following damage (Hawke and Garry, 2001).

Satellite cells lie in between the myofibers in a reversible G_0 state called quiescence, typically characterized by a high nucleus to cytoplasm ratio, presence of cell cycle inhibitors, and general metabolic and translational inactivity. They can be further identified by paired-box 7 (Pax7) transcription factor expression, which exclusively marks satellite cells in adult muscle (Dumont et al., 2015a). Upon muscle injury, signaling factors released by the damaged myofibers, fibroblasts, and immune cells induce satellite cell activation. Disintegration of the surrounding basement membrane and ECM serves the same purpose, as growth factors and matrix metalloproteinases (MMPs) previously sequestered are free to interact with satellite cells. For example, fibroblast growth factor 2 (FGF2) and hepatocyte growth factor (HGF) are both released from the matrix following injury and promote activation and proliferation via binding of FGF receptors and c-MET, respectively (Dumont et al., 2015a). Activated satellite cells migrate to the site of damage and proliferate, to generate the large number of cells required for muscle repair. Proliferating satellite cells, or myoblasts, continue to express

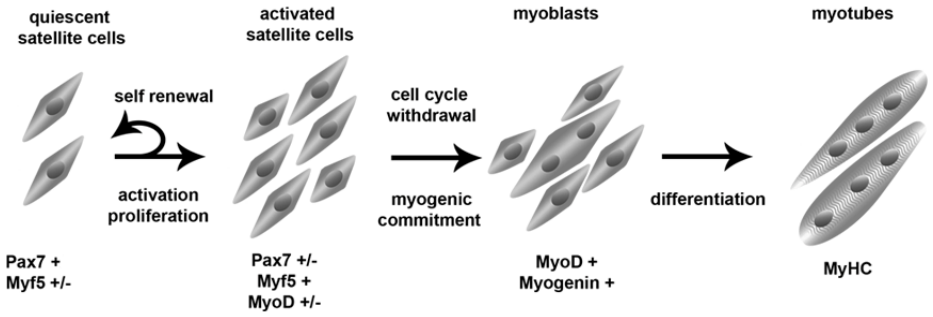

Figure 1. Satellite cell progression through the myogenic program

Satellite cells activated by muscle damage proliferate to expand their numbers. During this stage, a subset of cells will self-renew and return to quiescence, to maintain the stem cell pool. The rest of the satellite cells will commit to the myogenic program, becoming myoblasts. They exit the cell cycle, elongate, align, and fuse to make multinucleated myofibers. Myoblasts may fuse with existing myofibers as well.

Pax7, which induces expression of additional muscle specific transcription factors, like myogenic regulatory factor 5 (*Myf5*) and myoblast determination factor 1 (*Myod1*) (Rudnicki and Chang, 2014).

Satellite cells participate in regeneration by fusing with damaged myofibers or generating new myofibers *de novo*. To achieve this, myoblasts must downregulate *Pax7*, cease proliferation, and commit to myogenic differentiation. *Myod1* induces expression of transcription factor myogenin (*Myog*), which in turn suppresses cell cycle progression, and allows for terminal differentiation. The post-mitotic myoblasts elongate, align and fuse to generate myofibers that express structural proteins, like myosin heavy chains (MHCs). Over time, the new myofibers will mature and integrate into the newly regenerated muscle, thus restoring structure and function (Rudnicki and Chang, 2014).

Satellite cell plasticity

Unlike intestinal stem cells, or hematopoietic stem cells, which give rise to several different cell types, satellite cells are classified as monopotent, and only give rise to skeletal muscle. However, that may not entirely be the case, and given the right cues and conditions, satellite cells can adopt other lineages. For example, work from several groups demonstrates that satellite cells undergo adipogenesis, both *in vitro* and *in vivo*, particularly in obesity and aging models (Scarda et al., 2010; Sciorati et al., 2015; Shefer et al., 2004; Shefer and Yablonka-Reuveni, 2007; Vettor et al., 2009). Overexpression of the transcriptional regulator PRDM16 induces brown fat differentiation in primary satellite cell culture, via activation of Peroxisome proliferator-activated receptor γ (PPAR-γ) (Seale et al., 2008). Additionally, satellite cells treated with BMP7 in culture adopt an osteogenic lineage, as evidenced by positive alkaline phosphatase staining and

expression of osteogenic markers (Asakura et al., 2001). In non-mammalian species, satellite cells may adopt alternative lineages *in vivo*. In newts, Pax7+ satellite cells expanded in culture contribute to epidermis and cartilage in the regenerated limb after intramuscular injection (Morrison et al., 2006).

During development, satellite cells arise from somites, which also give rise to skeletal muscle, cartilage, bone, tendon, dermis, and fat (Relaix and Zammit, 2012). Thus, the ability of satellite cells to undergo adipogenesis, chondrogenesis and osteogenesis is consistent with their embryonic origin. However, it is unclear to what extent these events happen *in vivo* in mammals, if at all, as these experiments entailed *in vitro* manipulation, exposure to morphogens in culture, or alteration of gene expression. Taken together, these data hint at potential for expanded plasticity, which may change the way we think about satellite cell biology and perhaps mark satellite cells as an attractive source of autologous stem cells to be exploited for regenerative medicine therapeutics beyond skeletal muscle.

Bioengineering approaches for therapeutic exploitation

Attempts to harness satellite cells for medical treatments of muscle loss due to trauma or disease span the last few decades (Briggs and Morgan, 2013; Partridge et al., 1978). Donor myoblasts can be injected intramuscularly, where they contribute to muscle repair in both murine models and humans (Cornelison, 2018). Currently, this practice has limited reproducibility and functionality in a clinical setting, due to several hurdles.

Firstly, standard *in vitro* culture protocols do not recapitulate the complex mechanical, biological, and chemical cues that maintain satellite cell identity, stemness, and myogenic potential indefinitely. Cultured myoblasts are thus less likely to engraft,

contribute to muscle repair, and re-populate the stem cell niche. Satellite cells injected intramuscularly directly following isolation contribute to muscle regeneration significantly more than myoblasts maintained in culture first (Collins et al., 2005; Montarras et al., 2005). However, injection of satellite cells without *ex vivo* expansion has limited therapeutic applications. To repair a human tibialis anterior muscle, an estimated 2-4 kg of muscle tissue would be needed, demonstrating the impracticality of this method in a clinical setting (Borselli et al., 2011). Secondly, delivery of satellite cells to the damaged muscle has presented a challenge, contributing to the variability and lack of success encountered thus far. The majority of injected cells die within 3 days of transplantation, likely due to the stress of bolus delivery, and the immune reaction mounted subsequently (Péault et al., 2007). Finally, surviving satellite cells only migrate about 200 μm from the site of injection, posing a problem for human skeletal muscle, which may span over half a meter (Péault et al., 2007).

To address both the issues of delivery and cell culture, the use of biomaterials and bioengineering approaches has been explored at length. Synthetic materials often have tunable properties that allow for manipulation of parameters like patterning, rigidity, shape and functionalization much more readily than biological materials. The culture material stiffness is known to influence cell behavior, and several groups have explored how it affects satellite cell quiescence, proliferation and differentiation (Gilbert et al. 2010; Lacraz et al. 2015; Urciuolo et al. 2013). Other variables, like biomaterial topography, cyclic stretch and electric stimulation, or various ECM substrates have also been investigated (Dunn et al., 2019; Qazi et al., 2015). Sophisticated delivery methods that bypass injection have shown promise in mouse models. In an *mdx* (dystrophin null) model, delivery of wild type satellite cells on a nanopatterned PLGA (poly lactic-co-glycolic acid) patch surgically placed on the quadriceps muscles contributed significantly

to dystrophin production (Yang et al., 2014). Encapsulation of satellite cells along with insulin-like growth factor (IGF) and vascular endothelial growth factor (VEGF) in a shape-memory alginate scaffold improved functional recovery in mouse *tibialis anterior* (TA) injury model (Wang et al. 2014). However, it is unclear to what extent the success in mouse models will translate to human work, especially considering that several of these synthetic materials may not be well tolerated by the immune system, limiting their clinical use. Furthermore, many of these biomaterials and bioengineering studies use myoblast-like cell lines as satellite cell proxies, raising questions about whether the conclusions drawn can apply to primary satellite cells.

The stem cell niche and signaling pathways

Satellite cells were initially identified via electron microscopy based on their unique positioning within skeletal muscle. They occupy the space between the basal lamina and the myofiber sarcolemma (Mauro, 1961), and are often found in close proximity to blood vessels and neuromuscular junctions (NMJs) (Chargé and Rudnicki, 2004). Beyond providing mechanical and structural support, the muscle stem cell niche serves as a signaling center directing satellite cell survival, differentiation, proliferation and self-renewal. On the basal side, integrin α7 and the dystrophin-glycoprotein complex (DGC) anchor the satellite cell to the basement membrane. Frizzled-7 (FZD7), c-MET, and Syndecan-4 (Sdc-4) are likewise enriched basally. On the apical side, adhesion proteins like CD34, M-cadherin and NCAM form cell-cell interactions between the myofiber and the satellite cell. Transmembrane receptor Notch is also concentrated apically (Feige et al., 2018). Targeted disruption of some of these membrane receptors in satellite cells results in loss of quiescence, aberrant cell cycling, and spontaneous activation, highlighting the importance of the stem cell niche (Mashinchian et al., 2018).

Dystrophin null satellite cells, for example, display reduced asymmetric cell divisions, loss of polarity, and impaired mitotic spindle orientation, which likely exacerbates the muscle wasting phenotype in Duchenne's muscular dystrophy (DMD) (Dumont et al., 2015b). Double knock-out of M-cadherin and N-cadherin in satellite cells leads to spontaneous activation in the absence of injury (Goel et al., 2017).

Many of the highly conserved signaling pathways fundamental for metazoan embryonic development, like Notch, Wnt, Bone morphogenic protein/Transforming growth factor β (BMP/TGFβ), or Hedgehog dictate satellite cell behavior. Upon binding to its ligand, the Notch receptor undergoes a conformation change that exposes cleavage and results in release of the Notch intracellular domain (NICD). The NICD can translocate to the nucleus, and together with its binding partners (CSL transcription factors, p300/CBP, Maml1, etc.) act as a transcriptional activator for Notch target genes, like Hairy Enhancer of Split (*Hes*) and Hes-related with YRPW motif (*Hey*) (Carrieri and Dale, 2017). In the context of myogenesis, Notch activation is associated with stemness and inhibition of differentiation. Overexpression of Notch1 in satellite cells results in maintenance of *Pax7* expression and downregulation of myogenic regulatory factors (MRFs), while deletion of Notch pathway genes leads to loss of quiescence and premature differentiation (Bjornson et al., 2012; Conboy and Rando, 2002; Wen et al., 2012). Mechanistically, *Hes* genes can suppress *MyoD* and the cell cycle inhibitor p21 (Luo, Renault, and Rando 2005).

Once sufficient progenitor cells have been generated, Notch signaling activity is reduced, and canonical Wnt signaling promotes differentiation (Brack et al., 2008). Wnt ligands bind membrane receptor Frizzled (Fzd), which in turn leads to inhibition of Glycogen synthase kinase 3 β (GSK3β) activity. As a result, β-catenin, which is otherwise

targeted for degradation by GSK3β phosphorylation, accumulates in the cytoplasm and translocates to the nucleus, where it activates transcription of target genes along with DNA binding proteins of the LEF/TCF family (Rudnicki and Williams, 2015). In satellite cells, this results in upregulation of proteins that support myogenic differentiation (Girardi and Le Grand, 2018). However, non-canonical Wnt signaling promotes self-renewal instead, independent of βcatenin. Wnt7a binds to Fzd7 and Sdc-4 to promote symmetric expansion of satellite cells and enhance cell migration (Girardi and Le Grand, 2018).

Myostatin (Mstn) is the most notable member of the TGFβ family with a role in myogenesis. Activated TGFβ receptors form tetramers and exert their effects by phosphorylating the SMAD proteins, which act as transcriptional regulators in the nucleus. Myostatin inhibits satellite cell proliferation and differentiation, as it leads to p21 upregulation, and myogenin downregulation, respectively. Follistatin inhibits myostatin signaling, by directly binding to it (Dominique and Gérard, 2006; Huang et al., 2011; McCroskery et al., 2003).

A detailed understanding of how the signals from various pathways are integrated, and how each chemical and physical component of the niche influences satellite cell behavior will inform future efforts to enhance or manipulate satellite cell function for skeletal muscle repair and regenerative medicine.

CHAPTER 2

IDENTIFICATION OF SATELLITE CELLS FROM ANOLE LIZARD SKELETAL MUSCLE AND DEMONSTRATION OF EXPANDED MUSCULOSKELETAL POTENTIAL

Abstract

Lizards are evolutionarily the closest vertebrates to humans that demonstrate the ability to regenerate entire appendages containing cartilage, muscle, skin, and nervous tissue. We previously isolated PAX7-positive cells from muscle of the green anole lizard, *Anolis carolinensis*, that can differentiate into multinucleated myotubes and express the muscle structural protein, myosin heavy chain. Studying gene expression in these satellite/progenitor cell populations from *A. carolinensis* can provide insight into the mechanisms regulating tissue regeneration. We generated a transcriptome from proliferating lizard myoprogenitor cells and compared them to transcriptomes from the mouse and human tissues from the ENCODE project using XGSA, a statistical method for cross-species gene set analysis. These analyses determined that the lizard progenitor cell transcriptome was most similar to mammalian satellite cells. Further examination of specific GO categories of genes demonstrated that among genes with the highest level of expression in lizard satellite cells were an increased number of genetic regulators of chondrogenesis, as compared to mouse satellite cells. In micromass culture, lizard PAX7-positive cells formed Alcian blue and collagen 2a1 positive nodules, without the addition of exogenous morphogens to the culture medium. Mouse satellite cell micromasses did not consistently form chondrogenic nodules, and instead differentiated into multinucleated myofibers. Subsequent quantitative RT-PCR confirmed up-regulation of expression of chondrogenic regulatory genes and cartilage specific structural genes in

lizard cells. Taken together, these data suggest that tail regeneration in lizards involves significant alterations in gene regulation with expanded musculoskeletal potency.

Introduction

Lizards are evolutionarily the closest vertebrate group to humans with the ability to regenerate a complex appendage i.e., an entire tail (Eckalbar et al. 2012; Gilbert, Payne, and Vickaryous 2013; Koshiba-Takeuchi et al. 2009). The regenerated lizard tail is functional and structurally complex, containing *de novo* generated musculoskeletal tissues like skeletal muscle groups, tendons, a hyaline cartilage endoskeleton, as well as vasculature, peripheral and sensory nerves, and skin (Fisher et al., 2012; Hutchins et al., 2014). After an initial phase of wound healing in the lizard tail, the appendage regrows with an unique architecture distinct from the original tail (Fisher et al., 2012). Key differences include the development of a cartilage tube endoskeleton instead of segmented vertebrae, and axial muscle groups that run the length of the tail instead of segmental vertebral muscles (Fisher et al., 2012; Hutchins et al., 2014). Mammals have some regenerative capacity of appendages, limited to digit tip formation in neonatal mice and humans under age two (Yu et al., 2010). Neonatal mice can also regenerate limited damage to heart ventricular muscle during the first week of life (Darehzereshki et al., 2015; Porrello et al., 2011).

Regeneration of a multi-tissue structure such as the tail requires pools of proliferative stem cells capable of differentiating into different lineages. Regeneration capable species employ distinct strategies to generate these stem cell populations. In urodele amphibians, dedifferentiation of injured tissue results in proliferative, lineage restricted progenitors (Kragl et al., 2009). Resident tissue-specific stem cells that migrate to the site of injury can contribute to regeneration as well. For example,

amputation in the axolotl limb activates PAX7 positive satellite cells from adjacent muscle (Sandoval-Guzmán et al., 2014). Finally, dedifferentiated cells and stem cells can also transdifferentiate and change their fate to contribute to more than one tissue (Jopling et al., 2011). *A. carolinensis* skeletal muscle contains cells localized to the muscle stem cell niche (Kahn and Simpson, 1974). These cells have been previously shown to express *pax7,* and to fuse into multinucleated MHC positive myotubes upon serum withdrawal (Hutchins et al., 2014).

Several previous studies have profiled the transcriptomes of satellite cells in mammalian species such as mouse (Ryall et al., 2015) or human (Charville et al., 2015), among others. However, comparison of gene expression across vertebrate species remains a bioinformatic challenge, due to difficulties in identifying orthologous genes and differences in baseline gene expression. A useful framework for comparing transcriptome-wide expression profiles across species is based on testing whether a gene set that is specifically expressed in a species is shared with similar tissues or cell types in other species (Djordjevic et al., 2016).

In this study, we characterized the lizard muscle progenitor cells using XGSA cross species comparison, followed by a comparative analysis of expression of musculoskeletal and TGFβ/BMP pathway genes between mouse and lizard satellite cells. We further investigated the plasticity of mouse and lizard satellite cells and tested their ability to undergo chondrogenesis.

Results

XGSA analysis of satellite cell transcriptomes

Satellite cells were isolated from mouse and lizard limb skeletal muscle, and RNA was purified from PAX7 positive cells, an established marker of satellite cells in

mammals (Lepper et al., 2011; Sambasivan et al., 2011; Zammit et al., 2006). Analysis of genes expressed in lizard satellite cells was carried out using RNA-Seq transcriptomic analysis (Hutchins et al., 2014). Based on our previous data, we wanted to determine the similarity of the lizard PAX7 positive cells to the satellite cell population in mouse and human. We carried out this comparison using XGSA, a statistical method for cross-species gene set analysis (Djordjevic et al., 2016). We compared highly expressed genes in the lizard satellite cell transcriptome to a compendium of cell-type-specific gene sets, including 94 tissues from the mouse ENCODE project (Yue et al., 2014). Within the tissues examined, the lizard PAX7 positive cell had a significant similarity with the mouse satellite cell based on expression of cell-type-specific marker genes (p-value < 1.9×10^{-26}). It has more overlap with mouse satellite cell markers than markers of any other mouse cell types examined here (Figure 2A), and this result is robust against analysis parameters. Similarly, we compared lizard satellite cells with 139 tissues from the human ENCODE project and identified the greatest similarity with activated and quiescent human satellite cells (Figure 2B).

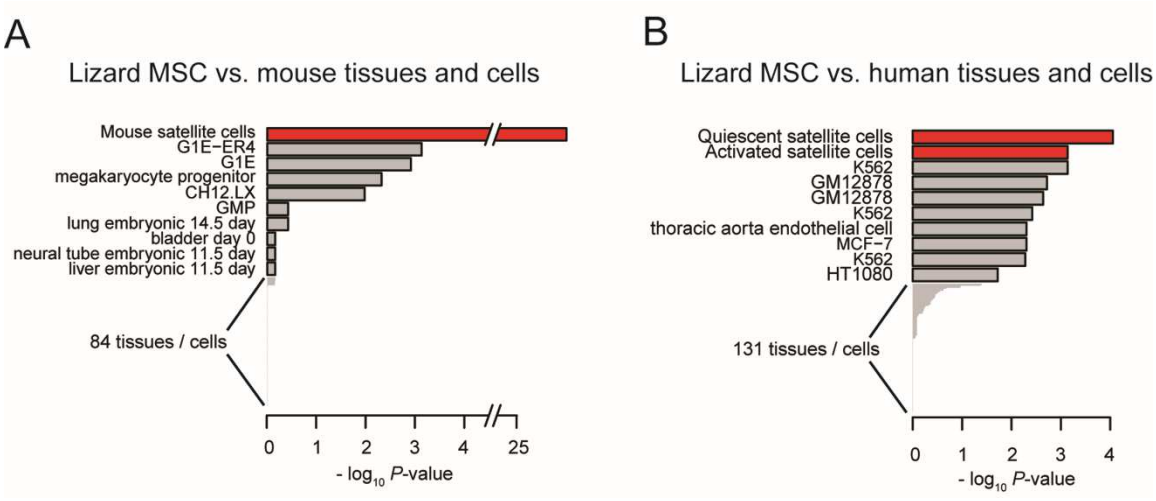

Figure 2. XGSA analyses comparing the transcriptome from lizard satellite cells to multiple tissues from the mouse and human ENCODE projects

XGSA comparison of marker genes with 94 mouse **(A)**, and 139 human **(B)** tissue reveals that the lizard satellite cell transcriptome displayed highest similarity with mouse and human satellite cell transcriptomes.

Gene rank comparison of mouse and lizard satellite cell transcriptomes

Bone morphogenic protein (BMP) and transforming growth factorβ (TGFβ) signaling pathways have important regulatory roles both in embryonic myogenesis and postnatal muscle regeneration (Friedrichs et al., 2011; George et al., 2013; McFarlane et al., 2011; Ono et al., 2010; Park et al., 2010; Sartori et al., 2014; Wang et al., 2010; Winbanks et al., 2013). We examined the differences in the expression of the TGFβ/BMP pathway genes by comparing the relative rankings of 105 TGFβ/BMP pathway genes (KEGG category mmu04350 and GO term GO:0030509) from lizard and mouse satellite cells (Figure 3A). Genes with higher rankings in lizard (closer to 1.0), as compared to a lower ranking in mouse (closer to 20,000), included *Bmp2, Bmp5, Bmp7, Dcn, Fst, Id4, Inhba, Pitx2, Smad9, Tgif2, Zfyve16, Msx1, Msx2, Rnf165, Grem2,* and *Sostdc1*. Follistatin (*Fst*) and *Pitx2* induce proliferation of satellite cells in regenerating muscle (Amthor et al., 2004; Gilson et al., 2009; L'Honoré et al., 2007; Lozano-Velasco et al., 2011). *Msx1* regulates the cellularization of myofibers, i.e., the conversion of multinucleated skeletal muscle fibers into mononuclear cells, during amphibian limb regeneration, as well as the cell cycle re-entry of resulting myoblasts. Ectopic expression of either *Msx1* or *Msx2* in mouse myofibers induced cellularization and inhibited myoblast differentiation (Echeverri and Zayas, 2018; Kumar et al., 2004; Odelberg et al., 2000; Yilmaz et al., 2015).

The expression of *Bmp2, Bmp5, and Bmp7*, which are important regulators of chondrogenesis and osteogenesis, ranked considerably higher in lizard satellite cells in comparison to mouse (Figure 3A) (King, Marker, and Seung 1994; Knippenberg et al. 2006; Shen et al. 2010; Shu et al. 2011; Tsuji et al. 2006). While mouse and human satellite cells and myoblasts typically only differentiate into skeletal muscle, high levels

of BMP ligands can induce these cells to undergo osteogenesis and chondrogenesis *in vitro* (Asakura et al., 2001; Katagiri et al., 1994; Shea et al., 2003; Wada et al., 2002). Other genes with lower expression levels in lizard satellite cells, as compared to mouse, included *Bmp6, Bmpr1b,Bmper, Fzd1, Lef1,* and *Sox11*. *Bmpr1b*, also known as *Alk6*, encodes a receptor specific for BMP7 and GDF5 (Yi et al. 2000; Yoon et al. 2005; Zhao et al. 2002). *Sox11* is expressed in condensing chondrocytes embryonically in mice (Cameron et al., 2009). *Bmper* (BMP binding endothelial regulator) can enhance or inhibit BMP signaling (Zhang et al., 2010). BMP6 regulates iron metabolism and is coexpressed in developing cartilage with BMP2 (Corradini et al., 2011; Luo et al., 2016). Therefore, the transcriptomic profile of lizard satellite cells was marked by the co-expression of genes involved not only in myogenesis, but also chondrogenesis and osteogenesis (Figure 3A).

Focusing on genes in the gene ontology terms 'skeletal muscle' and 'cartilage development and differentiation', we found that expression of key genes involved in satellite cell activation and proliferation, and muscle differentiation ranked higher in lizard as compared to mouse, e.g. *Mef2c, Pitx2, Srpk3, Hdac4, Axin2, Bcl9, Nr2f2,* and *Sulf1* (Figure 3B) (Black and Molkentin, 1996; Brack et al., 2012, 2008; Gill et al., 2010; Raines et al., 2015). *Nr2f2*, an orphan nuclear receptor, is upregulated in activated satellite cells and inhibits differentiation of stem cells in the skeletal muscle, cartilage, and bone marrow lineages (Gao et al., 2017; Zhu et al., 2016). The myogenic regulatory factors *Myod1*, myogenin (*Myog*), *Yap1*, and *Six4* were expressed at comparable levels in both species, but *Myf5* was expressed at a much lower level in lizard cells (Figure 3B). Other genes with known regulatory roles in muscle development and satellite cell function that demonstrated a lower level of expression in lizard satellite cells when compared to mouse included *Dll1, Six1, Ankrd2, Cited2, Gpc1, Fzd1, Megf10,* and *Smo*

(Figure 3B). Among these, *Megf10, Ankrd2, Fzd1*, and *Smo* induce differentiation of satellite cells (Brack et al., 2008; Holterman et al., 2007; Zhao and Hoffman, 2004).

These data suggest that these myoprogenitors express the myogenic transcriptional program, but are not differentiating, consistent with their status as proliferating single cells. This analysis further demonstrated that many genes involved in chondrogenesis, such as *Chsy1, Axin2, Tgfbr2, Fam101a, Fgf18, Col5a1,* and *Msx2*, had high levels of expression in lizard, but not in mouse satellite cells. *Fgf18* and *Chsy1* induce proliferation of early chondrocytes (Liu et al., 2007; Wilson et al., 2012), while *Msx2* is important for regeneration in amphibians and osteogenesis in mice. However, *Col27a1, Bmp4,* and *Bmpr1b,* which are also involved in cartilage differentiation (Lim et al., 2015; Plumb et al., 2011; Shu et al., 2011), have lower expression levels in lizard, as compared to mouse satellite cells (Figure 3B).

Based on the observed higher ranking of cartilage specific genes in the lizard transcriptome, we identified genes from the ranked lists whose expression level ranked between 1 and 5000 (highest levels of expression) with roles in 1) muscle development, differentiation, and regeneration, 2) cartilage development and differentiation or 3) tendon development (Figure 3C). We found 61 lizard genes and 70 mouse genes ranked in the respective transcriptomes with these functions. Of these genes, 49.2% had a role in muscle development, differentiation, and regeneration in lizard cells, whereas in proliferating mouse satellite cells 65.6% of the genes fell into this category. Further, 30.5% of lizard genes and 20.3% of mouse genes were involved in cartilage differentiation and development. Lastly, 20.3% of lizard genes and 14.1% of mouse genes had roles in both processes (Figure 3C). Overall, the XGSA analyses showed that although these cells were most transcriptionally similar to mammalian satellite cells,

there are notable differences, and taken together these data suggest that lizard satellite cells may have expanded differentiation potential.

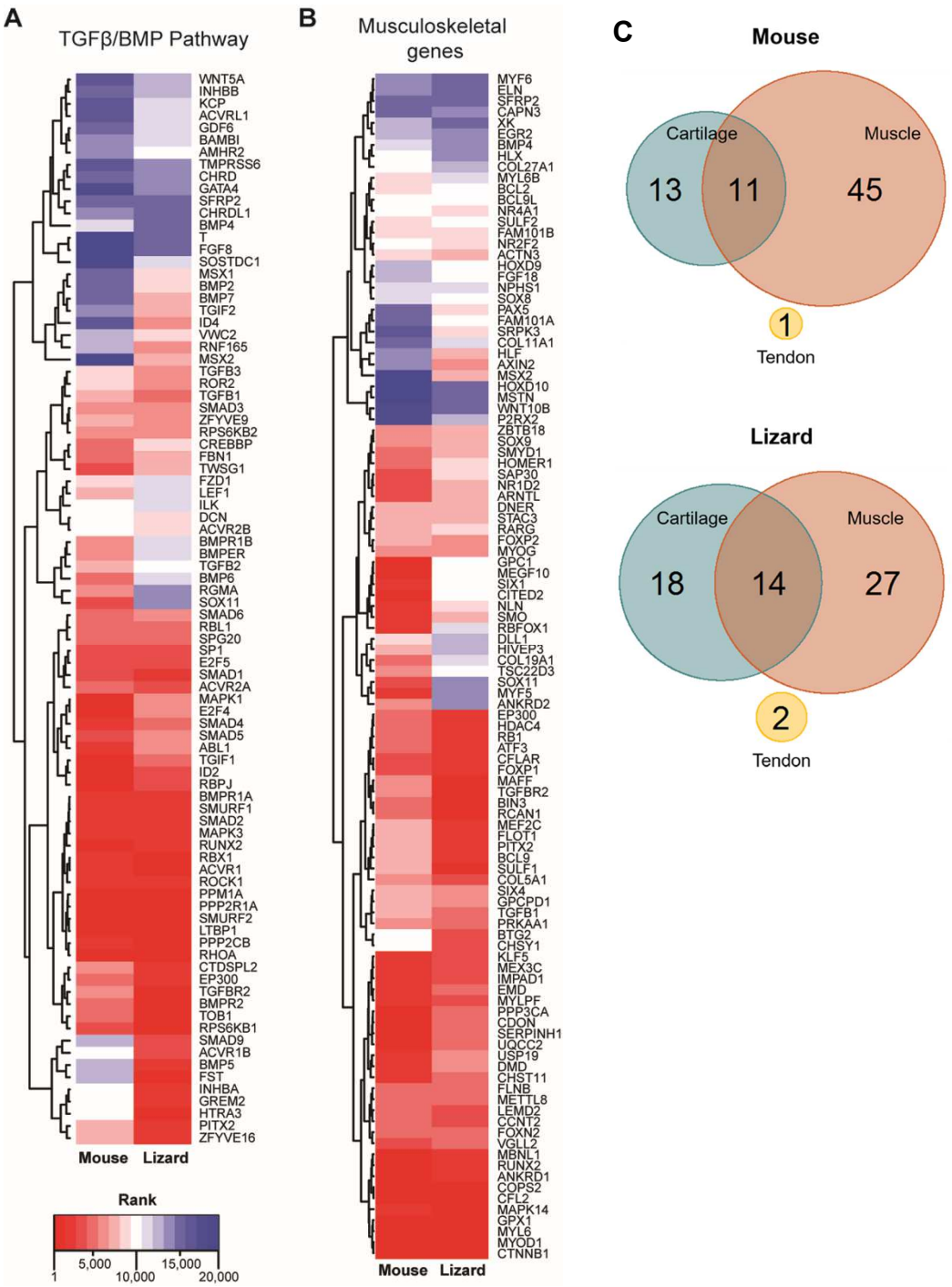

Figure 3. Gene rank comparison of mouse and lizard satellite cell transcriptomes.

Heatmaps of genes involved in the TGFβ/BMP signaling pathway **(A)** and musculoskeletal development **(B)** show differential rankings between mouse and lizard satellite cells. A functional comparison of the top ranked genes (1-5000) showed almost 30% of genes were cartilage-specific in lizard satellite cells, as opposed to 18.3% for mouse satellite cells **(C)**.

Analysis of chondrogenic potential by micromass culture

One of the most striking observations from our analyses were the high expression ranks of cartilage-promoting genes in the lizard satellite cells, such as *bmp2, bmp5,* and *bmp7* (Figure 3), which indicated that these cells might have expanded potential and could adopt the chondrogenic lineage. To examine this, lizard and mouse satellite cells were cultured at high density in micromasses in either growth medium or morphogen free chondrogenic differentiation medium. After 7 days in micromass culture, mouse satellite cells formed myotubes under either culture condition (Figure 4A, D), although differentiation was less extensive in chondrogenic differentiation medium (Figure 4, compare B to E). Lizard satellite cells formed large nodular structures comprised of condensed cells when cultured in chondrogenic medium (Figure 4J, K) and smaller nodules when cultured in growth medium (Figure 4G, H), which is indicative of chondrogenesis. The lizard cells formed sparse myotubes in both conditions, although they mostly remained as single cells (Figure 4H, K). To further investigate the chondrogenic nature of the nodular structures, micromasses were stained with Alcian blue, a cationic dye that binds specifically to sulfated glycosaminoglycans and proteoglycans. Lizard satellite cell micromasses formed Alcian blue positive nodules in both growth and chondrogenic media (Figure 4I, L). In growth medium, the micromasses averaged 30.8 small nodules (Table 1). In chondrogenic medium, there were fewer nodules, an average of 18 per micromass, but the average surface area was twice that of nodules formed in growth conditions (Table 1). Mouse micromasses demonstrated no Alcian blue positive nodules in growth medium, and less than one nodule per micromass in chondrogenic medium (Figure 4C, F, Table 1).

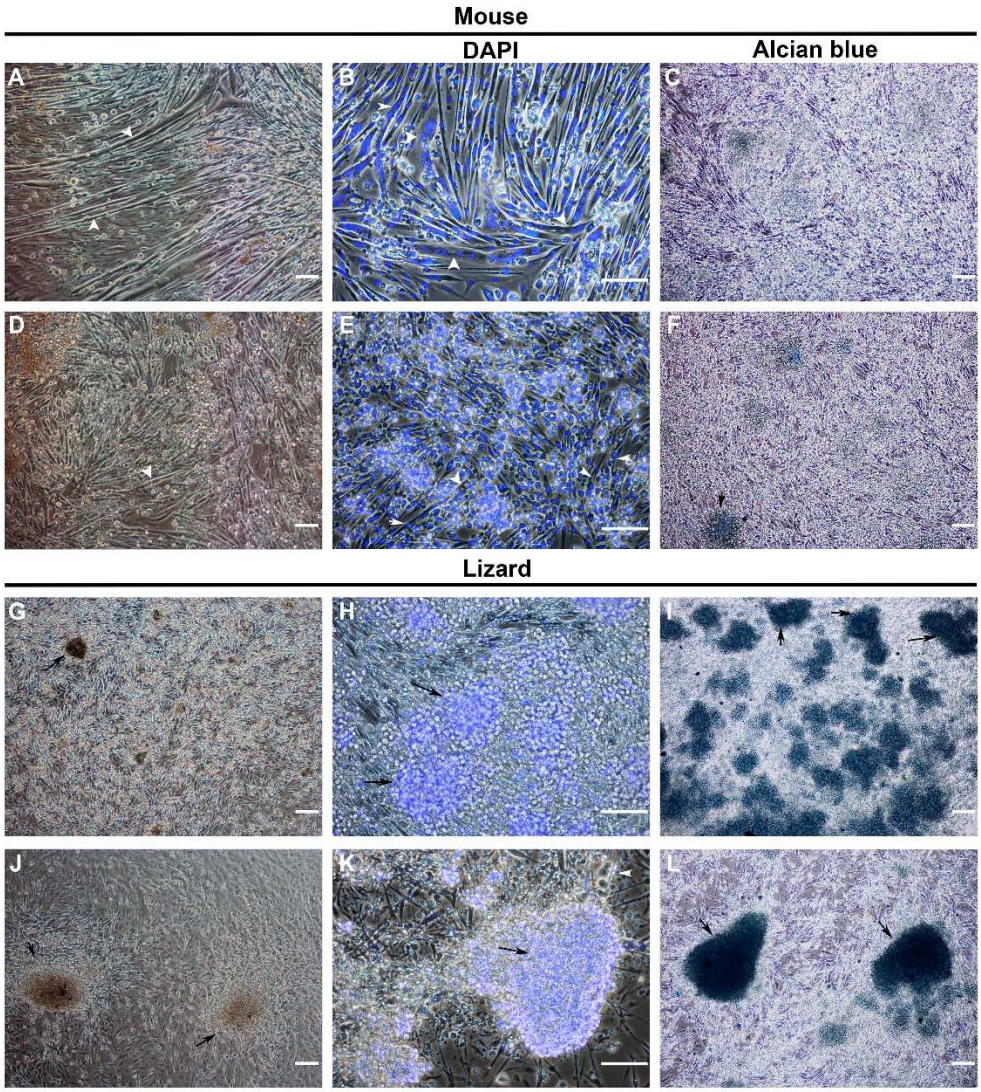

Figure 4. Micromass culture of lizard satellite cells results in condensation of cells into Alcian blue positive chondrogenic nodules

Mouse and lizard satellite cell micromasses were cultured in either growth **(A-C, G-I)** or chondrogenic differentiation medium **(D-F, J-L)** without added BMPs. Mouse satellite cells formed myotubes with many nuclei, as detected by DAPI nuclear stain, in growth medium **(A, B, white arrows)** and smaller myotubes in chondrogenic differentiation medium **(D, E, white arrows)**, but no defined nodules were noted. Lizard satellite cells in growth medium differentiated into a few small myotubes, and smaller nodules with undefined edges that stained positive with Alcian blue **(G-I, black arrows)**. Large Alcian blue positive nodules were found in micromasses cultured in differentiation medium, consistent with the onset of chondrogenesis *in vitro* **(J-L, black arrows)**. Photomicrographs are representative, magnification is 10× except for photomicrographs of DAPI stained micromasses, which are 20×; bars = 100 μm, n = 6 micromasses for each condition.

	GM	DM
	Average nodule number (average nodule surface area)	
Mouse	N/A	0.67 (0.029 mm^2)
Lizard	30.8 (0.027 mm^2)	18 (0.048 mm^2)

Table 1. Average number, and surface area of nodules in micromass.

The average number and surface area of nodules in day 7 micromasses was quantified using ImageJ (n = 6 micromasses for each experimental condition).

The expression of chondrogenic and myogenic marker genes in lizard and mouse satellite cells cultured in growth or chondrogenic medium was examined by RT-QPCR. CDNA was generated from total RNA isolated from high density micromass cultures after 7 days. Mouse cells significantly down-regulated *Pax7* expression, consistent with myotube differentiation, while this gene was up-regulated in lizard satellite cells, significantly so, in differentiation medium. This might reflect an increase in the number of satellite cells, as there were many single cells present at day 7 that did not participate in formation of myotubes or nodules in lizard micromasses (Figure 5). Analysis of MyoD (*Myod1*), a myogenic basic helix-loop-helix transcription factor (bHLH) up-regulated in actively proliferating satellite cells and myoblasts (Yin et al., 2013), revealed a small but significant decrease in expression in mouse satellite cells in growth medium (Figure 5). Conversely, *Myod1* expression demonstrated a small but significant down-regulation in lizard satellite cells cultured in chondrogenic medium, consistent with the onset of chondrogenesis. Additionally, we found that *Runx2*, a transcription factor important for proliferation and differentiation of chondrocytes and skeletal morphogenesis (Fujita et al., 2004; Takarada et al., 2013), was up-regulated in cells from both species. This occurred in both growth and chondrogenic differentiation conditions, suggesting that high cell density may be sufficient to trigger its expression. Interestingly, *Sox9*, a transcription factor necessary for chondrogenesis (Akiyama et al., 2002; Asou et al., 2002; Leung et al., 2011; Wright et al., 1995) was only significantly up-regulated in lizard cells cultured in micromass, and its expression level increased in chondrogenesis medium (Figure 5).

Given the differences in baseline expression of BMP pathway genes between lizard and mouse satellite cells, including elevated *Bmp2* and decreased *Bmp6*, we investigated whether further differences arose during chondrogenic differentiation in

micromass culture. For lizard satellite cells, *bmp2* transcription was significantly up-regulated undergrowth conditions, and culture in chondrogenic differentiation medium, further significantly increased the level of its expression (Figure 5). *Bmp6* is expressed in differentiating hypertrophic chondrocytes, but unlike *Bmp2*, its primary role is regulating iron metabolism, rather than orchestrating chondrogenesis (Camaschella, 2009). *Bmp6* expression was not up-regulated in lizard satellite cells in growth medium, but was increased in differentiation medium. *Bmp6* was up-regulated in mouse satellite cells when cultured at high density and in chondrogenic medium (Figure 5).

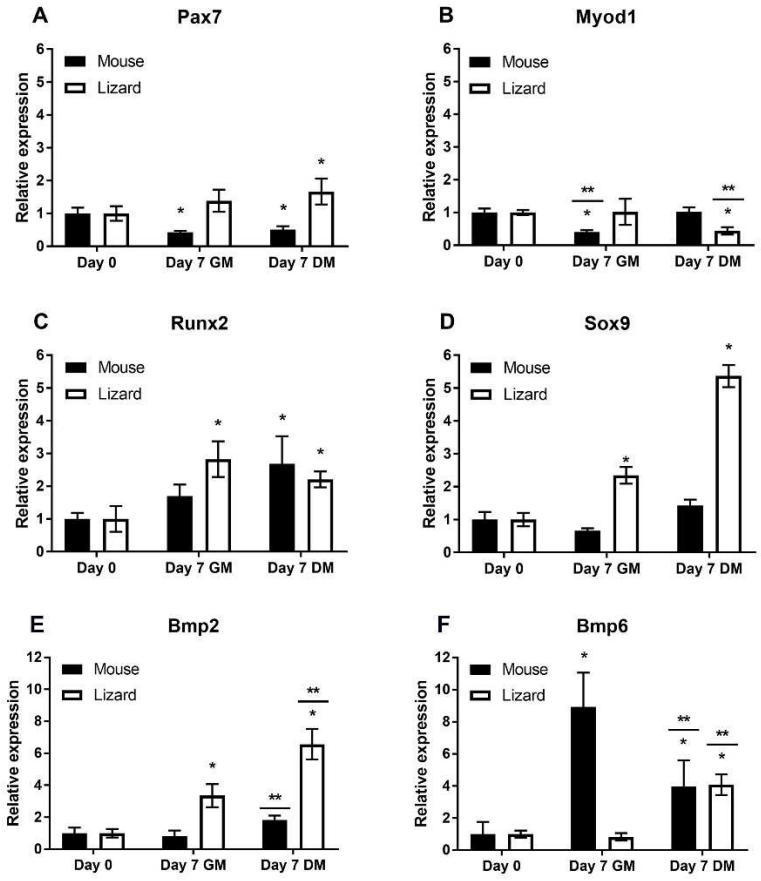

Figure 5. Expression of lineage-specific regulatory genes in lizard and mouse satellite cells cultured in micromass

Mouse satellite cells demonstrated decreased *Pax7* expression in micromass culture, while lizard cells up-regulated this gene **(A)**. Both species of satellite cells expressed *Myod1* and *Runx2* **(B, C)**, but only lizard cells significantly up-regulated the chondrogenesis regulator *sox9* **(D)**. Lizard satellite cells up-regulated *bmp2* expression significantly in growth medium (GM), and further increased expression significantly in chondrogenic differentiation medium (DM) **(E)**. Murine satellite cells demonstrated no significant change in the expression of *Bmp2* when compared to Day 0. Lizard satellite cells significantly up-regulated *bmp6* only when cultured in chondrogenic differentiation medium, while mouse cells demonstrated significant up-regulation of Bmp6 expression in growth medium as well **(F)**. Graphs are as labeled. Data are expressed as relative gene expression and are the result of 3 biological replicates, each done in triplicate. Statistical analysis was done by one way ANOVA; * indicates $p < 0.05$ when compared to Day 0 and ** denotes that DM and GM for that species are significantly different from each other ($p < 0.05$).

Cartilage is a hypocellular and avascular tissue, with few cells embedded in the extensive ECM. We further examined the expression of ECM proteins in micromass culture. Collagen I (*Col1a1*) is expressed in muscle, tendon, and bone (Reddi et al., 1977), whereas collagen 2A1 (*Col2a1*) is specific to cartilage. Both mouse and lizard cells significantly up-regulated *Col1a1* in micromasses, but only the lizard cells expressed and significantly up-regulated cartilage specific *Col2a1* (Figure 6). Aggrecan (*Acan*) is a cartilage specific ECM protein expressed during chondrogenic differentiation (Lauing et al., 2014), and expression of this gene was significantly up-regulated in the lizard micromasses. *Acan* was not detected in mouse micromasses regardless of culture conditions (Figure 6). Osteopontin, or secreted phosphoprotein 1 (*Spp1*), is expressed by a variety of cell types and has many roles, among which are muscle regeneration, inflammatory responses, and bone calcification (Pagel et al., 2014; Singh et al., 2014). Interestingly, while murine satellite cells up-regulated expression of this gene, the lizard satellite cells significantly down-regulated its expression in chondrogenic medium (Figure 6). We examined collagen 2a1 expression using ICC in micromasses at day 7. Cells were fixed in 4% formaldehyde and stained with an anti-collagen 2a1 antibody. Consistent with the RT-QPCR observations, mouse micromasses did not express collagen 2A1 (Figure 6, compare G to E, F), whereas lizard nodules demonstrated strong expression of this protein (Figure 6H, I). Taken together, our data demonstrates that the lizard cells express genes involved in chondrogenesis and can differentiate in culture by up-regulating the expression of BMP genes, cartilage specific transcription factors, and ECM genes.

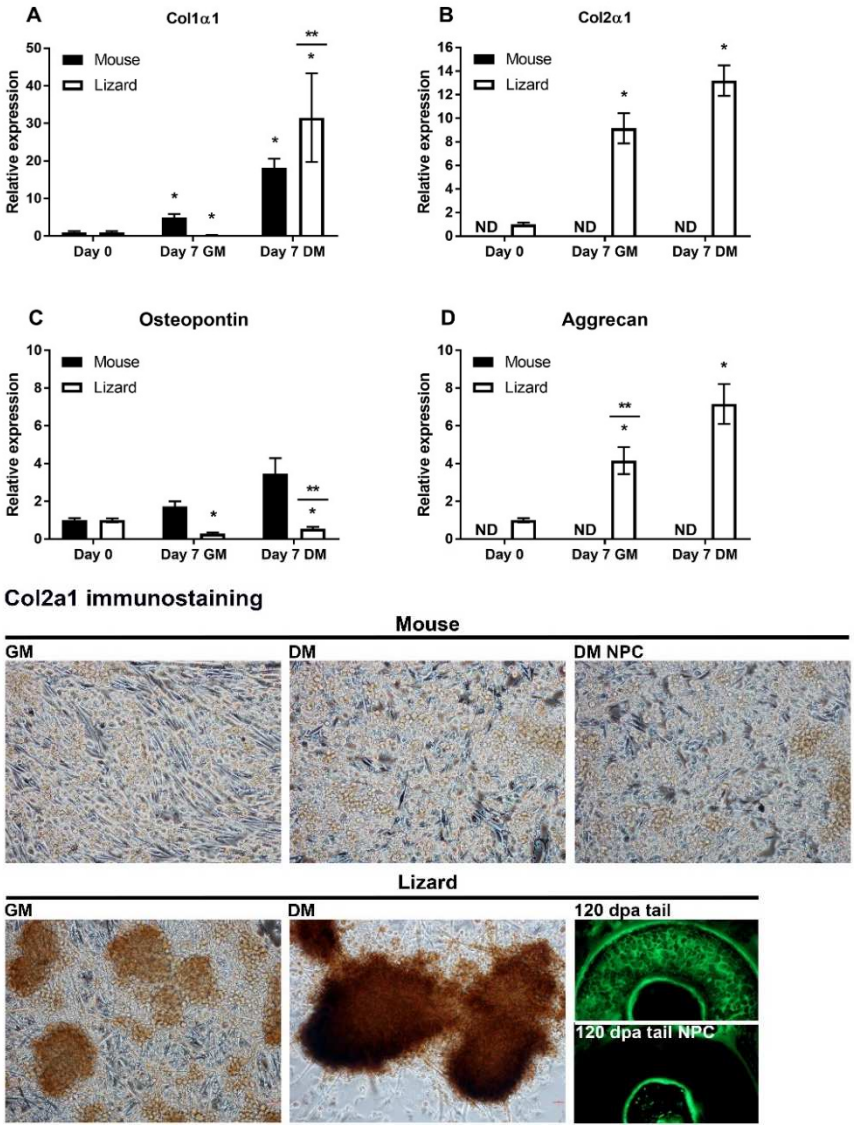

Figure 6. Lizard satellite cell micromass express cartilage-specific genes and proteins.

Col1a1 was up-regulated in both species in DM **(A)**, while *col2a1*, a cartilage specific collagen, was detected in lizard satellite cells only **(**B**)**. *Opn* was significantly down-regulated in lizard cells **(C)**. *Acan* expression was detected only in lizard micromasses, where it was significantly up-regulated in GM and further increased in DM **(D)**. Protein expression was determined by ICC. Mouse satellite cells exhibit background staining that is indistinguishable from the no primary antibody control (NPC) sample. Chondrogenic nodules express COL2A1 protein in lizard micromasses in both culture conditions, although the staining is more robust in DM. To show the specificity of the anti-COL2A1 antibody in lizard, IF was done with an anti-mouse-FITC secondary antibody on transverse sections of regenerating lizard tails at 120 days post autotomy (dpa). The matrix of the cartilage is evident compared to the NPC control. RT-QPCR data and tatistical analysis were carried out as previously stated (see figure 5); ND = not detected.

Discussion

Transcriptomic and histological analyses of regeneration in the *A. carolinensis* tail point to a stem cell-mediated process (Fisher et al., 2012; Hutchins et al., 2014). Our previous work demonstrated that lizard skeletal muscle contains PAX7 positive progenitor cells, and RNA-Seq analysis showed that the regenerating tail expressed marker genes of activated satellite cells and myoblasts (Hutchins et al., 2014). Using the cross-species analytical tool XGSA, we carried out comparative transcriptomic analysis of proliferating lizard satellite cells with mouse and human tissues from the ENCODE project. As expected, we found the closest match with satellite cells (Figure 2). However, the expression level of genes associated with chondrogenesis and osteogenesis were higher in lizard satellite cells when compared with their mouse counterparts (Figure 3).

BMP signaling induces different responses depending on ligand concentrations and exposure times. BMPs and their inhibitors define the spacial and temporal constrains of muscle formation (Hirsinger et al., 1997; Re'em-Kalma et al., 1995; Reshef et al., 1998). During skeletal muscle regeneration, low concentrations of BMP2, 4, and 7 maintain proliferation of satellite cells and myoblasts (Amthor et al., 1998; Friedrichs et al., 2011; Ono et al., 2010; Ozeki et al., 2007; Sartori et al., 2014; Wang et al., 2010), whereas high levels of BMP2, 4, 5, or 7 inhibit myogenesis, induce chondrogenesis, and ultimately, osteogenesis of satellite cells, C2C12 myoblasts, C3H10T1/2 mesenchymal stem cells (MSCs), and other MSCs, with continued exposure in culture (Bandyopadhyay et al., 2006; Friedrichs et al., 2011; Katagiri et al., 1994; Knippenberg et al., 2006; Liao et al., 2014; Ozeki et al., 2007; Schmitt et al., 2003; Shea et al., 2003; Takács et al., 2013; Zhou et al., 2016). Proliferating lizard satellite cells expressed *bmp2, 5*, and *7* at high levels, unlike their murine counterparts (Figure 3). A significant observation was the

endogenous up-regulation of *bmp2* by these cells in micromass culture and a further increase in its expression under conditions that favored cartilage differentiation, indicating the lizard satellite cells can adopt a chondrogenic fate. In mammals, BMP2 induces the expression of the transcriptional activators Runx2 and Sox9, which mediate chondrogenesis (Denker et al., 1999; Haas and Tuan, 1999; Hashimoto et al., 2008; Katagiri et al., 1994; Kwon et al., 2013; Liao et al., 2014; Schmitt et al., 2003; Shea et al., 2003; Zhou et al., 2016). The transcription factor RUNX2 regulates the differentiation of mesenchymal cells to chondrocytes, and chondrogenesis is disrupted in Runx2$^{-/-}$ mice (Inada et al. 1999; Komori et al. 1997; Takarada et al. 2013). SOX9 is a transcription factor that regulates differentiation of embryonic cartilage and induces chondrogenic differentiation of myogenic cells (Akiyama et al., 2002; Cairns et al., 2012; Liao et al., 2014; Wright et al., 1995; Zhou et al., 2016). In micromass culture, the lizard satellite cells concomitantly up-regulated expression of *bmp2, runx2,* and *sox9* significantly, and formed dense nodules (Figures 4–6). Expression of the SOX9 targets and cartilage specific matrix proteins *col2a1* and *acan* by lizard satellite cells was consistent with the onset of chondrogenesis (Figure 6). The presence of cartilage specific ECM in lizard satellite cell micromasses was also confirmed by Alcian blue staining (Figure 4), and detection of collagen 2A1 by ICC (Figure 6). By contrast, we found that mouse satellite cells in micromass culture did not initiate chondrogenesis (Figures 4-6). These data indicate that lizard satellite cells can enter a different musculoskeletal lineage by endogenously up-regulating expression of cartilage specific transcription factors and morphogens, and point to important differences in the regulation of these genes in the lizard. The up-regulation of cartilage specific regulators by lizard satellite cells suggests that these cells have greater potency as stem cells and are able to differentiate along multiple musculoskeletal lineages to form cartilage, skeletal muscle, and potentially even

tendon. Further research is required to confirm and elucidate the mechanisms underlying this process.

The expression of Msx1 and Msx2 was ranked higher in lizard compared to mouse satellite cells. These transcriptional repressors play important roles in embryonic chondrogenesis in mammals (Ishii et al., 2005; Odelberg et al., 2000; Satokata et al., 2000). In amphibians, these proteins are important for dedifferentiation of muscle during limb regeneration and are expressed in the blastema (Echeverri and Tanaka 2002). When C2C12 myotubes in culture expressed Msx1 or Msx2 from inducible viral promoters, these proteins caused delamination of single cells from the myotubes. The expression of myogenic marker genes was decreased in these cells, but less than 10% re-entered the cell cycle (Odelberg et al., 2000; Yilmaz et al., 2015). The expression of these two genes in proliferating lizard satellite cells may indicate they are necessary for either maintenance of proliferation, or another role in the increased plasticity of these cells. Not surprisingly, our data also showed that lizard satellite cells demonstrated changes in gene expression that are consistent with decreased fibrosis, which is important for successful regeneration. For example, Decorin (*Dcn*) encodes an ECM protein that decreases the fibrotic response during muscle regeneration (Li, Mcfarland, and Velleman 2008; Li et al. 2007; McCroskery et al. 2005) and is expressed at a higher level in lizard as compared to mouse satellite cells. Similarly, *Tgfb2* and *Fzd1* are both implicated in fibrosis in dystrophic and aged skeletal muscle (Biressi et al., 2015; Brack et al., 2007), and were expressed at much lower levels in lizard than in mouse myoprogenitors. Taken together, these data suggest that some lizard satellite cells have increased musculoskeletal potential governed by changes in the regulation of gene expression, as only the tail is regenerated. Further inquiry into these changes will not only shed light on the mechanisms of lizard tail regeneration, but also provide a means for approaching

improved tissue engineering of mammalian muscle and cartilage from satellite cells. Understanding the regeneration strategy employed by reptiles could provide important genetic information regarding specific pathways or genes whose regulation could be altered to improve the potential therapeutic uses of satellite cells in mammals.

Materials and Methods

Animals

CD-1 mice (Mus musculus) were bred and housed in a vivarium at Arizona State University (ASU) on a 10 h light:14 h dark schedule with ad libitum access to food and water. Adult *A. carolinensis* lizards were purchased from Charles D. Sullivan, Inc. (Nashville, TN) or Marcus Cantos Reptiles (Fort Myers, FL) and housed as described previously (Fisher et al., 2012). ASU is accredited by the Association for Assessment and Accreditation of Laboratory Animal Care (AALAC). All procedures were carried out in compliance with the ASU Institutional Animal Care and Use Committee and AALAC under approved research protocols.

Cell culture and Isolation

Muscle progenitor cells were isolated from 12 week old CD-1 mice and adult *A. carolinensis* lizards, as previously described (George et al., 2013; Hutchins et al., 2014). Hind limb quadriceps femoris muscles were excised, trimmed of fat and connective tissue, and finely minced to a pulp. For lizard cells, skeletal muscle was stripped from all limbs and proximal tail, trimmed of connective tissue, and treated as above. The muscle tissue was digested with 1.25 mg of protease XIV (Sigma-Aldrich, St. Louis, MO) for one hour at 37 °C, triturated to extract single cells and passed through a 100 μm nylon mesh. The cell suspension was spun down at 1500g for 10 mins and pre-plated in DMEM

(Corning, Corning, NY), 2% HS (Atlanta Biologicals, Flowery Branch, GA) and 100μg/mL Primocin (Invivogen, San Diego, CA) for 2 h, to remove fibroblasts and other debris. Satellite cells were grown on Matrigel (BD Biosciences, Bedford, MA) in Hams F-10 (Corning,),20% FBS (Atlanta Biologicals), 10 ng/mL bFGF (BD Biosciences) and 100μg/mL Primocin (Invivogen). Cells were cultured at 37 °C for mouse or 30 °C for lizard muscle progenitor cells in 5% CO2 humidified chamber. Cells from each isolation were plated onto Matrigel coated coverslips and PAX7 expression was determined by immunofluorescence (IF). The average percentage of PAX7 positive cells isolated was 98.8 ± 1.2% for mouse and 98.6 ± 2.2% s.d. for lizard cells, consistent with our previous data (George et al. 2013; Hutchins et al. 2014, data not shown)

Micromass culture

Satellite cells were seeded at 1 $\times 10^6$ cells/micromass in Matrigel coated 24 well plates. After a 1 h incubation (37 °C for mouse and 30 °C for lizard cells), the wells were flooded with growth medium (Ham's F-10supplemented with 20% FBS, 10 ng/mL bFGF and Primocin) or chondrogenic differentiation medium (Ham's F-10 supplemented with10% FBS, 1% ITS, 50 nM ascorbate-2-phosphate, 1 nM TGFβ1 (Preprotech, Rocky Hill, NJ), and Primocin, for 7 days. Medium was changed every 3 days.

RNA Isolation and quantitative RT-PCR (RT-QPCR)

Cells were lysed in Trizol (Invitrogen, Carlsbad, CA) for RNA isolation, per the manufacturer's protocols, and three biological replicate experiments were performed. RNA was quantified by Nanodrop prior to cDNA synthesis using SuperScriptIII reverse transcriptase (Invitrogen) with 2 μg of RNA. The cDNA was quantified using transcript specific, intron spanning primers and real time PCR with Sybergreen (Eurogentec,

Fremont, USA) on an ABI 7900 HTthermocycler using a 384 well format in 10µl reactions. Products from each primer set were sequenced and analyzed by BLAST (NCBI) to verify their identity. Primer efficiency was determined using a standard curve. For each transcript, three biological replicates were assayed in triplicate. All samples were normalized to the Gapdh transcript and relative gene expression was calculated using ΔΔCq analysis (Haimes and Kelley 2010). Primer sequences for mouse and lizard genes are in Table 2.

RNA-Sequencing and transcriptomic analysis

RNA-Seq analysis of *A. carolinensis* satellite cells (3 biological replicates) has been described previously by our group (Hutchins et al., 2014) and the data are deposited in the NIH Sequence Read Archive (SRR1502189, SRR1502190, and SRR1502191; BioProjectPRJNA253971). RNA-Seq data of mouse C57Bl/6J satellite cells (Ryall et al., 2015) (SRA accessions SRR1726676, SRR1726677) were supplemented by our RNA-Seq analysis of mouse CD1 satellite cells isolated as described above, using protocols outlined in Hutchins et al.,2014. Transcript reads were mapped to *A. carolinensis* (AnoCar2.0) or mouse (GRCm38) Ensembl annotated genomes with HISAT2 v2.0.1 using default parameters (Kim et al., 2015). Gene level read counts were generated using HTSeq v0.6.0 in intersection-nonempty mode (Anders et al., 2015). For lizard and mouse satellite cell transcriptomes, Reads Per Kilobase of transcript per Million mapped reads (RPKM) were generated using edgeR (Robinson et al., 2009). For human satellite cells, Fragments Per Kilobase of transcript per Million mapped reads (FPKMs) were generated from two biological replicates analyzed by RNA-Seq (Charville et al., 2015) using TopHat and Cuffnorm (Trapnell et al., 2010, 2009). For comparison with reported gene expression profiles for a library of different tissues, ENCODE

transcriptome profiles summarized as FPKMs were obtained for human (hg19; 139 tissues) and mouse (mm9; 94 tissues) (ENCODE ProjectConsortium, 2012 doi: 10.1038/nature11247; Mouse ENCODEConsortium et l., 2012 DOI: 10.1186/gb-2012-13-8-418). Gene symbols follow the recommendations of the International Committee on Standardized Genetic Nomenclature for Mice and the Anolis Gene Nomenclature Committee. In instances where the homologous genes in both mouse and lizard species are being referenced, the mouse nomenclature was used

Cross-species gene set analysis

For each RNA-Seq experiment containing RPKM or FPKM values, rank products were calculated for each gene using all available replicates (Breitling et al., 2004). We identified the 1500 most highly expressed genes in each cell type or tissue type. We then remove genes that are deemed highly expressed in more than 10% of the cell types, as these genes are likely ubiquitously expressed genes. The remaining genes are considered specifically expressed in each cell type or tissue type. We call this collection of gene sets the cell-type specific gene sets. Using the human and mouse ENCODE data collections, we generated a compendium of cell-type specific gene sets in humans and mice. Using a similar procedure, we used our lizard RNA-Seq data to generate a highly expressed gene set. We compared the lizard gene set against the human and mouse cell-type compendia using XGSA. A p-value is generated to represent whether the lizard gene set has significant overlap with a mouse or human cell-type-specific gene set. To confirm that our gene set analysis is robust against our choice of parameters, we repeated the same analysis with a range of parameters (number of top highly expressed genes: 500, 1000, 1500, 2000; % of cells containing marker gene: 1%, 2%, 3%, 5%, 10%, 15%, and 20%).

Alcian blue staining

Micromasses were fixed with 0.1% glutaraldehyde after 7 days in culture, and stained with 1% wt/vol Alcian Blue (VWR, Radnor, PA) in 0.1 M HCl overnight, at 4 °C. Excess stain was removed with 0.1 M HCl, followed by PBS.

Immunocytochemistry and Immunofluorescence

Monoclonal anti-Col2A1 antibody, II-II6B3, which was deposited to the Developmental Hybridoma Studies Bank by T.F. Linsenmayer (DSHB, Iowa City, IA) and biotinylated goat anti-mouse IgG/anti-rabbit IgG (BA-1400, Vector Laboratories, Burlingame, CA) were used for immunocytochemistry (ICC). Micromasses were fixed in 4% formaldehyde and permeabilized with 0.5% Triton X-100 PBS solution. After blocking non-specific binding with 10% goat serum (Invitrogen), micromasses were incubated overnight at 4 °C with primary antibody diluted in 1% serum, washed with PBS, and subsequently incubated for 1 h at 37 °C with secondary antibody in PBS and 1% serum. HRP-Streptavidin solution was added for 30 min, followed by PBS washes and DAB substrate incubation (Broad Spectrum HRP Histostain, Invitrogen). To visualize nuclei, fixed micromasses were stained with DAPI (Biotium, Fremont, CA), per manufacturer's instructions. Transverse vibratome sections of 120 DPA regenerated lizard tails were obtained and incubated with the anti-Col2A1 antibody. Briefly, sections were washed in 0.2% Triton X-100 PBS, blocked in 5% goat serum, and incubated overnight at 4 °C with anti-Col2A1 antibody diluted in 5% serum. Following Triton-PBS washes, sections were incubated with FITC conjugated anti-mouse IgG secondary antibody) (F-0257, Sigma-Aldrich) diluted in 5% serum overnight at 4 °C. Fluoro-Gel (Electron Microscopy Sciences, Hatfield, PA) was used to mount the sections. All images were obtained on a Nikon Eclipse TE2000-U microscope, using the 488 nm filter for

immunofluorescence (IF). Images were adjusted for contrast and color balance. The surface area of nodules was quantified using the "freehand tool" and "set scale" features of ImageJ that allow a known length to be assigned a specific number of pixels.

Primer name (mouse)	Primer sequence (5'-3')
Pax7 FWD	AACTACCCGCGCACCGGCTT
Pax7 REV	GGGTCGACCGTTGATGAAGACC
Myod1 FWD	TGATGGCATGATGGATTACAGCGG
Myod1 REV	AGATGCGCTCCACTATGCTGGACA
Runx2 FWD	AAACASGCCTCTTCAGCGCA
Runx2 REV	TCGCTCATCTTGCCGGGCT
Sox9 FWD	AGACCAGTACCCGCATCTGCACAA
Sox9 REV	AAGGGTCTCTTCTCGCTCTCGTT
BMP2 FWD	TACCGCAGGCACTCAGGCCA
BMP2 REV	AAGTTCCTCCACGGCTTCTTCGT
BMP6 FWD	AAGTCTTGCAGGAGCATCAGCACA
BMP6 REV	GCTGTGATGTCAAATTCCAGCCAACC
Col1α1 FWD	TTCAGCTTTGTGGACCTCC
Col1α1 REV	CAGATCAAGCATACCTCGGG
Col2α1 FWD	TGCTGCTGACGCTGCTCAT
Col2α1 REV	GATATCTCCAGGTTCTCCTTTCTGCC
Osteopontin FWD	GCTTGGCTTATGGACTGAGG
Osteopontin REV	CAACAGGGATGACATCGAGG
Aggrecan FWD	AACAACCATGTCCCTGACAGATGC
Aggrecan REV	ATTCAGACAAGGGCTTGAGAGGCA
Gapdh FWD	GGGAAGCCCATCACCATCTT
Gapdh REV	GCCTTCTCCATGGTGGTGAA
Primer name (lizard)	Primer sequence (5'-3')
Pax7 FWD	GAGAAGAAGGCCAAGCACAG
Pax7 REV	GGGTGTAGATGTCCGGGTAG
Myod1 FWD	GCTCAGCAAGGTCAACGAG
Myod1 REV	CCTGGAGGCTCTGCATGTAG
Runx2 FWD	CCTCCAGCCTGGGAAGAT
Runx2 REV	GAACGGAGCAGAGGAAGTTG
Sox9 FWD	TCCGACGAGGAAGCCTCTT
Sox9 REV	CTTCAGCACCTGCGAGAC
BMP2 FWD	TCGGGAGCAGGTCCAAGATA
BMP2 REV	CCATCTCCTTAGCGCTGGTG
BMP6 FWD	GCACAACTTGGGACTCCAGA
BMP6 REV	AGCCGTTCGAACATGAACCT
Col1α1 FWD	AAGATGGTCTGAATGGTCTCC
Col1α1 REV	ACCATCATGAGCTTTCTCCT
Col2α1 FWD	AGGCGAGAAGGGAGACTCTG
Col2α1 REV	AGGGAAGCCTCTCTCACCAC
Osteopontin FWD	GGGAATCGTGTTTGGCTCTC
Osteopontin REV	GACCGTCTGGACATTGAGTAC
Aggrecan FWD	CCCTGACATCAGTCCGCTGT
Aggrecan REV	TCCCAAAAGGTGCTCCACTG
Gapdh FWD	TGGTGAAAATCGGAGTCAACG
Gapdh REV	TGATTGCTGTAACTCGGACTT

Table 2. Comprehensive list of primers used for RT-QPCR for both mouse and lizard satellite cell samples.

CHAPTER 3

MOLECULAR ANALYSIS OF MUSCLE PROGENITOR CELLS ON EXTRACELLULAR MATRIX COATINGS AND HYDROGELS

Abstract

Development of an *ex vivo* culture system to expand satellite cells, the resident muscle stem cell population, will be necessary for their use as therapeutics. The loss of the niche environment is often cited as the reason that culture results in both the decreased myogenic potential and low re-engraftment rates of these cells. Studies have shown that culture of satellite cells on more elastic substrates maintained their quiescence and potential and increased re-engraftment, with limited proliferation. We examined whether substrates composed of extracellular matrix proteins, as either coatings or hydrogels, could support expansion of this population whilst maintaining the potency of these cells. The collagen-based hydrogels were very pliant and our studies demonstrate that stiffer substrates are necessary for *in vitro* proliferation and differentiation of satellite cells, and the ECM composition was not significantly important. Our data further indicates that culture on highly elastic substrates allowed satellite cells to down-regulate myogenic specific transcription factors, resulting in an expression profile similar to a Galert state. These satellite cells could be subsequently cultured on Matrigel and induced to differentiate. Proliferation and gene expression data further indicated that C2C12 cells are not a good proxy for studies of satellite cell proliferation and differentiation on alternative substrates. Examining the expression of lineage and cell cycle specific genes provided important insight into the behavior of both cell types, and pointed to fundamental differences that affect the interpretation of studies aimed at understanding the *in vitro* requirements of muscle progenitor cells.

Introduction

Satellite cells can be exploited therapeutically as an autologous source of stem cells for repair of volumetric muscle loss due to trauma or surgery, or as a source of genetically corrected stem cells to treat dystrophic muscle. However, satellite cells must be recovered from biopsies or surgical samples, thus in order to generate enough cells for therapeutic use, they require *ex vivo* expansion. Unfortunately, *ex vivo* culture is correlated with limited proliferation, loss of myogenic potential, and poor re-engraftment of these cells into the skeletal muscle niche. It has been hypothesized that this is a result of the loss of the niche environment, as the complex biochemical and biomechanical properties of the niche are difficult to replicate in traditional tissue culture (Boonen et al., 2009). To fully explore the therapeutic use of satellite cells, it is necessary to develop a culture system that promotes expansion without the loss of myogenic potential.

Recent studies of satellite cells in culture have focused on substrate stiffness (Gilbert et al. 2010), various ECM proteins as coatings (Grefte et al., 2016, 2012), and inhibition or stimulation of various signaling pathways (Charville et al., 2015; Quarta et al., 2016). C2C12 cells are reportedly able to form myotubes on substrate with a range of stiffness (Engler et al., 2004). Satellite cells require the support of an ECM coating, such as Matrigel, to attach, proliferate, and differentiate post-isolation (Chaturvedi et al., 2015; Osses and Brandan, 2002). However, Matrigel does not maintain satellite cell proliferation, nor myogenic potential, indefinitely (Montarras et al., 2005; Qu-Petersen et al., 2002; Sacco et al., 2008). A proteomic analysis of Matrigel composition found the most abundant ECM proteins were laminins, collagens I and IV, and fibronectin (Hughes et al., 2010). These same proteins are present in the ECM of the myofiber niche. Collagen

and laminin bind to α7β1 integrins on the satellite cell membrane (Sanes, 2003). Laminin has been shown to induce satellite cell proliferation and migration (Öcalan et al., 1988). Fibronectin is secreted by satellite cells as they remodel their niche in response to muscle damage and is necessary for satellite cell expansion (Collinsworth et al., 2002; Mathur et al., 2001; Öcalan et al., 1988; Qu-Petersen et al., 2002; Sanes, 2003). Collagen I is a structural component of the myofiber basal lamina and self-polymerizes under the right conditions, enabling us to design scaffolds that contain laminin and fibronectin without the support of synthetic materials.

The reported mechanical properties of native muscle fibers vary immensely. The Young's modulus of muscle fibers, as determined by atomic force microscopy (AFM), has been reported as 45.3 kPa (Collinsworth et al., 2002) and 24.7 kPa (Mathur et al., 2001). Others have noted that damaged myofibers are stiffer and reported a Young's modulus of 0.5 kPa for intact myofibers and 2.0 kPa for damaged myofibers (Mathur et al., 2001) or 12 kPa for intact and 16 kPa for damaged fibers (Urciuolo et al., 2013). The stiffness of the culture substrate has been shown to modulate proliferation and differentiation of satellite cells (Boonen et al. 2009; Gilbert et al. 2010; Quarta et al. 2016). For example, polymerized collagen I scaffolds with Young's or elastic moduli of 2 kPa or 12 kPa, as measured by atomic force microscopy (AFM), either maintained quiescence, or induced proliferation, respectively (Quarta et al., 2016). When cultured on laminin cross-linked PEG hydrogels that mimicked the stiffness of the muscle, fewer satellite cells underwent apoptosis or up-regulated myogenin (*Myog*), a marker of muscle differentiation. However, while differentiation was inhibited, the rate of satellite cell proliferation was unchanged on the PEG hydrogels (Gilbert et al. 2010). The stiffness and the protein composition of the substrate may have complementary or opposing effects on the potential and proliferation of satellite cells.

The reported Young's modulus of muscle ranges from 0.5 kPa to 45 kPa (Mathur et al., 2001; Urciuolo et al., 2013). These differences in measurement may be a result of experimental design, or the preparation and handling of the myofibers. Regardless, there was no consensus stiffness to mimic. In this study, we compared the effects of substrate elasticity and composition of hydrogels and coatings composed of ECM proteins on the proliferation, differentiation, and lineage status of C2C12 myoblasts, an immortalized myoblast cell line, and primary satellite cells. To examine the contributions of niche ECM components and stiffness of the culture matrix on the proliferation and lineage status of C2C12 myoblasts and primary satellite cells, we chose to culture these cells on collagen I based hydrogels with laminin, or laminin and fibronectin, or tissue culture plates coated with the same ECM proteins.

Results

Rheometry demonstrates that viscoelasticity varies with collagen concentration

We determined the relative stiffness of the collagen/laminin/ fibronectin hydrogels using rheology to calculate the storage moduli. Hydrogels polymerized on a humidified rheometer stage heated to 37°C as the storage and loss moduli were recorded continuously over 30 minutes. Storage moduli increased linearly as collagen I concentration increased from 0.96 Pa (1 mg/mL collagen I/100mg/mL laminin; 1-100) to 19 Pa (3 mg/mL collagen I/100mg/mL laminin; 3-100) (Figure 7), which is consistent with other rheometric measurements of collagen hydrogels (Miron-Mendoza et al., 2010). The addition of fibronectin modestly lowered the storage modulus several Pascals (Figure 7, G). Coated plates are a very stiff substrate with an elastic modulus ~10^6 kPa, orders of magnitude stiffer than skeletal muscle (Gilbert et al., 2010; Soofi et al., 2009).

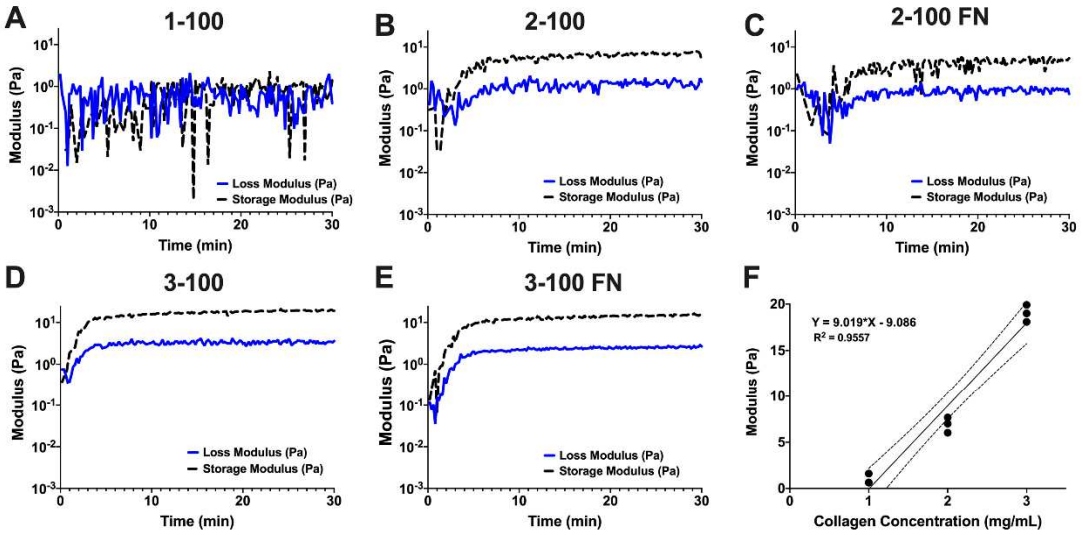

G

Hydrogel	Storage modulus (Pa)
1-100	0.96 ± 0.32
2-100	6.90 ± 0.48
2-100FN	4.65 ± 0.43
3-100	19.00 ± 0.53
3-100FN	14.61 ± 0.35

Figure 7. Collagen-based hydrogels have tunable properties

Rheometric analysis of collagen-based hydrogels shows the storage and loss moduli of the gels as they polymerized and then reached stable gel formation **(A-E)**. A direct linear correlation between the collagen concentration and storage modulus was observed for the collagen concentrations evaluated in this study (R^2=0.9557; **F**); dotted lines represent 95% confidence interval. Average storage modulus for each hydrogel formulation; mean ± SEM (n = 2-3; **G**).

Satellite cells do not proliferate on hydrogels

We determined if hydrogels or tissue culture plates coated with the same concentrations of the ECM proteins induced proliferation of satellite cells and C2C12 myoblasts. Cells were seeded at densities that ensured they would not reach confluency before 6 days (determined prior by seeding with various cell densities on Matrigel; data not shown) and proliferation was assayed at 1, 3, and 6 days using an MTT assay (Figure 8). Overall, C2C12 cells proliferated at a significantly higher rate than satellite cells on ECM coated plates, regardless of the composition of the coating ($p<0.05$; Figure 8A). Both C2C12 and satellite cells demonstrated decreased proliferation when cultured on 3-100FN ($p<0.05$ as compared to all other conditions). On this coating, satellite cells did not grow, and C2C12 cells demonstrated a lag in proliferation that was overcome at 6 days (Figure 8A). Overall, when cultured on hydrogels, both cell types demonstrated less robust proliferation (Figure 8B). C2C12 cells proliferated significantly better on the softest, 1-100, and the stiffest, 3-100FN, hydrogels (Figure 8B). Satellite cells demonstrated a marked lack of proliferation on hydrogels. We did not assay the 1 mg/mL collagen, 100 mg/mL laminin, 20 mg/mL fibronectin formulation, as this hydrogel would not polymerize consistently. On Matrigel coated plates, C2C12 cells proliferated significantly better than satellite cells. This ECM rich substrate induced better proliferation than any other coating or hydrogel assayed overall for both cell types ($p<0.05$; Figure 8C).

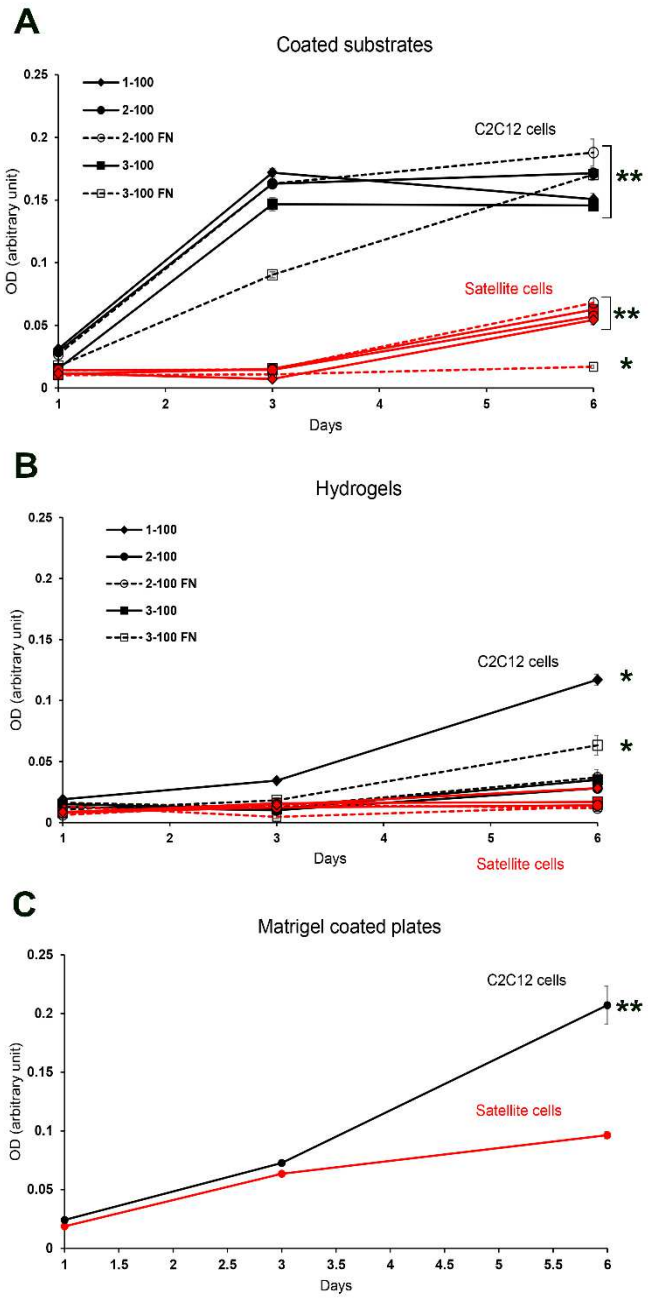

Figure 8. Satellite cells and C2C12 cells demonstrate differences in proliferation.

Cells were seeded on ECM coated plates **(A)**, hydrogels **(B)**, or Matrigel **(C)**, and MTT assays were carried out at days 1, 3, and 6. C2C12 cells proliferated significantly more robustly than satellite cells, regardless of substrate. Substrate composition did not significantly affect proliferation of either cell type. Day 6 data were analyzed by one way ANOVA with post-hoc Tukey test.; * $p<0.05$, significantly different from all other groups analyzed, and ** $p<0.05$, C2C12 cells are significantly different from satellite cells in all conditions. Data are mean+/- SEM of triplicate experiments.

Lack of proliferation can reflect a high level of cell death, rather than a true proliferation deficit. Therefore, we determined the viability of satellite cells on hydrogels using an ethidium homodimer/calcein AM assay. Cells were seeded on hydrogels in triplicates and viability was assayed at 24 and 72 hours post-seeding (Figure 9). A variety of hydrogel compositions were tested, ranging from 1-6 mg/mL collagen, and 10-100 μg/mL laminin. At 24 hours, greater than 90% of satellite cells were viable on hydrogels composed of 1 or 3 mg/mL collagen I. Hydrogels containing 6 mg/mL collagen I demonstrated a significant decrease in live cells, which may be due to technical issues, as these hydrogels are difficult to manufacture; they polymerize quickly, and do not adhere to tissue culture plastic as well (Figure 9A). Satellite cells grown on the 1-100, 2-100, or 3-100 hydrogels demonstrated 95.40%, 94.70%, and 99.09% live cells respectively at 72 hours (Figure 9C). Taken together, these data indicated that proliferation was not being masked by a high rate of cell death.

A

Collagen I (mg/mL)	Laminin (µg/mL)	% Live Cells
1	10	93.33%
1	100	97.15%
3	10	95.79%
3	100	96.46%
6	10	85.38%
6	100	83.02%

B

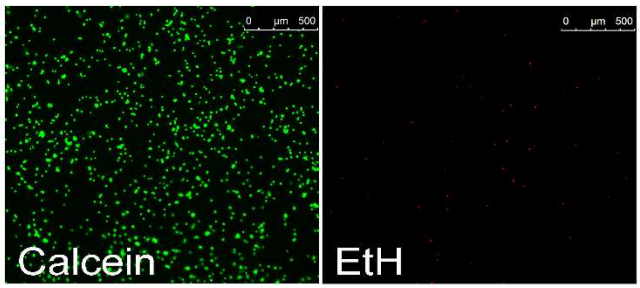

C

Collagen I (mg/mL)	Laminin (µg/mL)	% Live Cells
1	100	95.40%
2	100	94.70%
3	100	99.09%

Figure 9. Satellite cells maintain viability on hydrogels.

Viability of satellite cells seeded on hydrogels was tested using a calcein AM- ethidium homodimer assay either at 24 hrs **(A)** or 72 hours **(C)**. Live (green) and dead (red) cells were counted using ImageJ and the percentage of live cells was calculated for each condition **(B)**. Data are the result of triplicate experiments.

Satellite cells do not form myotubes on hydrogels

Previous studies indicated that softer substrates improved maintenance of myogenic potential of satellite cells *in vitro* (Ding et al., 2015; Padilla et al., 2017; Soofi et al., 2009). When cultured on plates coated with Matrigel, both satellite cells and C2C12 cells will form multinucleated myosin heavy chain positive (MHC+) myotubes within 3-5 days of serum withdrawal. We examined the differentiation of cells plated on hydrogels in growth medium for 24 hours, then differentiation medium for a further 3-5 days. Satellite cells did not migrate, align, or fuse into myotubes on any hydrogel, remaining instead as single cells (Figure 10). Conversely, C2C12 cells differentiated into multinucleated myotubes on all hydrogels, although differentiation was less robust on the 1-100 hydrogel (Figure 10).

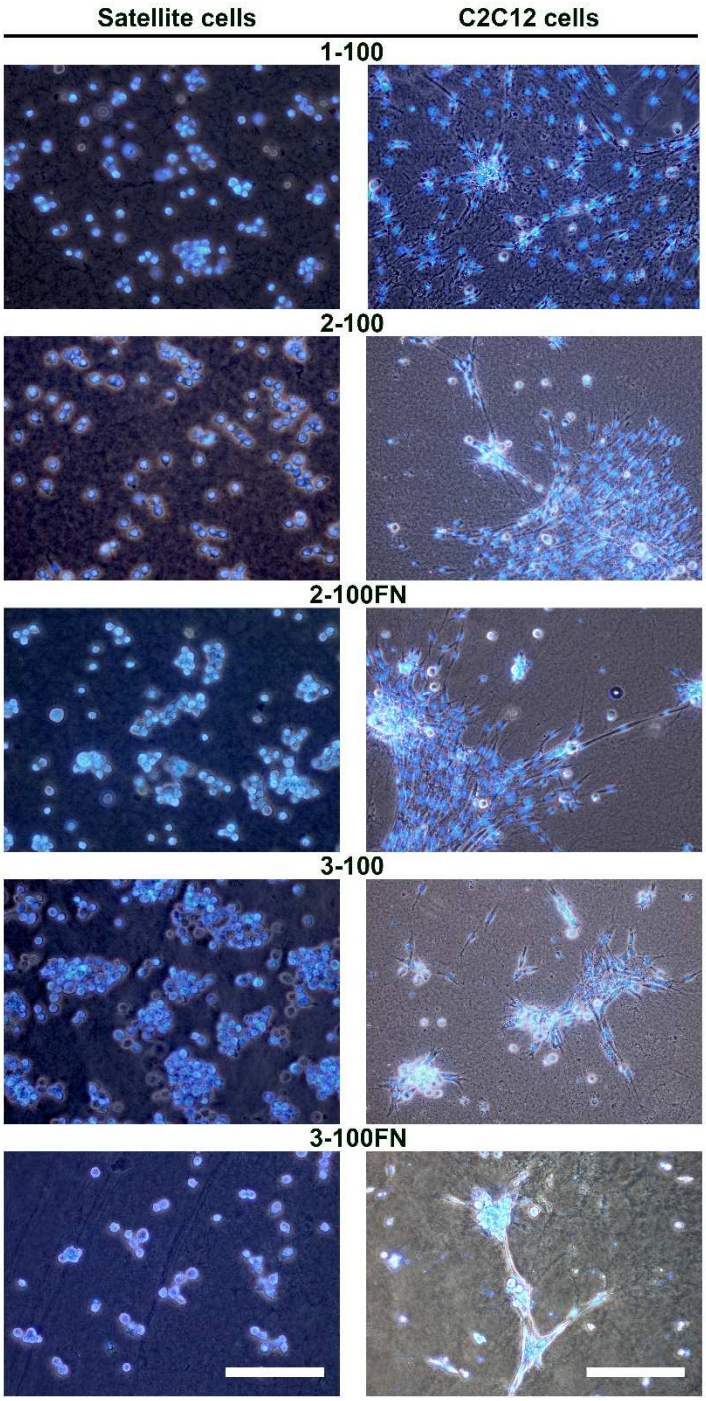

Figure 10. Culture on hydrogels inhibits satellite cell differentiation

Cells were grown on hydrogels 24 hrs, then in differentiation medium for 72 hrs. Cells were fixed and stained with DAPI (blue). Unlike C2C12 cells, satellite cells did not elongate and fuse to form myotubes. Images were obtained at 100x and 200X magnification, and the scale bar is 200 μm.

We next probed the differentiation potential of the satellite cells on the ECM coated plates. On Matrigel, satellite cells formed an average of 58.33± 9.71 MHC+ myotubes per field, with 10.42±5.05 nuclei per myotube. Satellite cells cultured on ECM coated plates also fused into MHC+ myotubes within 3 days, although the number of myotubes per field was significantly decreased when compared to Matrigel coating ($p<0.001$, Figure 11), ranging from 27.67±4.16 (1-100) to 18±5.2 (3-100FN). The average number of nuclei per myotube was likewise significantly reduced (3.9±0.68 for 1-100 and 4.42±0.17 for 3-100FN). While the various ECM formulations did not significantly alter differentiation, increasing the collagen concentration resulted in fewer numbers of myotubes per field. Robust myogenic differentiation *in vitro* requires nearly confluent cells. The proliferation assay data demonstrated lower levels of satellite cell proliferation on ECM coated plates, as compared to Matrigel (Figure 8). Thus, it was possible that the decreased number of myotubes and nuclei observed reflected reduced cell numbers, rather than a differentiation deficit caused by the ECM proteins or the stiffness of the plate. To examine this possibility, satellite cells were seeded on ECM coated plates at high density ($4.5x10^4$ cells/well) in growth medium for 24 hours, then in differentiation medium for a further 3 days. The number of MHC+ myotubes per field was statistically indistinguishable from Matrigel, and significantly higher when compared to cells plated at low density (Figure 11), demonstrating that ECM coatings supported differentiation. However, differentiation on ECM coated plates was not as robust, since the average number of nuclei per myofiber remained low when compared to Matrigel, regardless of plating density (Figure 11).

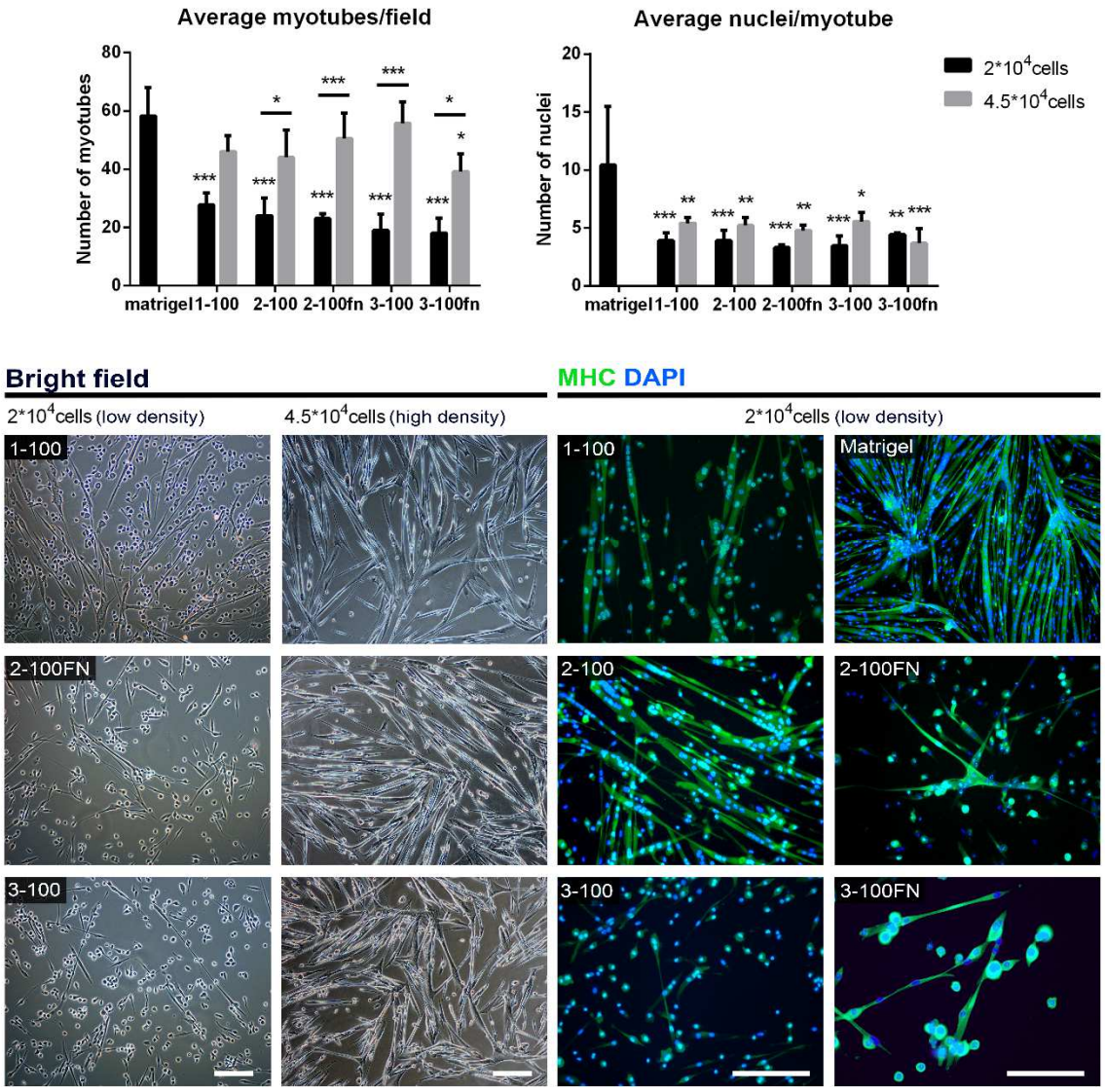

Figure 11. Satellite cells differentiate on coated plates

Satellite cells were seeded on ECM coated plates at low density, (2x10⁴ cells/well) or high density (4.5x10⁴ cells/well). After 3 days in differentiation medium, cells were fixed and stained using anti-MHC antibody (green) and DAPI (blue). At low density, there were fewer myotubes/field on ECM coated plates when compared to Matrigel, although that difference disappears when cells were seeded at high density. There were significantly fewer nuclei/myotube on ECM coated plates, regardless of cell density. Representative images for both low density and high density are shown, as labeled. Four fields at 100x magnification were analyzed for each condition, using ImageJ. Data are mean +/- s.d. of triplicate experiments. Statistical analysis was done with a one way ANOVA, and a Tukey post-hoc test; asterisks indicate significance when compared to Matrigel as follows: * for $p<0.05$, ** for $p<0.01$, and *** for $p<0.001$. Error bars are SD. Images were obtained at 100x and 200x magnification and the scale is 200 μm.

Elastic hydrogels maintain the myogenic potential of satellite cells

Our data showed that hydrogels maintain satellite cell viability but did not support proliferation or differentiation (Figures 8-10). Previous studies indicated that regardless of culture conditions, satellite cells lose myogenic potential *in vitro*(Charville et al., 2015). To examine if satellite cells cultured on hydrogels could differentiate, satellite cells were cultured on 2-100 hydrogels for 6 or 10 days in growth medium. The satellite cells were then retrieved from the hydrogels using collagenase, re-seeded onto Matrigel coated plates and incubated in differentiation medium. These retrieved satellite cells formed MHC+ multinucleated myotubes after 3 days of culture in differentiation medium (Figure 12). Quantitative analysis showed that the number of myotubes/field was not statistically different when compared to cells differentiated on Matrigel without previous culture on a hydrogel, although the mean number of nuclei/myotube was slightly reduced for the 6 day incubation (Figure 12). These data indicated that elasticity of the collagen hydrogel did not result in a loss of the myogenic potential of satellite cells.

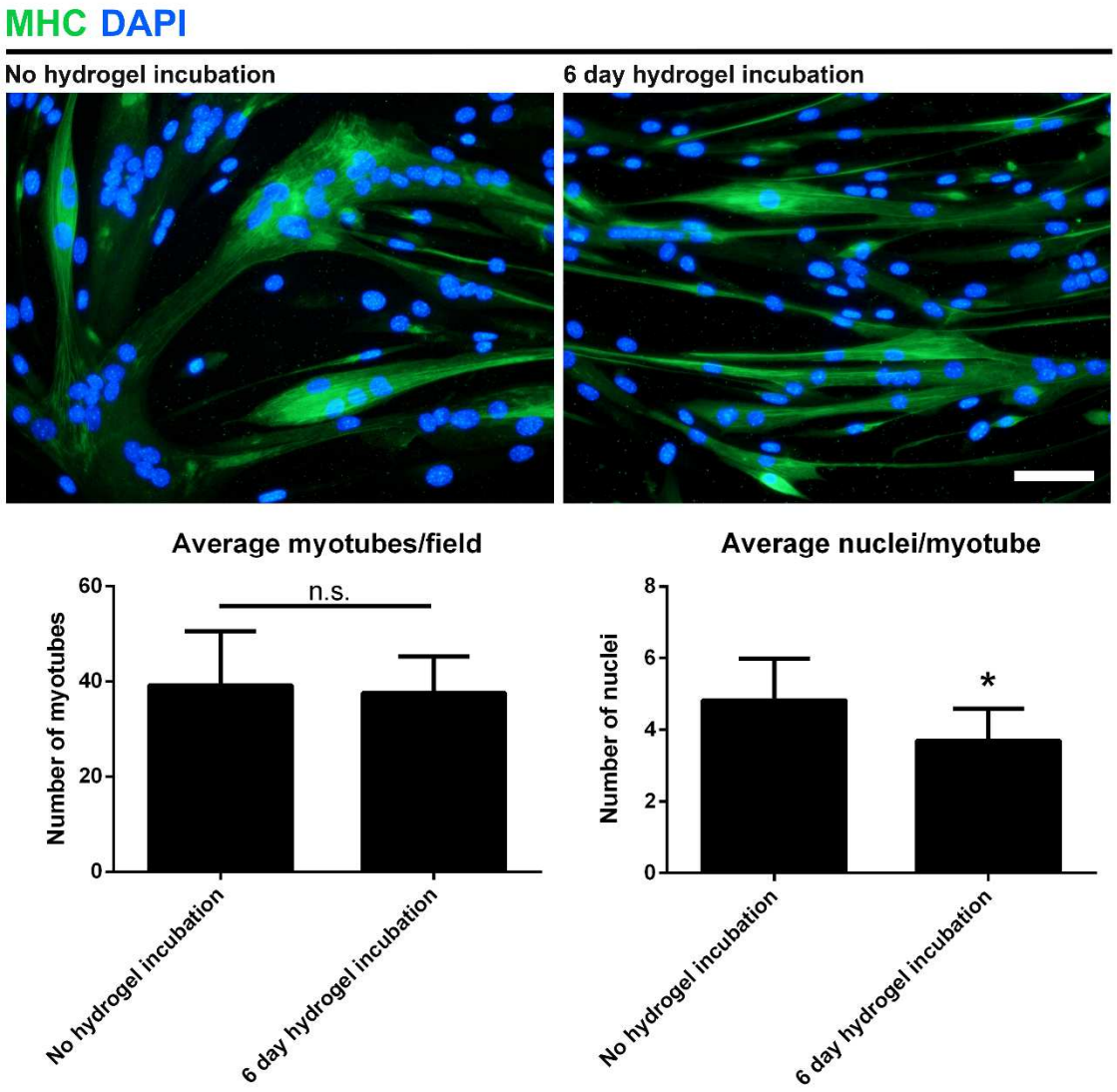

Figure 12. Satellite cells maintain their myogenic potential after prolonged incubation on hydrogels

Satellite cells were incubated on 2-100 hydrogels for 6 or 10 days prior to retrieval and reseeding on Matrigel coated plates. Satellite cells were then cultured for 3 days in differentiation medium, fixed, and stained with an anti-MHC antibody (green) and DAPI (blue). Cells incubated on hydrogels maintained their ability to differentiate into multinucleated MHC+ myotubes when switched to Matrigel coated plates. Analyses showed no significant difference in the mean number of myotubes/field from cells seeded directly onto Matrigel. The mean number of nuclei/myotube had a small but significant reduction for cells incubated for 6 days. Random fields at 100x magnification were analyzed for each condition, using ImageJ. Statistical analysis was done using a one way ANOVA, and a Tukey post-hoc test; asterisks indicate significance as follows: * for $p<0.05$, ** for $p<0.01$, and *** for $p<0.001$. Error bars represent the s.d. Images were obtained at 200x magnification and the scale is 100 μm.

There is a well understood pattern of gene expression for muscle differentiation during development and regeneration. The lineage status of myogenic progenitors can be identified based on the expression of specific genes: Pax7, a paired box domain transcription factor (Seale et al., 2000; Zammit et al., 2006), and three myogenic basic helix-loop-helix (bHLH) transcriptional regulators, MyoD *(Myod1), Myf5,* and myogenin (*Myog*). Quiescent satellite cells express *Pax7* and may express *Myf5*, thus they are *Pax7* positive (+), *Myf5+/negative (-).* Activated and proliferating satellite cells are *Pax7*+, *Myf5*+/-, *Myod1*+/-, but *Myog*-. These myogenic progenitors can either exit the cell cycle, commit to differentiation, and up-regulate *Myog* expression (*Pax7*-, *Myf5*-, *Myod1+/-, Myog+)* or self-renew, return to the niche, and re-express *Pax7* and *Myf5,* similar to the G_{alert} stage (Rodgers et al., 2014; Yin et al., 2013).

To examine how the ECM composition affected lineage status, C2C12 and satellite cells were cultured on coated plates in growth medium. After 3 days, total RNA was isolated and gene specific RT-QPCR was done. All samples were normalized to *Gapdh* and expressed as relative expression as compared to cells grown on Matrigel coating, using the ddC_t method (Figure 13). C2C12 cells were *Pax7*+, *Myf5*+, *Myod1+,* and *Myog*+. When compared to cells grown on Matrigel, there was a trend of decreased *Myf5* and *Myog* expression, significantly so on the 3-100FN coating. Additionally, C2C12 cells grown on 3-100 and 3-100FN coatings significantly up-regulated *Pax7* (Figure 13). This profile is consistent with proliferating myoblasts. Satellite cells expressed were similarly *Pax7*+, *Myod1*+, *Myf5*+ and *Myog*+. Satellite cells grown on the 3-100FN coating demonstrated significant up-regulation of *Pax7, Myf5,* and *Myod1*. In contrast, cells grown on the 3-100 coating down-regulated *Pax7*, indicating a potential role for fibronectin in inducing or maintaining *Pax7* expression (Figure 13). *Myog* expression

was significantly up-regulated on all coatings except 2-100 and 3-100FN (Figure 13). This profile is consistent with activated satellite cells that are poised to differentiate.

We repeated these experiments on the ECM hydrogels to examine the combined effect of an elastic substrate and ECM protein composition on myogenic gene expression. C2C12 cells maintained or up-regulated *Pax7* transcription on all hydrogels, significantly so on 3-100FN. *Myf5* expression was maintained but trended lower on all hydrogels, as compared to cells grown on Matrigel. *Myod1* and *Myog* expression in C2C12 cells increased significantly on all hydrogels, except those with the lowest storage moduli, 1-100 and 2-100 (Figure 13). Overall, these data indicate that C2C12 cells, which are myoblasts and thus *Myog*+, are poised differentiate, but have not withdrawn from the cell cycle. There were significant changes in expression on hydrogels with higher storage moduli, and fibronectin may act to maintain *Pax7* expression (Figure 13).

Satellite cells seeded on hydrogels in growth medium for 3 days significantly decreased *Pax7* expression, except for cells cultured on the 3-100FN hydrogel, which demonstrated the opposite trend. *Myf5* and *Myod1* expression was not significantly different than cells grown on Matrigel, while *Myog* expression was significantly up-regulated on all hydrogels tested (Figure 13). Since satellite cells demonstrated limited proliferation by day 6 and differentiated when re-plated onto Matrigel after 6 days of culture on hydrogels, we assessed expression at this timepoint as well. Interestingly, *Myf5* expression was significantly up-regulated and *Myod1* and *Myog* expression were significantly down-regulated. *Pax7* transcription was maintained but significantly decreased on all but the 3-100 hydrogel (Figure 13). These data are consistent with satellite cells returning to quiescence or a G_{alert} -like state (Rodgers et al., 2017; Yin et al., 2013).

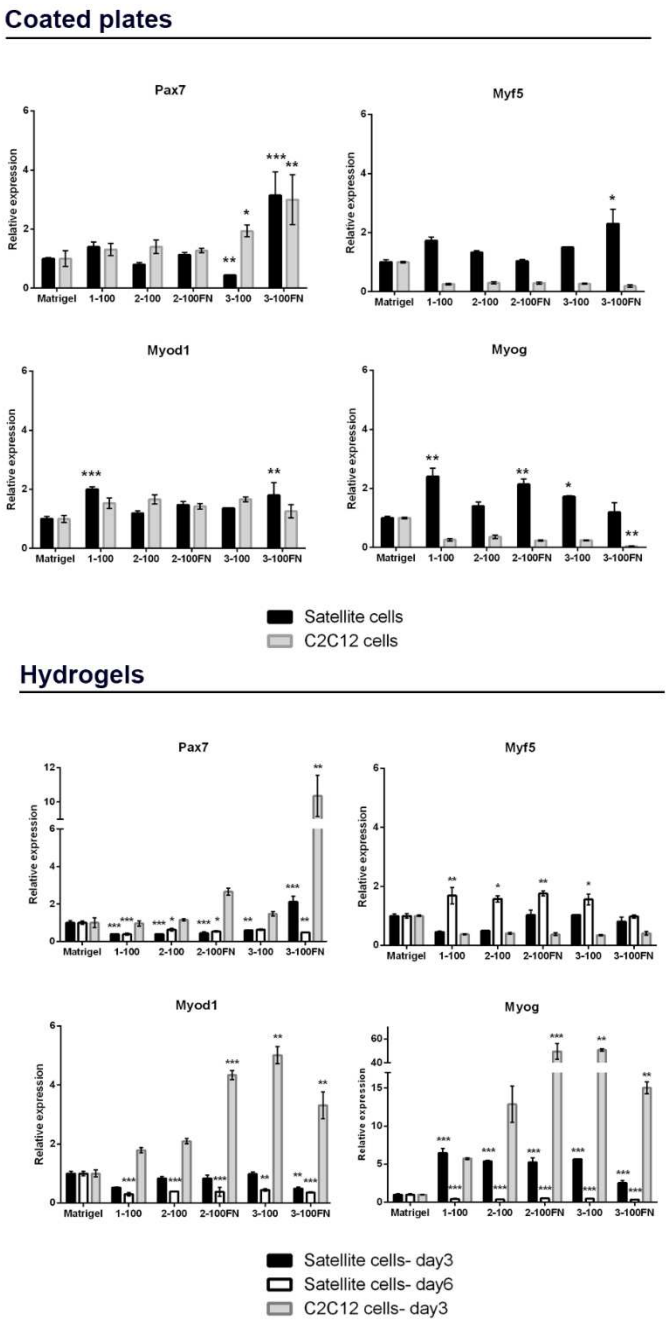

Figure 13. Myogenic gene expression analysis shows notable differences

Cells were grown on hydrogels or coated plates, and gene expression was determined by RT-QPCR 3 days after seeding for C2C12 cells, and 3 and 6 days after seeding for satellite cells. Data are expressed as relative gene expression as compared to cells grown on Matrigel and are the result of 2 biological replicates, each experiment done in triplicate. Statistical analysis was done by one-way ANOVA, with a Bonferroni post-hoc test; asterisks indicate significance when compared to Matrigel as follows: * for $p<0.05$, ** for $p<0.01$, and *** for $p<0.001$. Error bars represent the SD.

Myostatin expression limits satellite cell proliferation

We also examined the expression of p21 (*Cdkn1a*) an inhibitor of both the cell cycle and MyoD (Parker et al., 1995), and myostatin (*Mstn*), which inhibits proliferation of satellite cells and myoblasts (George et al., 2013; McCroskery et al., 2003). When cultured on coated plates, p21 transcription was decreased in C2C12 cells, significantly in those on the 2-100 and 3-100 coatings (Figure 14A). *Mstn* was not detectable in C2C12 cells regardless of culture substrate (Figure 14A, B), which is consistent with previous data (Artaza et al., 2002). Overall, this indicated C2C12 cells were actively proliferating myoblasts, and the exact composition of the substrate did not significantly affect these cells. Conversely, satellite cells expressed *Mstn* and significantly up-regulated p21 when grown on all coatings except for 2-100 (Figure 14A). Again, the differences in coating composition did not have a significant effect on gene expression. Satellite cells also significantly up-regulated transcription of p21 and increased *Mstn* expression in growth medium on all hydrogels after 3 days of culture (Figure 14B). However, by 6 days of culture, p21 transcription was down-regulated as compared to satellite cells grown on Matrigel. Interestingly, *Mstn* was also decreased, but detectable, at 6 days, indicating a shift towards a G_{alert} like state (Conboy and Rando, 2002; McCroskery et al., 2003).

Interestingly, C2C12 cells, which proliferated better than satellite cells on all conditions tested (Figure 8), did not express *Mstn* (Figure 14A, B). Satellite cells deficient for the fate determinant *Numb* overexpressed *Mstn* and had a proliferation defect. This phenotype was rescued by *Mstn* specific siRNA (George et al., 2013). We next determined whether siRNA knockdown of *Mstn* would induce proliferation of satellite cells on ECM hydrogels and coated plates. Initially, 3 commercially available siRNAs that target exons 1, 2, or 3 of *Mstn* were used to knock down *Mstn* expression in

satellite cells either separately, or together. Total RNA was isolated 48 hours post transfection and RT-QPCR was used to determine the level of *Mstn* knockdown. Knockdown efficiency ranged from 71-93% when compared to cells transfected with a negative control siRNA (Figure 14C). Satellite cells were seeded onto the 1-100 or 3-100 coated plates or the 3-100 hydrogels in growth medium and transfected with validated *Mstn* specific siRNA #1 or control siRNA 24 hrs post-plating. Proliferation was measured by MTT assays at 1, 3, and 6 days after seeding. *Mstn* knockdown increased proliferation, although not equivalent to Matrigel levels (Figure 14D-F; compare to Figure 8). Satellite cells on the 3-100 hydrogel demonstrated increased proliferation initially, but this decreased by day 6 (Figure 14D). These data demonstrated that myostatin knockdown increased the proliferation of satellite cells but did not rescue it completely.

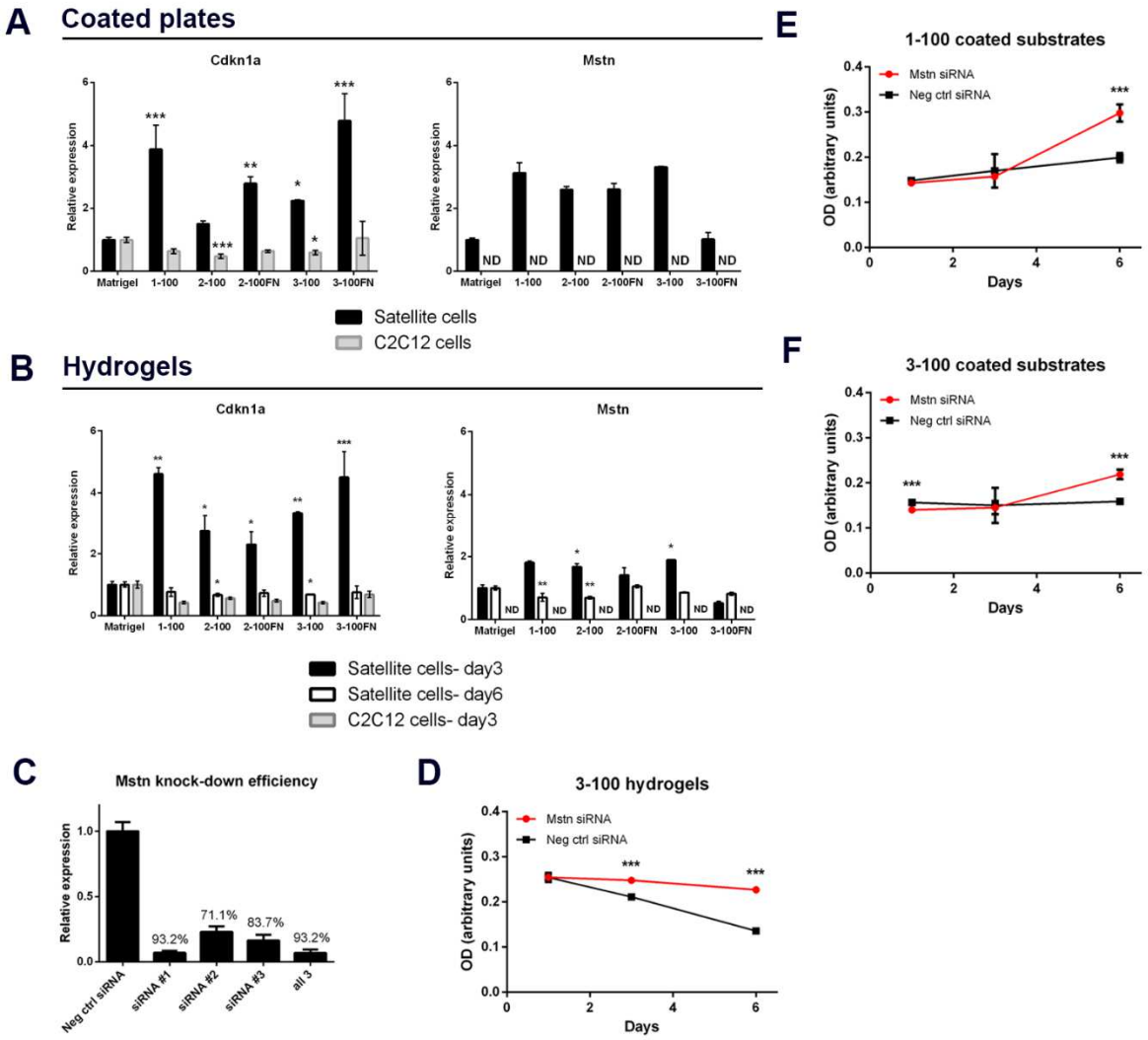

Figure 14. Analysis of p21 (*Cdkn1a*) and *Mstn* expression reveals major differences between C2C12 and satellite cells

RT-QPCR was done to determine gene expression in C2C12 cells and satellite cells on either coated plates, or hydrogels **(A, B)**. To assess whether *Mstn* knock-down affects satellite cell proliferation, the efficiency of three siRNA constructs targeting *Mstn* was tested in satellite cells using RT-QPCR **(C)**; siRNA construct #1 was used for all subsequent experiments. Satellite cells were seeded in triplicates on hydrogels **(D)** and coated plates **(E, F)**, and transfected with either a universal negative control construct, or the *Mstn* targeting construct. MTT assays were carried out at days 1, 3 and 6. Proliferation is significantly improved by day 6 when *Mstn* is knocked down in all conditions tested. RT-QPCR data and statistical analysis were carried out as previously stated (see figure 13); ND = not detected. For the MTT assay, statistical analysis was done using a two sample t test **(D-F)**; asterisks indicate significance as follows: * for $p<0.05$, ** for $p<0.01$, and *** for $p<0.001$ **(A-F)**. Duplicate experiments were carried out in triplicates. Error bars represent the s.d. on all graphs **(A-F)**.

Discussion

The collagen/laminin/fibronectin hydrogels are pliant substrates with storage moduli that range from 0.96 to 19 Pa, as measured by rheology (Figure 7). We found that these very elastic substrates did not induce proliferation of satellite cells, and C2C12 proliferation was less robust when compared to Matrigel coated plates (Figure 8). The exception was C2C12 cells grown on the 1-100 hydrogel, which proliferated significantly better. However, we observed that after several days in culture, C2C12 cells remodeled this hydrogel, degrading it and migrating on the tissue culture plate below (data not shown). This behavior, which was not observed in C2C12 cells cultured on the stiffer hydrogels, is likely the cause for the higher proliferation rate. Further, on plates coated with ECM proteins, C2C12 cells proliferated significantly better than satellite cells on all substrates. Satellite cells had a lag of 3 days before there was demonstrable proliferation on coated plates, and the specific composition of the substrates did not alter this (Figure 8). C2C12 cells grown on the 3-100FN coated plates also demonstrated a lag in proliferation, although these cells caught up by 6 days (Figure 8). Laminin and fibronectin have been shown to induce proliferation of satellite cells (Bentzinger et al., 2013; Öcalan et al., 1988) but our observations indicate a need for a stiffer substrate than these ECM based hydrogels provide to induce proliferation. However, satellite cells cultured on fibronectin containing hydrogels and coatings up-regulated *Pax7* expression, which may indicate that they are activated and poised to proliferate.

Differentiation of myogenic progenitor cells into multinucleated MHC positive myotubes is used as a metric of myogenic potential. Our experiments demonstrated that the hydrogels did not support satellite cell differentiation, whereas C2C12 cells formed myotubes on these substrates (Figure 10). It has been reported that satellite cells lose

myogenic potential in culture within 3 days (Montarras et al., 2005). However, satellite cells cultured on hydrogels did not lose their myogenic character; in fact, after 10 days of hydrogel culture, these cells formed MHC positive multinucleated myotubes when re-plated onto Matrigel coated plates (Figure 12). When satellite cells were cultured on plates with ECM coatings, differentiation was cell density dependent, indicating that the lack of proliferation was a limiting factor (Figure 11). Interestingly, satellite cells differentiated on ECM coated plates indicated an inhibitory role for collagen I at its highest concentration, and this was more pronounced when fibronectin was also present. This is consistent with previous reports that collagen I and fibronectin inhibited differentiation (Grefte et al., 2016, 2012). The hydrogels we used were comprised only of niche specific ECM proteins, and when polymerized, had low storage moduli. Our data indicates that a stiffer substrate is necessary for differentiation and assessing how new culture substrates affect myogenic potential requires consideration of cell density before withdrawal of growth factors.

When examining myogenic regulatory gene expression in C2C12 cells grown on coated plates, we found that *Pax7* and *Myod1* transcription was increased, while that of *Myf5* and *Myog* was decreased, as compared to cells grown on Matrigel (Figure 13). This pattern is consistent with a population of proliferating transit amplifying cells (Biressi and Rando 2010; Yin, Price, and Rudnicki 2013). On hydrogels, C2C12 cells up-regulated *Myog* and *Myod1* transcription, indicative of preparation to differentiate (Figure 13). C2C12 cells proliferated on all substrates, and did not express *Mstn* in any growth condition, consistent with observations that this gene was only expressed in C2C12 myotubes (Artaza et al., 2002; Diel et al., 2008). Satellite cells displayed a dynamic pattern of expression when cultured on hydrogels, initially significantly up-regulating *Mstn* and p21 by day 3, but eventually down-regulating *Mstn* and p21, while increasing

expression of *Myf5* by day 6 (Figures 13, 14). Knockdown of *Mstn* by siRNA in satellite cells grown on hydrogels and coated plates improved proliferation in all conditions tested, indicating the differences in the regulation of expression of this gene between C2C12 cells and satellite cells has functional implications on cell behavior. Much research has been done towards understanding the dynamics of satellite cells in response to muscle damage, and often C2C12 cells are used as a proxy for primary cells (Khodabukus and Baar, 2009; Perniconi et al., 2014; Pumberger et al., 2016). The disparate responses of the two cell types in our experiments indicates a limitation to using this immortalized cell line. While these cells recapitulate some of the primary cell behavior, their responses were fundamentally different in proliferation assays and regulation of *Mstn* expression. Other groups have likewise found behavioral discrepancies between C2C12 cells and primary myoblasts (Boontheekul et al., 2007; Sengupta et al., 2012). Thus, when trying to extrapolate data to predict primary cell responses, the use of C2C12 cells may bias the data.

Our data indicated that during the initial 3 days of culture on viscoelastic hydrogels, satellite cells up-regulated cell cycle inhibitors and myogenin, and decreased *Pax7* expression, a pattern consistent with myoblast differentiation. This is within the timeframe other studies have indicated as the point at which satellite cells lose myogenic potential add10 However, this might represent an early response, as we observed an increase in *Myf5* expression, and a decrease in transcription of *Myog, Myod1*, and *Mstn* by day 6. The hydrogels we tested are very soft substrates, and consistent with other findings, gene expression analysis indicated that the satellite cells were in a state similar to G_{alert} (Rodgers et al., 2017) which could signal that they are returning to quiescence. A number of studies have found that more elastic substrates maintained the myogenic character and increased re-engraftment of satellite cells in short term culture, but these

were much stiffer than the hydrogels used (Gilbert et al., 2010; Quarta et al., 2016). For effective therapeutic use of satellite cells in regeneration after volumetric muscle loss, or as a source of edited stem cells for neuromuscular diseases, it will be necessary to induce proliferation while maintaining the ability of these cells to both re-engraft the niche and actively regenerate myofibers. The potential return to quiescence on the hydrogels after initially up-regulating myogenin and myostatin indicates that there is a possibility to develop a multistep *in vitro* culture protocol. This protocol would have phases that supported expansion, followed by a phase involving transfer to a substrate that would induce a return of satellite cells to an activated state.

Materials and Methods

Mouse husbandry and satellite cell isolation

Swiss-Webster mice were purchased from Charles River, and maintained as previously described; satellite cells were isolated and cultured as previously described (see previous chapter Materials and Methods). C2C12 cells were maintained in growth medium containing DMEM, 10%FBS, 10U/mL penicillin and 10mg/mL streptomycin (Cellgro, Manassas, VA).

Hydrogel and coated plates assembly

Collagen scaffolds were fabricated according to standardized protocols (ibidi USA, Fitchburg, WI). Briefly, sterile PBS, 7.5% w/v sodium bicarbonate, 10x Ham's F10 pH 5.0 (Sigma-Aldrich), laminin 111 from EHS murine sarcoma basement membrane (Sigma-Aldrich), and bovine plasma fibronectin (Sigma-Aldrich) were mixed to the desired concentrations. Following a 10 min incubation on ice, collagen I (Corning) was

added, and contents were immediately mixed and plated into disc shapes in 24 well plates. The plates were incubated 30 minutes at 37°C to allow for collagen polymerization. ECM coated plates were made by adding laminin, collagen and fibronectin in coating buffer (0.15 M sodium carbonate, 0.35 M sodium bicarbonate in sterile dH_20) to desired concentrations. The mixture was added to 24 well plates and incubated for 2 hours at room temperature, on a shaker. Excess substrate was aspirated, and the plates were rinsed thoroughly with PBS prior to cell seeding.

Rheology

Parallel plate rheological measurements were completed using a Physica MCR101 rheometer (Anton Paar, Graz, Austria) to determine the storage and loss moduli of collagen-based gels of predetermined formulation. Briefly, 500 μL gels were pipetted onto the fixed plate immediately following mixing and the moving plate was lowered to a height of 0.5 mm. The gels were tested at 0.5% strain with an oscillatory frequency of 1 Hz. The stage was heated to 37°C and maintained within a humid environmental chamber to enable polymerization. Storage and loss moduli measurements were collected every 0.2 min for 30 min. Average moduli values were calculated from the last 10 min of each rheometer run with n = 2-3 per group.

Proliferation assays

C2C12 cells were seeded at $1x10^4$ cells/well (hydrogels) or $8x10^3$ cells/well (coated plates). Satellite cells were seeded at $2.5x10^4$ cells/well (hydrogels) and $2x10^4$ cells/well (coated plates). On days 1, 3, and 6, post-plating, cells were incubated with 12 mM MTT (Molecular Probes, Eugene, OR) in phenol red free Ham's F10/F12 with 10% FBS (Cellgro) for 4 hours, at 37°C. Sodium dodecyl sulfate- hydrochloric acid (SDS-HCl) was

added, cells were incubated an additional 4 hours at 37°C, and absorbance was read at 570 nm. MTT assays were carried out in triplicate.

Viability/Cytotoxicity

Satellite cells were seeded at $2x10^4$ cells/well and viability/toxicity assays (Biotium, Hayward, CA) were conducted at 24 and 72 hrs post-seeding. Medium was removed, the cells were washed in PBS, and incubated with 2 μM Calcein and 4 μM EthD-III for 30 min, at room temperature. The cells were imaged using a Leica DMI6000B.

Differentiation assays

C2C12 cells and satellite cells were switched to differentiation medium (DMEM, 2% HS, 100 μg/mL Primocin) 24 hours post-plating. Medium was changed every 24 hours. Cells were cultured for 72 hrs for satellite cells, or 96 hrs for C2C12 cells before fixation and imaging. Quantitative analysis was done using the manual cell counter feature in ImageJ. For cells initially cultured on hydrogels, satellite cells were seeded at $3x10^4$ cells/well in growth medium. After 6 or 10 days, 3.09 mg/mL collagenase type II (Worthington, Lakewood, NJ) was used to dissolve the hydrogels and retrieve the satellite cells, which were subsequently seeded on Matrigel coated plates ($3x10^4$ cells/well) for differentiation assays. These assays were completed in duplicate with triplicate replicates.

Immunofluorescence

Cells were fixed in 4% formaldehyde and permeabilized with 0.5% Triton X-100 PBS. Samples were blocked with 10% goat serum (Invitrogen) for 1 hr and incubated overnight at 4°C with anti-myosin antibody, MY-32 (Sigma-Aldrich). Cells were washed in PBS, incubated with FITC conjugated anti-mouse IgG antibody (Sigma-Aldrich) for 1 hr at 37°C, then incubated with DAPI (Biotium), according to manufacturer's instructions. Cells were mounted in glycerol PBS containing phenylenediamine, and images were obtained on a Nikon Eclipse TE2000-U epifluorescence microscope.

RNA isolation and Quantitative RT-PCR (RT-QPCR)

Cells were seeded in 24 well plates at a density of $1.5x10^4$ cells/well (C2C12 cells) or $4x10^4$ cells/well (satellite cells) onto polymerized hydrogels and incubated at 37°C in growth medium. After 72 hours in culture, cells were lysed in TRIzol (Thermo Fisher Scientific, Waltham, MA) for RNA isolation. All data are the result of triplicate replicates from two biological samples. RNA isolation, cDNA generation, and RT-QPCR was carried out as described previously (see previous chapter Materials and Methods). Sequence for primers are in Table 3.

Myostatin siRNA knock-down experiments

Three validated *Stealth* siRNA constructs against mouse Myostatin (*Mstn*) (Invitrogen) were tested, using Lipofectamine RNAiMAX and OptiMEM I (Thermo Fisher Scientific), according to the manufacturer's protocol. Satellite cells were transfected 24 hrs post-seeding with either *Stealth* Universal Negative Control construct (Invitrogen), or *Stealth* anti-*Mstn* constructs, and 48 hrs later, RNA was harvested for

RT-QPCR. The construct with the greatest knock-down efficiency (siRNA #1, MSS237302) was used for all subsequent experiments. For MTT assays, satellite cells were seeded on 3-100 hydrogels ($2.5x10^4$ cells/well) and 1-100, and 3-100 coated substrates ($2x10^4$ cells/well) in antibiotic free medium and transfected with either anti-*Mstn* or negative control siRNA 24 hrs post plating. MTT assays were done in triplicate for each condition, as described previously, at days 1, 3, and 6.

Primer name	Primer sequence (5’ to 3’)
GapDH Fwd	GGGAAGCCCATCACCATCTT
GapDH Rev	GCCTTCTCCATGGTGGTGAA
Pax7 Fwd	TCTTACTGCCCACCCACCTA
Pax 7 Rev	CACGTTTTTGGCCAGGTAAT
MyoD Fwd	TGATGGCATGATGGATTACAGCGG
MyoD Rev	AGATGCGCTCCACTATGCTGGACA
Myf5 Fwd	CCCGAAAGAACAGCAGCTTTGACA
Myf5 Rev	CCACAATGCTGGACAAGCAATCCA
Myogenin Fwd	ATGGTGCCCAGTGAATGCAACTC
Myogenin Rev	TGGACGTAAGGGAGTGCAGATTGT
Myostatin Fwd	TGACAGCAGTGATGGCTCTTTGGA
Myostatin Rev	GCTTGCCATCCGCTTGCATTAGAA
p21 Fwd	TCCACAGCGATATCCAGACA
p21 Rev	AGACAACGGCACACTTTGCT
Integrin alpha 7 Fwd	TCTGTCAGAGCAACCTCCAGCT
Integrin alpha 7 Rev	CTATGAACGGCTGCCCACTCAA

Table 3. Comprehensive list of primers used for RT-QPCR.

CHAPTER 4

NUMB PLAYS A ROLE IN MUSCLE REPAIR AND SATELLITE CELL FUNCTION

Introduction

The adaptor protein Numb was first described in *Drosophila*, where it acts as a Notch signaling inhibitor and cell fate determinant during neurogenesis. In sensory organ precursor cell division, Numb asymmetrically segregates, allowing the two daughter cells to adopt different fates and generate the various cell types necessary for sensory organs (Rhyu et al., 1994). Mechanistically, Numb inhibits Notch signaling by 1) recruiting the E3 ligase Itch to the NICD, thus targeting it for degradation, and by 2) hindering recycling of the Notch receptor back to the plasma membrane (Dho et al., 1999; McGill and McGlade, 2003).

Numb can asymmetrically segregate during satellite cell division as well, where it may direct cell fate decision making (Conboy and Rando, 2002). Since Notch signaling supports activation, proliferation, and inhibition of differentiation in satellite cells, it is plausible that an asymmetric cell division event may result in a Numb-positive daughter cell that downregulates Notch and differentiates, and a Numb-negative daughter cell that maintains both Notch activity and its myogenic progenitor status. However, studies investigating Numb function in satellite cells point to a more complex mechanism.

Conditional deletion of *Numb* from satellite cells using murine models resulted in poor skeletal muscle repair following injury. Surprisingly, loss of *Numb* did not significantly affect expression of Notch target genes, nor did it result in uncontrolled expansion of satellite cells, as might be expected (George et al., 2013; Le Roux et al., 2015). Instead, *Numb* deficient satellite cells had a marked proliferation defect, and

upregulated expression of myostatin and p21. Knock-down of myostatin rescued the proliferation defect *in vitro* (George et al., 2013).

The function of NUMB in mammalian satellite cells may be complicated due to the existence of Numblike (*Numbl*), a less well-studied Numb homolog, which has both distinct and redundant roles as *Numb*, depending on context (Liu et al. 2011; Shenje et al. 2014; Wilson et al. 2007; Zhong et al. 1997). Indeed, the conditional Numb knock out mouse models were created in mice with a *Numbl* null mutation in order to generate a phenotype (George et al., 2013; Le Roux et al., 2015). Moreover, there are four Numb isoforms, generated by alternative splicing of exons 3 and 9 of the *Numb* transcript. The resulting proteins, with molecular masses of 65, 66, 71 and 72 kDa, may have different functions, especially since exons 3 and 9 are located within a phosphotyrosine binding (PTB) domain and proline rich region (PRR), respectively (Dho et al., 1999). In cell culture overexpression studies, the Numb isoforms with the PTB insert (PTBi, p66 and p72) associated with the plasma membrane, while those without the insert (PTBo, p65 and p71) were cytoplasmic. Additionally, a switch from the Numb isoforms lacking the PRR (PRRo, p65 and p66) to those containing the PRR (PRRi. p71 and p72) takes place during neuronal differentiation of embryonal carcinoma P19 cells (Dho et al., 1999). Similar findings that hint at different roles for the different isoforms have been reported by other groups, with the emerging paradigm that Numb p65 and p66 (the "short" isoforms) support differentiation and maturation, whereas Numb p71 and p72 (the "long" isoforms) are associated with proliferation and stemness (Abballe et al. 2018; Bani-Yaghoub et al. 2007; Dooley et al. 2002; Toriya et al. 2006; Verdi et al. 1999; Yoshida et al. 2003).

Expression of Notch target genes was not significantly affected in *Numb* null satellite cells, indicating that, at least in part, its role in satellite cells is independent of Notch inhibition. This is not necessarily surprising, as NUMB facilitates the ubiquitination and subsequent proteasomal degradation of several proteins and functions as a cargo selective endocytic adaptor for recycling endosomes. NUMB has protein binding domains beyond the PTB and PRR, such as the Eps15 homology (EH) binding motif, and tripeptide motifs DPF and NPF, which all impart NUMB its extensive scaffolding role and allow it to complex proteins together (Gulino et al., 2010; Pece et al., 2011). For example, Numb mediates the ubiquitination of Gli1, a transcription factor downstream of Hedgehog signaling (Marcotullio et al. 2011; Marcotullio et al. 2006). Another E3 ligase, mouse double minute 2 (Mdm2) binds Numb at the PTB domain (Colaluca et al., 2013). This interaction sequesters Mdm2 and prevents it from degrading p53, which has crucial implications for various cancers, and makes Numb a *bona fide* tumor suppressor (Pece et al., 2011). However, the opposite relationship has been found in satellite cells, where Numb deficiency resulted in p53 upregulation instead (Le Roux et al., 2015), highlighting the complex and context-dependent set of protein-protein interactions Numb might have in the cell.

There are two main avenues for endocytosed membrane-associated proteins: lysosomal degradation, via transport to late endosomes, or recycling back to the plasma membrane (Grant and Donaldson, 2009). Numb colocalizes with EH-domain (EHD) proteins to recycling endosomes and clathrin coated structures, where it acts as a negative modulator of endocytic recycling for various proteins (Smith et al. 2004; Santolini et al. 2000). Notably, Numb prevents the recycling of adhesion junction cadherins and integrins back to the plasma membrane, thus modulating cell adhesion

and migration, which has implications for epithelial to mesenchymal transition (EMT), a hallmark of cancer metastasis (Nishimura and Kaibuchi 2007; Wang et al. 2009).

Given the repertoire of proteins Numb binds, and its pleiotropic involvement in signaling pathways crucial for stem cells and cancer biology, it's likely that it plays several yet undiscovered functions in satellite cells independent of Notch inhibition, and possibly in an isoform-specific manner. The aim of this study is to explore which isoforms are present in satellite cells, and to investigate the mechanisms by which *Numb* deficient satellite cells fail to activate, proliferate, and contribute to muscle repair.

Results

Numb isoform expression varies across different cells and tissue types

To investigate *Numb* mRNA isoform expression, we generated primer pairs that span exons 2-6 and give products at 307 or 340 base pairs (bp), depending on whether exon 3 is included (PTBi) or omitted (PTBo). The second set spans exons 7-10 and gives products of 404 bp when exon 9 is included (PRRi) or 260 bp when exon 9 is omitted (PRRo) (Figure 15 diagram). The "long" isoforms of Nb are PRRi (p71, p72), while the "short" isoforms are PRRo (p65, p66). For a quantitative approach, primers that allow for the calculation of a splicing index of the long isoforms were employed instead, as previously described (Figure 15 diagram) (Rajendran et al., 2016). Lastly, to investigate protein isoform expression, a pan-NUMB antibody that recognizes all isoforms was used. Notably, the PRRi and PRRo isoforms of NUMB migrate as a doublet on a 12% SDS-polyacrylamide gel (SDS-PAGE) due to the considerable difference in mass, but the PTBi versus the PTBo isoforms cannot be resolved via conventional Western blot. RT-PCR analysis showed the predominant mRNA isoform present in satellite cells is PRRo, with no apparent change in expression levels as differentiation proceeds from proliferating

myoblasts (day 0) to differentiated myotubes (day 3). The PRRi transcript is present as a faint band that disappears over time (Figure 15 A). RT-QPCR data follows the same trend and shows a significant decrease in the splicing index for PRRi Numb (*i.e.* as differentiation proceeds, less of the total *Numb* transcript is made up of *Numb* PRRi, Figure 15 E). Both PTBi and PTBo are present at the mRNA level (Figure 15 B). Additionally, myotubes and reserve cells collected after differentiation (day 3) did not express significantly different levels of Numb, when compared to proliferating cells (Figure 15 C-E). Taken together, these data show that Numb p65 and p66 are likely the most abundant transcripts in proliferating satellite cells, with p71 and/or p72 making only a minor contribution.

Immunofluorescence and confocal imaging were used to investigate NUMB expression and subcellular localization in satellite cells. NUMB is present in the cytoplasm and is often enriched at one pole of the cell, both in single myoblasts (Figure 16, top panel) and in multinucleated myofibers (Figure 16, bottom panel). However, since the antibody recognizes all isoforms, it is impossible to distinguish endogenous isoforms with this method. A Western blot revealed that only the PRRo isoform(s) is/are present in satellite cells, regardless of differentiation status, which contrasts the RT-PCR data (Figure 16, compare to Figure 15 A). However, it is unknown whether this is due to post transcriptional regulation that prevents the PRRi mRNA from being translated, or a lack of detection due to the sensitivity of the Western blotting technique, especially considering the low abundance of the PRRi transcript. Notably, all NUMB isoforms appear to have higher molecular weights than expected on the Western blot, as p65 and p66 migrated with the 70 kDa protein marker, and p71, p72 migrated with the 100 kDa marker. This is likely due to phosphorylation of NUMB, and/or other post-translational modifications.

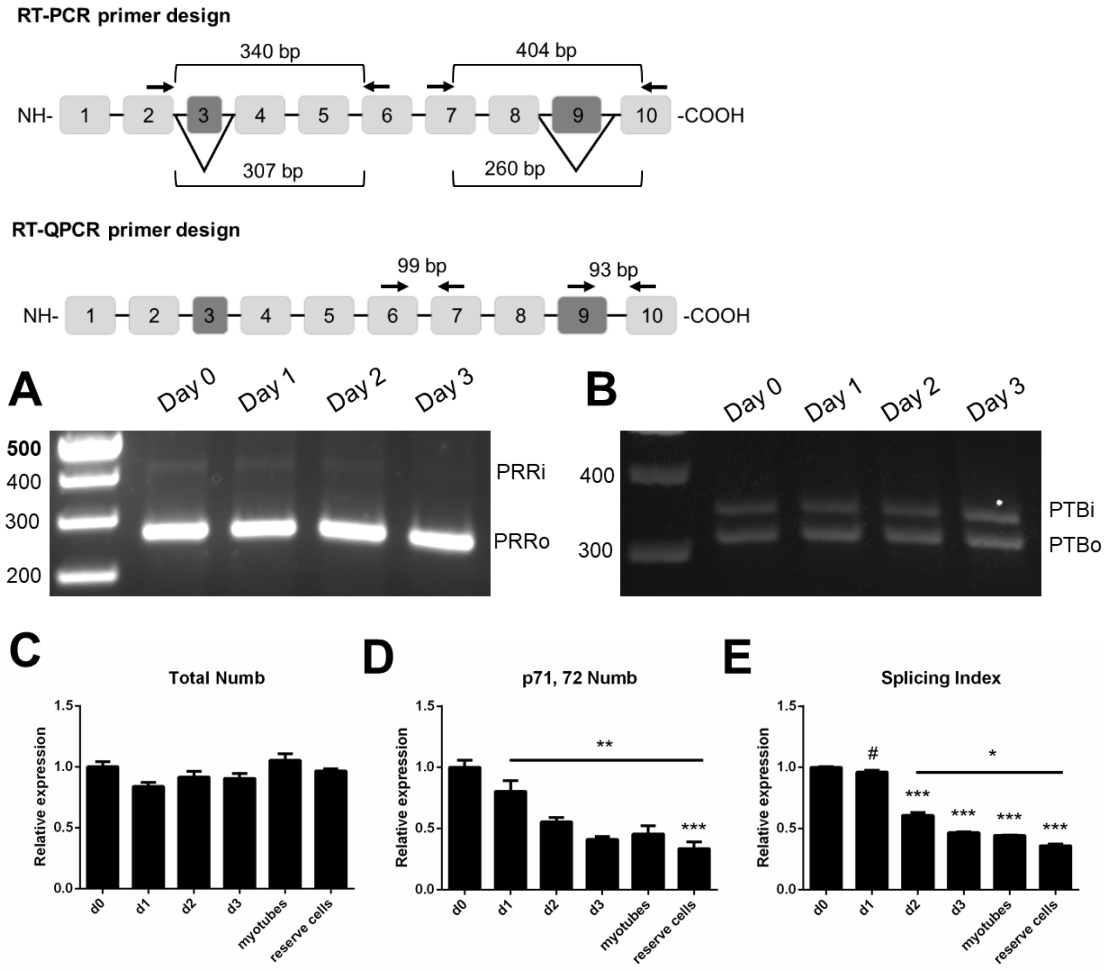

Figure 15. Satellite cells predominantly express Numb mRNA p65 and p66

Satellite cells were cultured in differentiation medium, and RNA was harvested every 24 hours. RT-PCR was done with primers flanking the PRR region and the PTB region, as diagramed. *Numb* PRRo is the predominant transcript, with only a faint band for Nb PRRi, which disappears as satellite cells undergo differentiation **(A)**. Both PTBi and PTBo are present in all samples **(B)**. RT-QPCR was done with intron spanning primers as diagramed above, to detect either total *Numb* **(C)** or *Numb* PRRi only **(D)**, and a splicing index was calculated **(E)**. The quantitative data corroborates A and B, as Nb PRRi decreases as differentiation proceeds. Samples enriched for myotubes or reserve cells by differential trypsinization after 3 days in differentiation medium do not have significantly different levels of *Numb* isoforms **(C-E)**. RT-QPCR data are expressed as relative gene expression as compared to cells grown on Matrigel and are the result of 2 biological replicates, each done in triplicate. Statistical analysis was done by one-way ANOVA, with a Tukey post-hoc test; asterisks indicate significance when compared to Matrigel as follows: * for $p<0.05$, ** for $p<0.01$, and *** for $p<0.001$; # is significantly different from all groups. Error bars represent the SD.

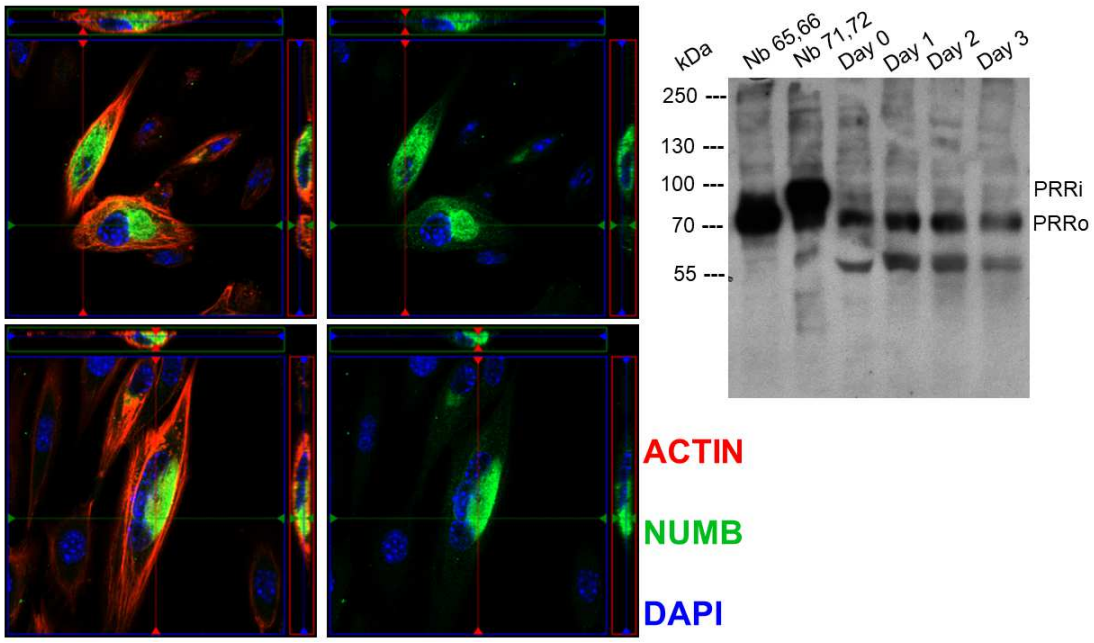

Figure 16. Satellite cells express the short isoforms of NUMB only

For immunofluorescence, satellite cells were cultured on coverslips, fixed and stained for F-actin (conjugated phalloidin, red), NUMB (anti-NUMB antibody, green), and DNA (DAPI, blue). Numb is present in the cytoplasm, predominantly localized to one side of the cell. The images were obtained at 63x and are displayed as orthogonal projections. A Western blot of total protein lysates from satellite cells during differentiation was used to resolve which protein isoforms are present (lanes 3-6). Only the Nb PRRo isoforms were detected at the protein level. As positive controls, lysates from HEK 293T cells transfected with either Nb 65 and 66, or Nb 71 and 72 were included as well (lanes 1, 2).

Given the importance of *Numb* in development, we sought to understand the pattern of Numb isoform expression in muscle cells in that context. During mouse embryonic development, Pax3+ myogenic progenitors populate the forelimb bud, and MRFs are expressed in those cells as early as embryonic day 11.5 (e11.5) (Cheng et al., 1993; Lee et al., 2013). We isolated whole forelimb RNA and protein to examine Numb expression in embryonic muscle. Numb is important for heart compaction and cardiomyocyte cell cycle withdrawal (Hirai et al., 2017; Yang et al., 2012), as well as neurogenesis (Bani-Yaghoub et al. 2007; Dooley et al. 2002; Q. Shen et al. 2002; Zhong et al. 1997). Thus, we also investigated Numb isoform expression in the neural tube and embryonic heart. Notably, we attempted to harvest RNA and protein from e10.5- e12.5 embryos, but only reliably obtained enough protein for Western blot analysis from e11.5 and e12.5 (Figure 17). All embryonic tissues investigated expressed both PTB isoforms, with a strong band for PTBi (Figure 17 B). PRRi was likewise strongly expressed, unlike in satellite cells where PRRi was barely detected (Figure 17 A, compare to Figure 15 A). RT-QPCR analysis showed a significant decreasing trend in splicing index for PRRi as embryonic development proceeds, which was mirrored at the protein level (Figure 17 C-F). These data show that p71/72 are abundant during development in all tissues assayed, and there is no discrepancy between isoform expression at the RNA level and protein level, as found in satellite cells.

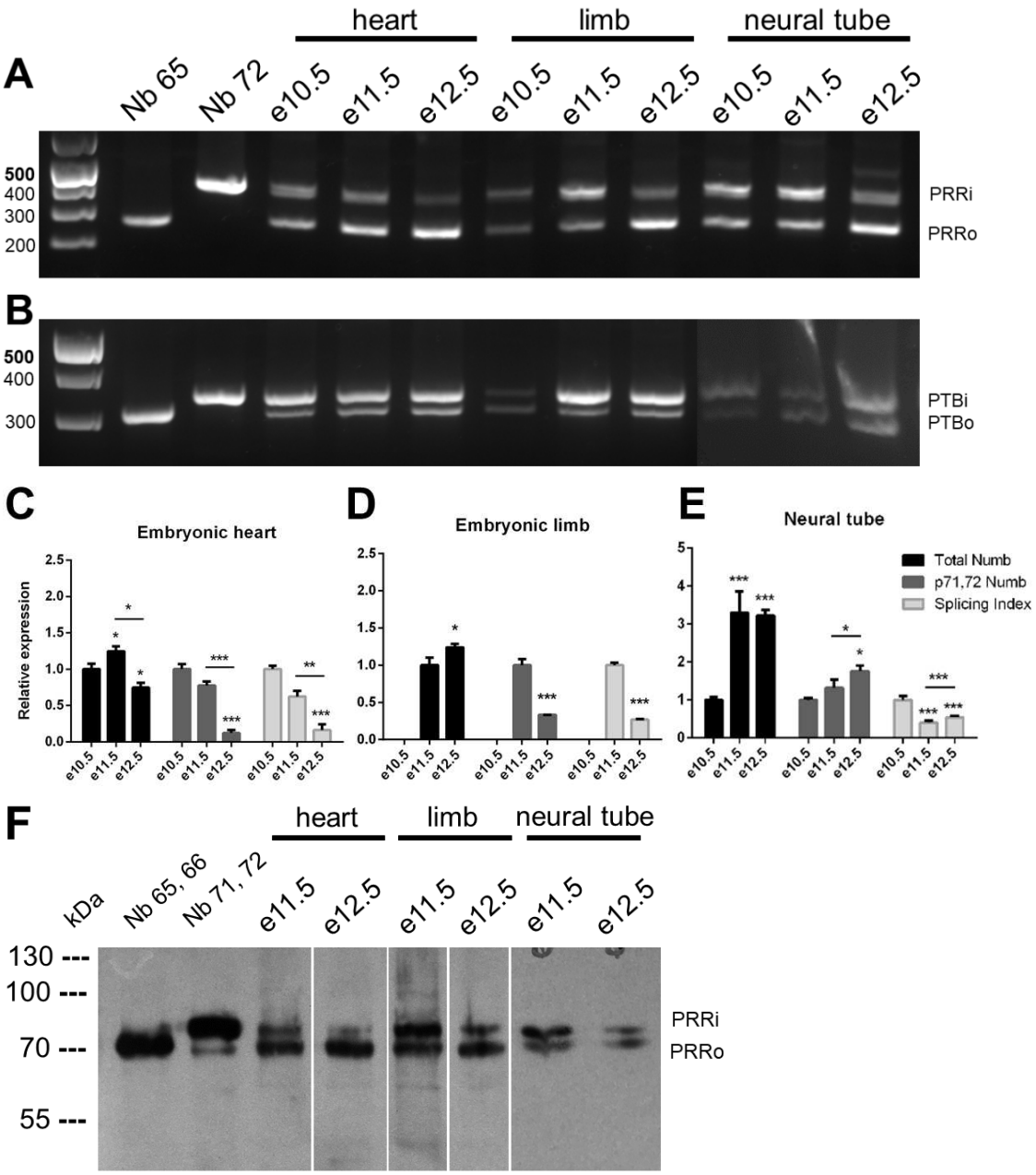

Figure 17. Numb p71/72 expression declines over embryonic time at the RNA and protein level.

Embryos were harvested at days e10.5-1 e2.5 for total RNA and total protein. Numb transcript isoforms containing the PRRo and PRRi, as well as PTBo and PTBi are present in embryonic heart, limb, and neural tube **(A, B)**. RT-QPCR data shows a trend of PRRi decline over time **(C-E)**, and the protein expression analysis corroborates those findings **(F)**. For RT-QPCR, data are expressed as relative gene expression as compared to the earliest time point a single biological replicate experiment done in triplicate and statistical analysis was done as described previously (Figure 15).

Numb interacts with a vast network of proteins during satellite cell activation and proliferation

Since a deficiency of *Numb* in myogenic progenitors cells did not result in significant changes in Notch signaling (George et al., 2013; Jory et al., 2009; Le Roux et al., 2015), we sought to investigate other potential interactors of Numb in satellite cells, to better understand its role during activation and proliferation. To this end, we performed an immunoprecipitation (IP) proteomics experiment.

First, satellite cells were isolated from hindlimb skeletal muscles, and cultured *in vitro* until sufficient numbers of cells were generated. Treatment with the proteasome inhibitor MG132 was used to preserve interactions with binding partners that might otherwise be rapidly degraded, and total protein was harvested with a mild NP-40 based lysis buffer. NUMB and its binding partners were immunoprecipitated overnight with agarose beads and anti-NUMB antibody and eluted by boiling in SDS buffer (Figure 18 A). Coomassie staining showed strong staining bands in the total lysate and the supernatant from the IP, demonstrating that our protein lysis and IP techniques do not result in protein degradation. The NUMB IP has several bands along the length of the lane, indicating that numerous proteins co-immunoprecipitated. The distinct bands at 50 kDa and 25 kDa in the NUMB IP lane mark the heavy and light chains of the anti-NUMB antibody (Figure 18 B). A Western blot done with the anti-NUMB antibody shows the presence of NUMB PRRo isoforms at the protein level in total lysate, and to a lesser extent, in the supernatant. NUMB is only detected in the NUMB IP lane, and not in the isotype control antibody lane (Figure 18 C).

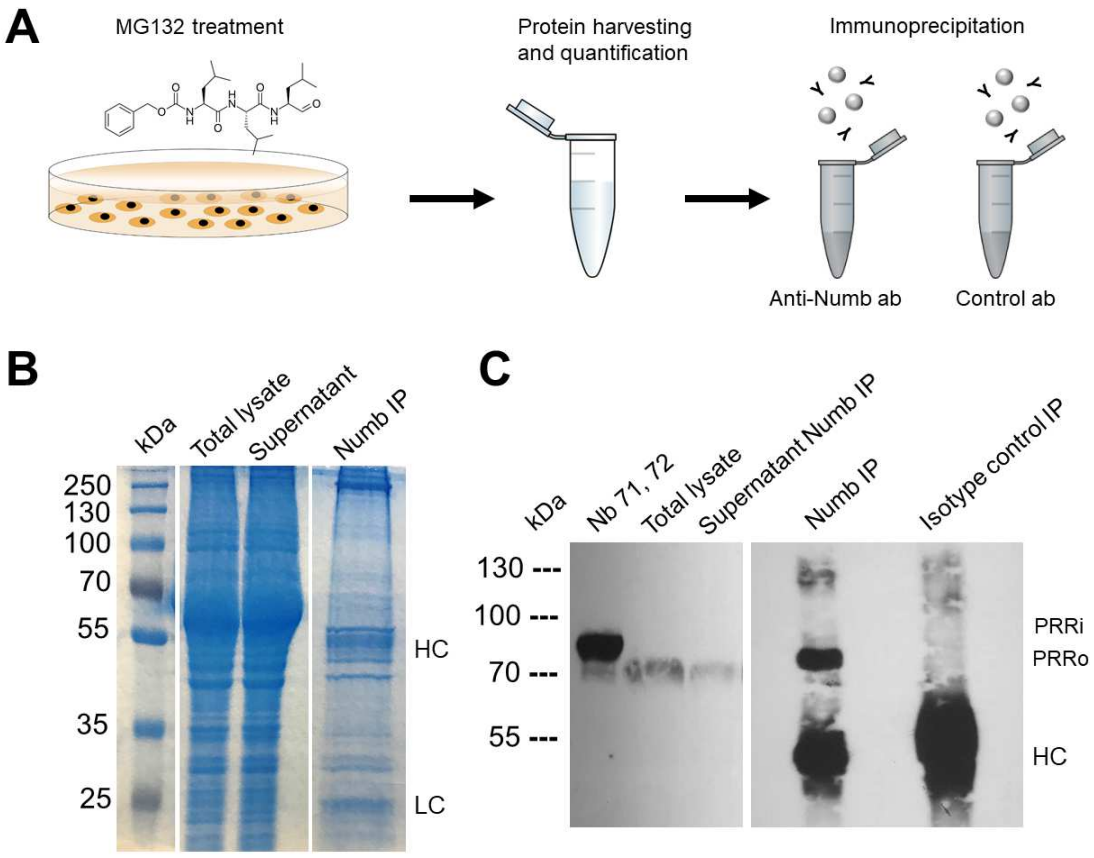

Figure 18. Immunoprecipitation of NUMB from MG132 treated satellite cell lysates

Satellite cells were treated with MG132 to inhibit the proteasome, followed by lysis and IP with either anti-NUMB antibody or isotype control antibody and Protein A/G agarose beads **(A)**. Coomassie stained gel of the IP shows protein bands spanning 250 kDa- 25 kDa, indicating multiple proteins co-precipitated with Numb. The bands at 50 kDa and 25 kDa represent the heavy chain (HC) and light chain (LC) of the antibody used for the IP **(B)**. Western blot with anti-NUMB antibody shows that only the PRRo isoform of the protein is detected in the IP **(C)**. Lysate from HEK 293T cells transfected with p71 and p72 was loaded as a positive control **(C, lane 1)**.

To identify Numb binding partners and better understand its role in satellite cell activation and proliferation, a top-down proteomics approach was taken. The IP samples were subjected to in-gel digestion and LC-MS/MS, and a total of 821 and 462 proteins were identified for the Numb IP and isotype control antibody IP, respectively (Figure 19 B); 227 of those proteins were shared among the two data sets. As expected, NUMB was identified in the anti-NUMB IP exclusively (Figure 19 D). Surprisingly, mapping of the identified peptides revealed overlap with PRRi (exon 9), suggesting the presence of Numb 71 and/or 72 in proliferating satellite cells, which is not supported by the Western blot analysis (Figure 19 C, compare to Figure 16 G). Numb was identified with a sequence coverage under 50%, despite its enrichment in the sample (Table 4), which is expected, given its trypsin cleavage pattern (Krieger et al., 2013). Various subtypes of keratin are common contaminants resulting from sample preparation during the gel staining, slicing and handling, and were prevalent in both data sets (Table 4).

Among the top unique hits in the Numb IP are actin-binding, FERM domain containing proteins Moesin (Msn), Radixin (Rdx) and Ezrin (Ezr), the intermediate filament binding Plectin (Plec), and other cytoskeleton-associated proteins. Calmodulin binding protein Caldesmon1 (Cald1) was likewise uniquely identified in the Numb IP. The control IP top unique hits included structural proteins like Vimentin (Vim) and Myosin heavy chains (Myh1) (Table 4).

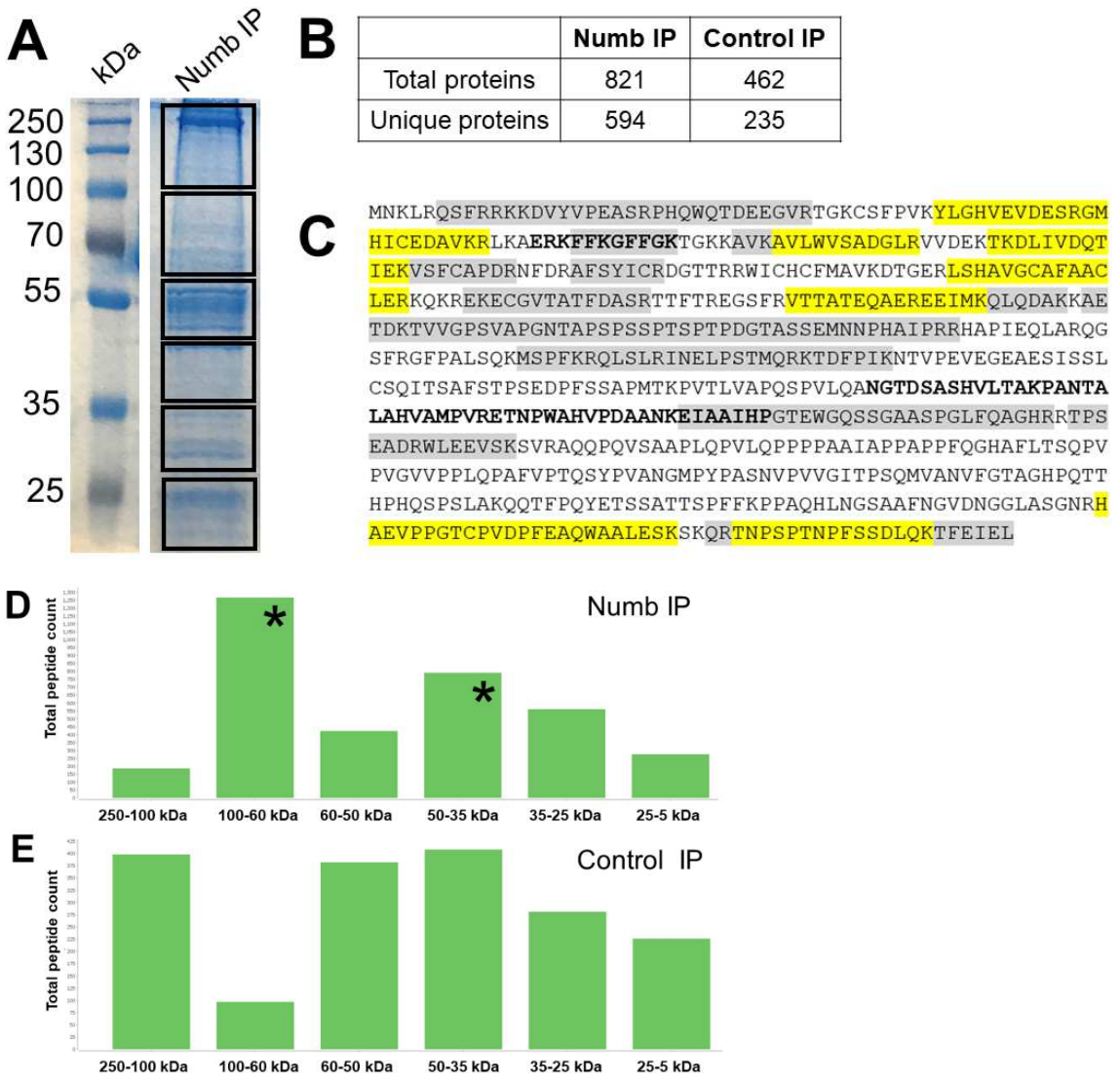

Figure 19. Mass spectrometry experiment overview

IP samples separated via SDS-PAGE and stained with Coomassie were subjected to in-gel digestion and LC-MS/MS. For better resolution, each lane was divided into 6 pieces which were individually processed for mass spectrometry, as depicted (A). A total of 594 unique proteins were identified in the Numb IP sample, with 227 proteins found in both the Numb IP and isotype control IP (B). A breakdown of peptides identified show an enrichment in the 100-60 and 50-35 kDa fractions in the Numb IP. Peptides corresponding to Numb were identified in the Numb IP exclusively (D, E; the fractions containing Numb are marked with a * symbol; graphs were generated with PeptideShaker 1.16.43). Mapping the identified Numb peptides on the amino acid sequence for Numb 72 shows sequence coverage in both PTBi and PRRi, indicating the presence of Numb 71 or 72 in satellite cells (C; PTBi and PRRi are bolded; mapped peptide sequences are highlighted yellow for high confidence hits, and gray for low confidence hits).

Numb IP								
Entry	Protein name	Gene name	Score	Coverage	# Proteins	# Unique Peptides	# Peptides	PSM
P26041	Moesin	Msn	126.64	74.52	1	18	71	111
Q3TQ13	Uncharacterized protein	Hspa8	120.53	72.14	6	20	54	99
A0A068F126	Glyco-gag polyprotein		97.70	44.80	4	1	32	64
Q6NXH9	Keratin, type II cytoskeletal 73	Krt73	89.22	39.52	7	1	25	67
Q3TZU7	Sorting nexin	Snx9	87.88	68.24	2	16	50	77
Q9R0X4	Acyl-coenzyme A thioesterase 9	Acot9	80.65	70.16	1	13	37	68
B9EKE9	Ddx3x protein	Ddx3x	80.22	65.51	6	3	51	85
Q3U8B3	Replication protein A subunit	Rpa1	78.43	56.52	3	17	45	68
Q80UT7	Rpl7a protein (Fragment)	Rpl7a	71.08	58.15	4	11	25	47
Q62095	ATP-dependent RNA helicase	Ddx3y	68.78	67.63	5	1	48	78
B2RTP7	Krt2 protein	Krt2	68.01	46.96	6	5	31	64
Q3UL48	FERM domain-containing protein	Ezr Vil2	65.91	64.85	3	6	50	63
A0A1S6GWJ8	Uncharacterized protein	Hnrnpm	64.97	77.26	6	13	91	220
Q3TH46	FERM domain-containing protein	Rdx	64.12	63.47	3	6	49	65
P02535	Keratin, type I cytoskeletal 10	Krt10	62.63	33.33	16	5	21	51
O88569	Heterogeneous nuclear ribonucleoproteins	Hnrnpa2b1	58.78	61.76	2	7	22	50
Q8C7C3	Uncharacterized protein	Tpm3	57.10	76.21	1	5	26	52
Q3T9U9	Uncharacterized protein	Rpl3	56.35	56.58	6	8	34	58
Q04586	Env polyprotein	Mela H52	55.70	30.49	11	8	15	27
P05064	Fructose-bisphosphate aldolase A	Aldoa	55.68	84.34	4	13	29	45
Q8BN32	Polyadenylate-binding protein	Pabpc1	54.93	63.84	8	9	44	61
B9EKB0	Laminin B1 subunit 1	Lamb1	53.98	34.08	4	9	46	71
P58771	Tropomyosin alpha-1 chain	Tpm1	53.63	78.52	3	2	35	64
Q9QXS1	Plectin	Plec	53.31	39.65	15	10	175	231
Q61656	Probable ATP-dependent RNA helicase	Ddx5	53.28	48.21	5	10	39	89
A0A0R4J259	Heterogeneous nuclear ribonucleoprotein Q	Syncrip	52.47	65.24	9	11	34	49
Q5FWB6	60S acidic ribosomal protein P0	Rplp0	51.49	64.67	1	11	21	46
Q9JHS4	ATP-dependent Clp protease	Clpx	50.34	60.09	1	12	37	51
Q9D1R6	Uncharacterized protein	Tpm2	50.21	85.21	2	1	33	47

A2AIM4	Tropomyosin beta chain	Tpm2	49.23	76.76	1	1	29	43
P60843	Eukaryotic initiation factor 4A-I	Eif4a1	46.45	67.98	5	8	29	42
Q925I1	ATPase family AAA domain-containing protein 3	Atad3	44.20	69.54	1	11	42	76
P53026	60S ribosomal protein L10a	Rpl10a	41.77	51.61	3	7	17	49
Q9QZS3	Protein numb homolog	Numb	40.86	47.78	3	8	28	39
A2A7S7	Tyrosine--tRNA ligase	Yars	39.67	74.11	1	11	39	54
Q8QZY1	Eukaryotic translation initiation factor 3 subunit L	Eif3l	39.35	49.65	1	8	28	37
Q8R2P1	Kelch-like protein 25	Klhl25	39.11	86.59	2	9	50	85
Q3TF40	Uncharacterized protein (Fragment)	Nono	38.51	57.77	3	6	41	109
Q8BP47	Asparagine--tRNA ligase, cytoplasmic	NARS1	37.68	57.60	1	9	35	49
Q99LF8	Polyadenylate-binding protein (PABP)	Pabpc4	34.47	53.64	8	5	34	44
Q3TG12	B5 domain-containing protein (Fragment)	Farsb	34.04	69.22	3	10	36	55
Q6A0F1	MKIAA0002 protein (Fragment)	Cct8	33.94	55.86	4	12	29	49
Q9QWL7	Keratin, type I cytoskeletal 17	Krt17	32.97	60.74	18	4	28	49
P05213	Tubulin alpha-1B chain	Tuba1b	32.49	46.12	4	7	15	20
Q80UG5	Septin-9	Septin9	31.92	58.32	2	8	34	46
E9QA15	Caldesmon 1	Cald1	31.42	51.95	4	8	46	73
A1E2B8	Inducible heat shock protein 70		31.41	49.14	4	5	22	38

Control IP

Entry	Protein name	Gene name	Score	Coverage	# Proteins	# Unique Peptides	# Peptides	PSMs
Q3TWV0	IF rod domain-containing protein	Vim	275.86	83.05	4	3	60	176
A2A513	Keratin, type I cytoskeletal 10	Krt10	66.37	26.56	14	4	16	50
P14869	60S acidic ribosomal protein P0	Rplp0	66.16	73.19	1	11	20	42
Q3UB67	Uncharacterized protein	Rpl3	48.65	52.85	4	8	27	42
B2RWX0	Myosin, heavy polypeptide 1	Myh1	32.96	44.70	5	6	86	129

Table 4. List of unique identified proteins

The top uniquely identified proteins from each experiment with a protein score above 30 are listed. Proteins identified in both experiments are excluded. The UniProt entry identifier, gene and protein name, protein score, % coverage, numbers of proteins, unique peptides, and total peptides, as well as peptide to spectrum matches (PSMs) are provided. Reviewed proteins are highlighted in gray, and unreviewed proteins are not highlighted (according to UniProt, “reviewed” refers to manually annotated proteins, while “unreviewed” proteins are automatically generated and annotated from -omics data). In the Numb IP, 47 proteins have a score above 30, as opposed to only 5 identified proteins in the control IP.

Gene ontology (GO) analysis of the unique data set revealed significantly enriched categories that are in line with Numb's previously described roles, such as *Membrane Trafficking (R-MMU-199991)* and *Clathrin-mediated endocytosis (R-MMU-8856828)* (Table 5). These categories included members of the Ywhae (14-3-3) family, which act as a scaffolding hub for hundreds of proteins (Fan et al. 2019), and the AP-2 complex found in clathrin coated pits (Song and Lu, 2012). Other notable endocytosis related proteins present exclusively in the Numb IP include sorting nexins (Snx9, 18), EHD proteins and Epidermal growth factor receptor substrate proteins (EPS15, 8), and DP-ribosylation factor GTPase-activating proteins (Arfgap 2, 3). Numb's involvement in proteasomal degradation is highlighted by categories like *GLI3 is processed to GLI3R by the proteasome (R-MMU-5610785)* and *Regulation of PTEN stability and activity (R-MMU-8948751),* which identify many proteasome complex proteins (Psma4, Psmb3, Psmc1,2,4 and 5, Psmd3,11 and 13) or ubiquitin ligases and associated proteins (Rnf34, Rnf181, Spop, Prkaca, Trim25). *Protein serine/threonine kinase activity (GO:0004674)* and *Cyclin-dependent protein serine/threonine kinase activity (GO:0004693)* included an extensive list of kinases as putative Numb-interacting proteins (Table 5).

Interestingly, *Focal adhesion (GO:0005925)* and *Actin polymerization or depolymerization (GO:0008154)* were significantly enriched in the Numb IP data set, and contained proteins involved in cell adhesion, migration, and polarity establishment. Notable transcription factors Myog, Runt related transcription factor 1 (Runx1), and Sox15 were included in the *DNA-binding transcription factor activity (GO:0003700)* category.

GO category- Molecular Function	P-value	Identified proteins
ribonucleoprotein complex binding (GO:0043021)	3.11E-06	C1qbp, Eif2a, Srp68, Srpra, Eif2a, Eef2, Srp72, Abce1, Hnrnpu
signaling receptor binding (GO:0005102)	2.88E-04	Grb10, Gdf15, Gnas, Lamb1, Ifna6
cyclin-dependent protein serine/threonine kinase activity (GO:0004693)	6.65E-03	Ccn1, Ccnd3, Cdk1, Cdk9, Cdk18, Cdk4
DNA-binding transcription factor activity (GO:0003700)	8.79E-03	Sox15, Pura, Ubp1, Zfp558, Myog, Runx1
protein serine/threonine kinase activity (GO:0004674)	1.34E-02	Ccn1, Ccnd3, Csnk1a1, Camk2d, Dapk3, Cdk1, Mark2, Vrk1, Csnk2a, Eif2ak2, Camk2g, Cdk9, Csnk1d, Dapk2, Cdk18, Cdk4, Gsk3b
repressing transcription factor binding (GO:0070491)	1.70E-02	Rbpj, Mta1, Mta2
GO category- Pathways		
Membrane Trafficking (R-MMU-199991)	1.60E-05	Ywhae, Tubb6, Cyth1, Fnbp1l, Eps15, Ap2a1, Klc2, Tmed9, Kifc1, Klc1, Snx18, Cope, Rae1, Clint1, Dnm2, Kif27, Ap2m1, Necap2, Nsf, Cttn, Arpc2, Arcn1, Ubc, Ank1, Capzb, Tuba1b, Arfgap3, Preb, Csnk1d, Dennd1b, Epn1, F5, Mvb12a, Snx9, Pacsin2, Racgap1, Hspa8, Picalm, Actr3, Dync1i2, Arfgap2
GLI3 is processed to GLI3R by the proteasome (R-MMU-5610785)	2.35E-05	Tubb6, Psmc1, Prkar2b, Psmd11, Prkaca, Csnk1a1, Psmc2, P4hb, Psma4, Psmd13, Ubc, Tuba1b, Psmc4, Psmb3, Numb, Psmd3, Ift140, Prkar2a, Psmc5, Spop, Gsk3b
Clathrin-mediated endocytosis (R-MMU-8856828)	3.97E-03	Fnbp1l, Eps15, Ap2a1, Snx18, Dnm2, Ap2m1, Necap2, Cttn, Arpc2, Ubc, Epn1, Snx9, Pacsin2, Hspa8, Picalm, Actr3
Interferon Signaling (R-MMU-913531)	1.95E-03	Eif4a3, Trim25, Camk2d, Eif4a1, Ptpn2, Eif2ak2, Camk2g, Eif4g1, Abce1, Ifna6, Eif4e
Regulation of PTEN stability and activity (R-MMU-8948751)	7.02E-03	Psmc1, Psmd11, Mta2, Psmc2, Gatad2b, Csnk2a1, Psma4, Psmd13, Ubc, Gatad2a, Psmc4, Psmb3, Mta1, Psmd3, Hdac2, Psmc5
Regulation of TP53 Activity (R-MMU-5633007)	4.60E-02	Ywhae, Polr2e, Npm1, Ppp2r1a, Mta2, Rfc4, Rae1, Rnf34, Cdk1, Gatad2b, Ywhag, Gtf2f2, Csnk2a1, Rpa2, Ubc, Gatad2a, Cdk9, Rfc3, Gtf2f1, Hdac2, Prmt5, Rfc2, Rpa1
GO category- Molecular Component		
extracellular region (GO:0005576)	1.31E-07	Gdf15, Serpinb6b, Hba, Timp1, Lamb1, Serpinh1, Ifna6
focal adhesion (GO:0005925)	7.63E-04	Zyx, Ctnnd1, Parva, Cttn, Amotl2, Lims1, Plec, Parvb
plasma membrane part (GO:0044459)	3.15E-03	Grm5, Cacnb1, Camk2d, Dnm2, Pcdha11, Dnah8, Gnas, Fmr1, Ssna1, Cttn, Camk2d, Ephb4, Cd163, Camk2g, Bsg, Ank1, Map1b, Abi1, Ift140, Nedd1, Eps8, Hspa8, Picalm, Gsk3b
GO category- Biological Process		
intracellular signal transduction (GO:0035556)	1.59E-02	Rala, Ccdc125, Prkaca, Nos1, Gnas, Mark2, Amotl2, Kctd10, Depdc5, Eps8
negative regulation of Wnt signaling pathway (GO:0030178)	1.61E-02	Emd, Grb10, Csnk1a1, Gsk3b
actin polymerization or depolymerization (GO:0008154)	2.00E-02	Baiap2l1, Cttn, Arpc2, Vasp, Capzb, Actr3
response to endoplasmic reticulum stress (GO:0034976)	3.12E-02	Pdia4, P4hb, Ufd1, Canx, Pdia2

Table 5. GO lists of Numb unique identified proteins

Several GO categories, with P-values and lists of proteins from that category for the Numb IP unique data set are shown. These categories were not significantly identified in the Control IP unique data set.

Discussion

Previous work has uncovered that during neurogenesis, a switch in *Numb* isoforms from PRRi to PRRo takes place as differentiation proceeds (Bani-Yaghoub et al. 2007; Rajendran et al. 2016), and our analysis showed a similar trend in embryonic skeletal muscle (limb bud), embryonic heart, and satellite cells (Figures 15-17). However, NUMB PRRi was only detected by Western blot at the protein level in embryonic tissues, suggesting that in the context of muscle, long isoforms are necessary for development, but not for adult stem cells. The regulators of *Numb* isoform expression are not well understood, although splicing factors like Polypyrimidine tract binding protein (Ptbp1), Splicing factor 1 (Sf1) and Quaking (QKI) have been implicated in Numb alternative splicing (Rajendran et al., 2016; Zong et al., 2014). Interestingly, all three of those proteins were present in the Numb IP unique proteins data set.

The immunoprecipitation-proteomics experiment aimed to uncover potential binding partners for Numb in satellite cells during activation and proliferation. However, the data were obtained from a single biological replicate, and are thus very limited and preliminary. Additionally, since our anti-Numb antibody detects all isoforms, our data does not provide any specificity regarding which identified protein interacts with which isoform(s). Indeed, previously published work using tagged Numb isoforms for IP-proteomics experiments found that Numb 72 has a significantly higher affinity for certain endocytic proteins than Numb 66 (Krieger et al., 2013), raising the possibility that some of our identified proteins might have similar isoform preferences.

Limitations aside, this experiment identified a series of potential Numb binding partners that may shed light on its function in satellite cell proliferation and activation. Many of these proteins have been previously identified by other groups (Krieger et al.,

2013; Nishimura et al., 2003), thus validating our approach. However, several well established Numb interacting proteins that are expressed in satellite cells, (*e.g* Notch, Gli2/3, Itch) were not identified in our experiment, either because Numb does not bind those proteins in proliferating satellite cells, or very likely due to technical limitations.

Interestingly, the MRF myogenin was identified in the Numb IP. Since myogenin promotes myoblast cell cycle exit and differentiation, a possible model where Numb targets it for degradation could, in part, explain the Numb deficient satellite cell phenotype, and might warrant further exploration. Other transcription factors found in the dataset include Sox15 and Runx1. In satellite cells, Sox15 activates Forkhead box protein K1 (Foxk1), to promote proliferation and inhibit differentiation. $Sox15^{-/-}$ mice have myoblasts with perturbed cell cycle kinetics, and impaired skeletal muscle regeneration following injury (Béranger et al. 2000; Lee et al. 2004; Meeson et al. 2007). Runx1 may drive proliferation and inhibit premature differentiation in satellite cells as well (Bao et al., 2018; Umansky et al., 2015). To our knowledge, interactions between Numb and these transcription factors have not been previously described.

Numb has over two dozen serine/threonine phosphorylation sites, some of which have been validated *in vitro* and *in vivo* (Krieger et al., 2015; Tokumitsu et al., 2005). Calcium/calmodulin protein kinase types I, II and IV (Camk1, 2, 4) phosphorylate Numb, resulting in recruitment of the 14-3-3 proteins (Tokumitsu et al., 2005). Our IP experiment identified Camk2 subunits delta and gamma (Camk2d, Camk2g) and 14-3-3 proteins, along numerous cell cycle associated kinases, further highlighting a potential role for Numb in regulating myoblast cell cycle kinetics.

The E3 ubiquitin ligases Itch and Mdm2, whose ability to bind Numb has been extensively studied (Colaluca et al. 2013; Marcotullio et al. 2011; McGill and McGlade

2003), were conspicuously absent from the data set. However, several other ubiquitin ligases were identified instead (*e.g*. Rnf181, Trim56, Nosip, Ppil2, Rnf34, Mid1, Znf598, Ube2s), along with many components of the proteasome complex, suggesting that in satellite cells, Numb's involvement in ubiquitination and protein degradation may be carried out in concert with different ubiquitin ligases.

Enrichment for GO categories pertaining to focal adhesions and actin dynamics indicates Numb might play a role in directing myoblast fusion, migration, and adhesion. Although this has not been previously explored in satellite cells, it is in agreement with Numb's reported roles in other contexts (Nishimura and Kaibuchi 2007; Wang et al. 2009). Among the top hits were actin binding proteins Msn, Rdx and Ezr, which make up the ERM trio, and serve as crosslinkers between the plasma membrane and the cytoskeleton, where they direct cell-cell adhesion, and cell migration (Kawaguchi et al., 2017; Michie et al., 2019). On the same line, Plectin (Plec), a cytoskeleton linker necessary for sarcomeric and neuromuscular junction integrity, was uniquely identified (Mihailovskaa et al., 2014; Rezniczek et al., 2016), along numerous other cadherin, integrin, and actin binding proteins (*Actin polymerization or depolymerization (GO:0008154)*).

Given the multifaceted and pleiotropic roles of Numb, it is likely and possible that its function in satellite cells could involve several biochemical processes and signaling pathways. Thus, validation of the IP experiment, and further investigation into Numb's binding partners will help uncover those mechanisms and expand our understanding of the vast repertoire of proteins regulating satellite cell behavior during muscle regeneration.

Materials and Methods

Mouse husbandry, satellite cell isolation and cell culture

Swiss-Webster mice were purchased from Charles River, and maintained as previously described; satellite cells were isolated and cultured as previously described (see chapter 2 Materials and Methods). For myogenic differentiation, satellite cells were cultured in serum withdrawal conditions as previously described (see chapter 3 Materials and Methods).

Differential trypsinization was performed after 3 days in differentiation medium, to separate myotubes from reserve cells. Briefly, the plates were washed with PBS and trypsin was added. The cells were monitored under a microscope every 20-30 seconds, and once the majority of the myotubes detached from the plate, the supernatant was retrieved and considered to be the myotube enriched fraction. The remaining cells were incubated with trypsin until they detached from the plate. The supernatant was again retrieved and considered to be the reserve cell enriched fraction.

RT-PCR and RT-QPCR

RNA harvesting, cDNA library generation, and RT-QPCR was carried out as previously described (see chapter 2 Materials and Methods). Primer sequences are in Table 6.

Numb immunofluorescence and confocal imaging

Satellite cells were grown on coverslips and fixed in 4% formaldehyde. The cells were then were permeabilized with 0.5% Triton X-100 in PBS and non-specific binding was blocked with 10% goat serum for 1 hour. The primary anti-Numb antibody (C29G11, Cell Signaling Technology) was used at a 1:800 dilution with an overnight incubation at 4 °C. Excess antibody was washed 3 times for 5 minutes in PBS, and anti-rabbit IgG Alexa-Fluor 488 secondary antibody (Molecular Probes) was used at a 1:1000 dilution for 1 hour at 37 °C. Excess antibody was washed again, and phalloidin conjugated to a 568 fluorophore (Biotium) was used to label filamentous actin, according to the manufacturer's instructions. Nuclei were stained with DAPI (Sigma-Aldrich) and finally, coverslips were mounted in anti-fade media (10% PBS, 90% glycerol, phenylenediamine) and images were captured with a Zeiss LSM800 confocal microscope. Z-stacks were captured at 63x magnification, and image processing was carried out in Zen 2 (Blue edition).

Embryonic tissue isolation

Embryos were isolated from Swiss-Webster females at e10.5, 11.5 and 12.5. Using sterile scalpel and fine forceps, hearts, forelimbs, neural tubes, and tail tips were dissected in PBS. From each litter (9-12 embryos), half of the tissue was lysed in RIPA lysis buffer (50 mM Tris pH 8.0, 0.5% sodium deoxycholate, 0.1% SDS, 1% NP-40, 150 mM NaCl and protease inhibitor cOmplete mini (Roche)) for protein extraction, while the other half was lysed in TRIzol for RNA extraction, according to manufacturer's protocols.

Protein isolation and quantification

Cells were rinsed in ice-cold PBS and lysed in Darnell extraction buffer (50 mM Tris pH 8.0, 1 mM DTT, 0.5% NP-40, 10% glycerol and protease inhibitor), manually scraped into a tube, and centrifuged for 15 minutes at 14000 rpm, at 4°C, to pellet the debris. The supernatant was transferred to a fresh tube, and total protein content was assayed using the Bradford method. Briefly, the protein samples were diluted 1:20 in ultrapure water, and added to Bradford reagent solution (BIORAD Protein Assay). Protein standards of known concentration were generated using bovine serum albumin (BSA) in Darnell lysis buffer, as serial dilutions spanning 4 mg/mL to 0.125 mg/mL. Each sample was prepared in triplicates, in a 96 well plate, and absorbance at 595 nm was recorded. Total protein concentration was determined using a linear fit generated with the absorbance values of the protein standards.

SDS-PAGE and immunoblotting

Protein lysates of known concentration were denatured by boiling in laemmli buffer (Tris HCL pH 6.8, SDS, glycerol, bromo-phenol blue, 2-mercaptoethanol) for 5 minutes, at 97°C, and loaded onto a 12% polyacrylamide gel, along with Page Ruler PLUS Prestained ladder (Thermo Scientific). The gel was run in a glycine based running buffer (25 mM Tris, 190 mM glycine, 0.1% SDS), in a minigel set up (Mini-PROTEAN Tetra Vertical Electrophoresis Cell, BIORAD) at 80-110 volts. For transferring, the Transblot Semi-dry BIORAD Transfer Cell apparatus was used, according to the manufacturer's instructions. The PVDF membrane (MiliporeSigma) was activated in 100% methanol for 10 seconds, followed by ultrapure water for 30-60 seconds, and an incubation in cold methanol-free BSN-TB buffer (48 mM Tris, 39 mM glycine, 0.04% SDS) for 3-5 minutes.

The gel was likewise soaked in cold BSN-TB buffer for 5-10 minutes before transferring. The prepared membrane and gel were then layered onto the apparatus in between pieces of BSN-TB soaked filter paper, and the transfer was carried out for 25 minutes at 15 volts. The membrane was briefly rinsed in ultrapure water and incubated overnight in 10% milk TBS-T (10 mM Tris pH 7.5, 140 mM NaCl, 0.05% Tween-20) solution, at 4°C, with constant agitation, to block non-specific binding. After 3 washes in TBS-T for 5 minutes each, the membrane was incubated for 1 hour with anti-Numb monoclonal rabbit antibody (C29G11, Cell Signaling Technology), used 1:2000 in TBS-T, at room temperature, with constant agitation. Excess antibody was washed 3 times with TBS-T, for 5 minutes, and a 1:10,000 dilution of HRP conjugated anti-rabbit IgG secondary antibody (sc-2004, Santa Cruz) was added to the membrane for 1 hour. Finally, the membrane was washed in TBS-T, and the signal was detected using chemiluminescent kit Pierce ECL Western Blot Substrate (Thermo Scientific) and CL-Xposure film (Thermo Scientific).

Immunoprecipitation

A total of 3 mg of protein lysate was incubated with 1 µg anti-Numb antibody for 1 hour at 4°C with constant agitation. After adding 50 µL Protein A/G PLUS agarose beads (Santa-Cruz) to the antibody-lysate complex, the samples were incubated overnight, at 4°C, on a rotating platform. The beads were collected via centrifugation for 5 minutes at 2500 rpm, in 4°C, and the supernatant was removed. After a total of 4 washes in 500 µL of Darnell lysis buffer, the beads were resuspended in 40-50 µL of laemmli buffer, added to a fresh centrifuge tube, and the proteins were eluted via boiling at 97°C for 5 minutes. The immunoprecipitation was also carried out with 3 mg of total

lysate and 1 μg isotype control rabbit IgG antibody (Thermo Scientific) using the same protocol.

Sample preparation for mass spectrometry

Satellite cells were isolated from one litter (4 females, 4 males) of 3-month-old Swiss-Webster mice, and maintained in culture until 6 10 cm plates of confluent cells were generated. The cells were treated with 50 μM MG132 (MiliporeSigma) in DMSO, to inhibit the proteasome, and samples were harvested 4 hours later with Darnell lysis buffer. Total protein concentration was determined using the Bradford method, and 3 mg of total lysate was used for immunoprecipitation. A fraction of the precipitated sample (10 μL) was kept for Western blot analysis, while the rest of the sample was used for mass spectrometry.

In-gel protein digestion

Materials used for the preparation and handling of the gel were cleaned with 100% methanol and autoclaved, when possible. Glass tools and containers were used instead of plastic. The samples were loaded and run using SDS-PAGE as described above. After the 15 kDa protein marker in the ladder reached the bottom of the gel, electrophoresis was stopped, and the gel was washed 3 times for 5 minutes in ultrapure water, with gentle agitation. The gel was then stained in BioSafe Coomassie G-250 stain (BIORAD) until distinct bands became apparent (~1 hour), followed by de-staining in ultrapure water until the background was almost clear (~1 hour). Using the ladder as a guide, each lane was cut out of the gel with a sterile scalpel in 6 pieces: 250-100 kDa,

100-60 kDa, 60-50 kDa, 50-35 kDa, 35-25 kDa, and 25-10 kDa. Each piece was cut further in 1 mm x 1 mm cubes, added to a Protein LoBind 1.5 mL centrifuge tube (Eppendorf), and covered with ultrapure water. To remove the Coomassie stain, the water was discarded, and the pieces were covered with 1:1 solution of acetonitrile (ACN): 100 mM ammonium bicarbonate buffer (ABC) and incubated 10 minutes, twice. Next, the gel pieces were covered with 100% ACN, until opaque. The disulfide bonds were reduced with 10 mM DTT, for 30 minutes at 60°C. After the samples cooled to room temperature, DTT was discarded and ACN was added until the gel pieces were opaque again. For alkylation, iodoacetamide (IAA) incubation in the dark, for 30 minutes at room temperature was used. The IAA was discarded, and the gel pieces were washed with ACN until opaque. To remove traces of IAA, 3 wash steps of 10 minutes each were carried out with 100 mM ABC, followed by 1:1 ACN:ABC, then ACN. Next, the gel samples were incubated in mass spectrometry grade Trypsin Gold, at 20 ng/µL, overnight at 37°C, to digest the proteins. The supernatant containing the peptides was transferred to new low-protein binding tubes. Residual peptides were extracted from the gel with incubations of 15 minutes each in ACN:ABC, 5% formic acid, then ACN, twice. The peptide supernatant was then dried in a speed vac, resuspended in 15 µL 0.1% formic acid, placed in the autosampler vial, and injected. The injections and data analysis were carried out by Dr. Natalie Mitchell, using Mayo Clinic's mass spectrometry core facilities. Additional data analysis was carried out using freely available ProteoWizard software and protocols outlined in CompOmics' "Bioinformatics for Proteomics" tutorials.

Data analysis

To create "unique hits" lists for each experiment, the UniProt accession IDs from both data sets were filtered for duplicate values, which were subsequently sorted and removed using Excel. The Retrieve/ ID mapping feature in UniProt was then used to convert the accession IDs into protein and gene names, and generate the unique proteins lists for both the Numb and Control IPs. Gene ontology categories were generated for both unique data sets with AmiGO 2's Term Enrichment Service, using the standard parameters (Fisher's Exact test, with Bonferroni correction for multiple testing, and P-value <0.05). For the Numb data set, 563 out of 573 proteins were identified and mapped, while 224 out of 227 were mapped for the Control data set. The categories explored include GO-Slim Biological Process, GO-Slim Cellular Component, GO-Slim Molecular Function, and Reactome Pathways. Table 5 lists several of the significantly enriched categories, along with the P-value, and the proteins in said category. The table 5 list is not exhaustive and presents only a snapshot of the results.

Primer name (RT-QPCR)	Primer sequence (5’ to 3’)
GapDH Fwd	GGGAAGCCCATCACCATCTT
GapDH Rev	GCCTTCTCCATGGTGGTGAA
Total Numb Fwd	TTGCAAGATGCCAAGAAAGC
Total Numb Rev	GGGAGAGGTGGGAGAGGATG
PRRi Numb Fwd	TCCCTGATGCTGCTAACAAG
PRRi Numb Rev	CCTGGAAGAGACCTGGAGAG
Primer name (RT-PCR)	Primer sequence (5’ to 3’)
PTB Fwd	AGAGGAATGCACATCTGTGAAGA
PTB Rev	AACAGGCTGCAAAAGCACAG
PRR Fwd	CGCATCAATGACTTGCCTTCC
PRR Rev	GCCTGGAAGAGACCTGGAGA

Table 6. Comprehensive list of primers used for RT-QPCR and RTPCR.

CONCLUSIONS

Satellite cells are adult stem cells capable of undergoing repeated rounds of repair in healthy skeletal muscle. However, satellite cell function declines steeply with age and with the sustained, chronic muscle damage common in myopathies and dystrophies. This work aims to further understanding of muscle stem cell biology through different molecular and bioengineering approaches.

Mammals have poor regeneration capabilities when compared to other classes of animals, like fish, amphibians, and reptiles. Evolutionarily, lizards are the closest vertebrates to humans with significant regeneration ability. For example, *Anolis carolinensis* lizards autotomize their tails when threatened, and regenerate a replacement with a cartilage endoskeleton, skin, nerves, vasculature, connective tissue, and functional skeletal muscle groups with tendinous attachments and NMJs. The anatomy of the regenerated tail has been described at length, as has the transcriptomic signature, but very little is known about its stem cell populations. We characterized *A. carolinensis* satellite cells using an *in vitro* culture model. Transcriptomic data set analysis using XGSA showed that lizard satellite cells are more transcriptionally similar to mouse, and even human satellite cells, than any other cell or tissue type investigated. However, lizard satellite cells express chondrogenic markers at higher levels, and when cultured in micromass format, will condense into chondrogenic nodules. These nodules express cartilage specific proteins, like sulfated glycosaminoglycans and collagen 2a1. Mouse satellite cells cultured in micromasses do not aggregate into nodules consistently, nor do they express cartilage specific ECM genes. The lizard satellite cells underwent differentiation in the absence of exogenously added morphogens, and intrinsically upregulated chondrogenic specific transcription factors. These data suggest that lizard

satellite cells have expanded musculoskeletal plasticity, and given the right context, may adopt non-myogenic fates, unlike their mammalian counterparts. Our findings may help explain, in part, some of the discrepancy in regeneration ability across different animal classes.

While our data present a compelling case for satellite cells as a stem cell source that contribute to the regenerating cartilage endoskeleton and skeletal muscle, it will be necessary to validate these findings *in vivo*. Performing immunofluorescence or *in situ* hybridization for satellite cell markers in the tail at different time points post autotomy will give us a better understanding of where these cells are during regeneration, as would lineage tracing and ablation experiments. Recent advancements in CRISPR-Cas9 editing lizard oocytes will hopefully lead to those genetic tools being developed in the near future. For example, knocking out Pax7 will result in adult animals lacking satellite cells in their skeletal muscle. Autotomy experiments in $Pax7^{-/-}$ lizards will provide tremendous insight into the role of satellite cells during regeneration.

Furthermore, the full extent of lizard satellite cell expanded musculoskeletal plasticity has not been characterized. During development, the paraxial mesoderm gives rise to not only to skeletal muscle and cartilage, but tendon, bone, and dermis, and whether lizard satellite cells can adopt those lineages or not remains to be determined. Additionally, mammalian satellite cells likely represent a heterogeneous stem cell, with subsets of the stem cell population having different characteristics in terms of self-renewal, myogenic potential, and gene expression. At the moment, it is unknown whether lizard satellite cells also exhibit heterogeneity, and whether expanded plasticity is a feature of the entire stem cell pool, or only a select subset of the total population. Finally, the mechanisms that drive endogenous upregulation of chondrogenic

transcription factors in lizard satellite cell micromasses have not been explored. A comparative analysis of the genetic regulatory regions that control expression of Sox9, and BMP genes will shed light on what leads to expanded plasticity in lizard satellite cells and provide important genetic information regarding specific pathways whose regulation could be altered to improve the potential therapeutic uses of satellite cells.

However, before we can apply lessons learned from anole satellite cells to human regenerative medicine, it will be necessary to establish an *in vitro* culture system that maintains satellite cell myogenic potential. Biomaterials and various bioengineering techniques are currently being explored for improving satellite cell culture and delivery into damaged muscle. We cultured mouse satellite cells on hydrogels comprised of proteins that are present in the muscle stem cell niche, and assayed proliferation, differentiation, and gene expression. We cultured the cells on tissue culture plates coated with the same ECM proteins, to investigate how stiffness influences behavior, and finally, we repeated the experiments with C2C12 cells, a myoblast cell line, in a comparative study aimed at describing how the primary stem cells are similar to, or different from their immortalized proxy.

Overall, stiffness altered cell behavior more drastically than the ECM protein composition. We also found notable differences in satellite cell behavior when compared to C2C12 cells. The hydrogels did not support proliferation or differentiation of satellite cells, and gene expression analysis done at 3- and 6-days post culture showed that the cells initially attempt to differentiate, but eventually return to a quiescent-like state. Interestingly, the phenotype observed after prolonged culture was reversible, as satellite cells retrieved from hydrogels and reseeded onto Matrigel coated plates maintained their myogenic potential and differentiated into myotubes. C2C12 cells did proliferate and

differentiate on hydrogels, albeit to a lesser extent when compared to substrate coated plates. Gene expression analysis showed that myogenic inhibitor myostatin was not expressed in these cells under any conditions tested, and may, in part, explain the discrepancies between satellite cells and C2C12 cells, especially since knock-down of myostatin in satellite cells slightly improved proliferation on both hydrogels and coated substrates.

For satellite cells to become a safe, reliable and autologous source of stem cells for therapeutic purposes, parameters for an *in vitro* culture system that maintains stemness and myogenic potential must be outlined. Our study describes how ECM and stiffness cues affect cell behavior, but many other variables remain to be explored. For example, satellite cells are polarized *in vivo*, and express a different set of cell surface proteins on their apical side, which contacts the myofiber, when compared to the basal side, which contacts the basal lamina- a feature that is lost when cells are cultured on a flat surface. Additionally, the niche environment is dynamic, its stiffness and composition changing constantly with aging, exercise, injury, disease, stress, nutrition, and is influenced by neighboring NMJs, blood vessels, and resident fibroblasts. Other features of the stem cell niche and skeletal muscle, like pressure, stretch, oxygen level, etc. have also been explored in various contexts. Determining how these variables dictate satellite cell behavior and understanding how to recapitulate them *in vitro* may help overcome some of the current challenges. One approach that could integrate several of the aforementioned variables into one dynamic, complex culture protocol is microfluidics miniaturized total analysis systems (μTAS) technology. While the initial microfluidics efforts focused on diagnostics and medical devices, later applications included lab-on-a-chip and organ-on-a-chip tools that aim to better mimic the *in vivo* environment and provide means for improved drug testing and research. These have

already been used to model vasculature, the blood-brain barrier, lungs, and other organs or tissues with multiple cell types and complex organization, and could be used to inform future efforts for satellite cell *in vitro* culture protocol design.

The endocytic adaptor and cell fate determinant Numb has been extensively studied in development and cancer, but little is known about its contribution to muscle stem cell activation and proliferation. Numb deficient satellite cells fail to repair muscle following injury and upregulate myogenic and cell cycle inhibitors myostatin and p21. We investigated Numb isoform expression in satellite cells as they differentiate, and in various embryonic tissues as development proceeds. Limb bud, neural tube, and embryonic heart express PRRi and PRRo isoforms of Numb, both at the RNA and protein level, with PRRi declining over time. Satellite cells express predominantly the PRRo isoform of Numb, and the PRRi is virtually absent.

A small preliminary proteomics experiment identified many putative Numb binding proteins in freshly isolated, proliferating satellite cells. Our findings confirmed Numb's previously known roles in clathrin-dependent endocytosis and protein ubiquitination and suggested a few novel implications in actin dynamics, focal adhesion, and cell division, which have not been previously investigated in satellite cells. Possible interactions with myogenin and other transcription factors important for satellite cell function were also identified. However, further validation and experiments will be necessary to determine the biological significance of our data set. First, repeating the IP-proteomics to generate n=3-5 will confirm which proteins are reliably and consistently identified. Interactions with proteins of interest, like myogenin, will need to be confirmed via co-IP Western blot. To test our hypotheses, establishing a Numb (and Numblike) deficient satellite cell culture system, either with CRISPR-Cas9 or shRNA,

will be necessary. It will be interesting to determine whether the localization, activity, and expression levels of myogenin and other transcription factors changes in the absence of Numb. Likewise, staining for F-actin, integrins or cadherins, and investigating cell migration and fusion in Numb$^{-/-}$ satellite cells will determine how Numb influences focal adhesion and cytoskeletal dynamics. Finally, the identified 14-3-3 family of proteins and the EHD proteins implicate Numb in trafficking, sorting, and endocytosis during activation and proliferation, and exploring those processes further will shed light on the mechanisms responsible for the Numb$^{-/-}$ satellite cell phenotype.

References

Abballe, L., Mastronuzzi, A., Miele, E., Carai, A., Besharat, Z.M., Moretti, M., De Smaele, E., Giangaspero, F., Locatelli, F., Ferretti, E., Po, A., 2018. Numb Isoforms Deregulation in Medulloblastoma and Role of p66 Isoform in Cancer and Neural Stem Cells. Front. Pediatr. 6, 1–10. https://doi.org/10.3389/fped.2018.00315

Akiyama, H., Chaboissier, M.C., Martin, J.F., Schedl, A., De Crombrugghe, B., 2002. The transcription factor *Sox9* has essential roles in successive steps of the chondrocyte differentiation pathway and is required for expression of *Sox5* and *Sox6*. Genes Dev. 16, 2813–2828. https://doi.org/10.1101/gad.1017802

Amthor, H., Christ, B., Weil, M., Patel, K., 1998. The importance of timing differentiation during limb muscle development. Curr. Biol. 8, 642–652. https://doi.org/10.1016/S0960-9822(98)70251-9

Amthor, H., Nicholas, G., McKinnell, I., Kemp, C.F., Sharma, M., Kambadur, R., Patel, K., 2004. Follistatin complexes Myostatin and antagonises Myostatin-mediated inhibition of myogenesis. Dev. Biol. 270, 19–30. https://doi.org/10.1016/j.ydbio.2004.01.046

Anders, S., Pyl, P.T., Huber, W., 2015. HTSeq-A Python framework to work with high-throughput sequencing data. Bioinformatics 31, 166–169. https://doi.org/10.1093/bioinformatics/btu638

Artaza, J.N., Bhasin, S., Mallidis, C., Taylor, W., Ma, K., Gonzalez-Cadavid, N.F., 2002. Endogenous expression and localization of myostatin and its relation to myosin heavy chain distribution in C2C12 skeletal muscle cells. J. Cell. Physiol. 190, 170–179. https://doi.org/10.1002/jcp.10044

Asakura, A., Komaki, M., Rudnicki, M., 2001. Differentiation: Muscle Satellite Cells Are Multipotential Stem Cells tha Exhibit Myogenic, Osteogenic, and Adipogenic Dinfferentiation. Differentiation 245–253.

Asou, Y., Nifuji, A., Tsuji, K., Shinomiya, K., Olson, E.N., Koopman, P., Noda, M., 2002. Coordinated expression of scleraxis and Sox9 genes during embryonic development of tendons and cartilage. J. Orthop. Res. 20, 827–833. https://doi.org/10.1016/S0736-0266(01)00169-3

Bandyopadhyay, A., Tsuji, K., Cox, K., Harfe, B.D., Rosen, V., Tabin, C.J., 2006. Genetic analysis of the roles of BMP2, BMP4, and BMP7 in limb patterning and skeletogenesis. PLoS Genet. 2, 2116–2130. https://doi.org/10.1371/journal.pgen.0020216

Bani-Yaghoub, M., Kubu, C.J., Cowling, R., Rochira, J., Nikopoulos, G.N., Bellum, S., Verdi, J.M., 2007a. A switch in numb isoforms is a critical step in cortical development. Dev. Dyn. 236, 696–705. https://doi.org/10.1002/dvdy.21072

Bani-Yaghoub, M., Kubu, C.J., Cowling, R., Rochira, J., Nikopoulos, G.N., Bellum, S., Verdi, J.M., 2007b. A switch in numb isoforms is a critical step in cortical development. Dev. Dyn. 236, 696–705. https://doi.org/10.1002/dvdy.21072

Bao, M., Liu, S., Yu, X.Y., Wu, C., Chen, Q., Ding, H., Shen, C., Wang, B., Wang, S., Song, Y.H., Li, Y., 2018. Runx1 promotes satellite cell proliferation during ischemia -

Induced muscle regeneration. Biochem. Biophys. Res. Commun. 503, 2993–2997. https://doi.org/10.1016/j.bbrc.2018.08.083

Bentzinger, C.F., Wang, Y.X., Von Maltzahn, J., Soleimani, V.D., Yin, H., Rudnicki, M., 2013. Fibronectin regulates Wnt7a signaling and satellite cell expansion. Cell Stem Cell 12, 75–87. https://doi.org/10.1016/j.stem.2012.09.015

Béranger, F., Méjean, C., Moniot, B., Berta, P., Vandromme, M., 2000. Muscle differentiation is antagonized by SOX15, a new member of the SOX protein family. J. Biol. Chem. 275, 16103–16109. https://doi.org/10.1074/jbc.275.21.16103

Biressi, S., Miyabara, E.H., Gopinath, S.D., Carlig, P.M.M., Rando, T. a, 2015. A Wnt-TGFβ2 axis induces a fibrogenic program in muscle stem cells from dystrophic mice 6, 1–25. https://doi.org/10.1126/scitranslmed.3008411.A

Biressi, S., 2010. Heterogeneity in the muscle satellite cell population. Semin. cell Dev. Biol. 21, 845–854. https://doi.org/10.1016/j.semcdb.2010.09.003.Heterogeneity

Bjornson, C.R.R., Cheung, T.H., Liu, L., Tripathi, P. V., Steeper, K.M., Rando, T.A., 2012. Notch signaling is necessary to maintain quiescence in adult muscle stem cells. Stem Cells 30, 232–242. https://doi.org/10.1002/stem.773

Black, O.B., Molkentin, J., 1996. Cooperative activation of muscle gene expression by MEF2 and myogenic BHLH proteins. E. FASEB J. 10, 1125–1136.

Boonen, K.J.M., Rosaria-Chak, K.Y., Baaijens, F.P.T., Van Der Schaft, D.W.J., Post, M.J., 2009. Essential environmental cues from the satellite cell niche: Optimizing proliferation and differentiation. Am. J. Physiol. - Cell Physiol. 296, 1338–1345. https://doi.org/10.1152/ajpcell.00015.2009

Boontheekul, T., Hill, E.E., Kong, H.-J., Mooney, D.J., 2007. Regulating myoblast phenotype through controlled gel stiffness and degradation. Tissue Eng. 13, 1431–42. https://doi.org/10.1089/ten.2006.0356

Borselli, C., Cezar, C.A., Shvartsman, D., Vandenburgh, H.H., Mooney, D.J., 2011. The role of multifunctional delivery scaffold in the ability of cultured myoblasts to promote muscle regeneration. Biomaterials 32, 8905–8914. https://doi.org/10.1016/j.biomaterials.2011.08.019

Brack, A.S., Conboy, I.M., Conboy, M.J., Shen, J., Rando, T.A., 2008. A Temporal Switch from Notch to Wnt Signaling in Muscle Stem Cells Is Necessary for Normal Adult Myogenesis. Cell Stem Cell 2, 50–59. https://doi.org/10.1016/j.stem.2007.10.006

Brack, A.S., Conboy, M.J., Roy, S., Lee, M., Kuo, C.J., Keller, C., Rando, T.A., 2007. Increased Wnt signaling during aging alters muscle stem cell fate and increases fibrosis. Science (80-.). 317, 807–810. https://doi.org/10.1126/science.1144090

Brack, A.S., Murphy-seiler, F., Hanifi, J., Deka, J., Keller, C., Aguet, M., Rando, T. a, 2012. BCL9 is an essential component of canonical Wnt signaling that mediates the differentiation of myogenic progenitors during muscle regeneration. Dev. Biol. 335, 93–105. https://doi.org/10.1016/j.ydbio.2009.08.014.BCL9

Breitling, R., Armengaud, P., Amtmann, A., Herzyk, P., 2004. Rank products: A simple, yet powerful, new method to detect differentially regulated genes in replicated

microarray experiments. FEBS Lett. 573, 83–92. https://doi.org/10.1016/j.febslet.2004.07.055

Briggs, D., Morgan, J.E., 2013. Recent progress in satellite cell/myoblast engraftment - Relevance for therapy. FEBS J. 280, 4281–4293. https://doi.org/10.1111/febs.12273

Cairns, D.M., Liu, R., Sen, M., Canner, J.P., Schindeler, A., Little, D.G., Zeng, L., 2012. Interplay of Nkx3.2, Sox9 and Pax3 regulates chondrogenic differentiation of muscle progenitor cells. PLoS One 7, 1–17. https://doi.org/10.1371/journal.pone.0039642

Camaschella, C., 2009. BMP6 orchestrates iron metabolism. Nat. Genet. 41, 386–8. https://doi.org/10.1038/ng0409-386

Cameron, T.L., Belluoccio, D., Farlie, P.G., Brachvogel, B., Bateman, J.F., 2009. Global comparative transcriptome analysis of cartilage formation in vivo. BMC Dev. Biol. 9, 1–17. https://doi.org/10.1186/1471-213X-9-20

Carrieri, F.A., Dale, J.K., 2017. Turn It Down a Notch. Front. Cell Dev. Biol. 4, 1–9. https://doi.org/10.3389/fcell.2016.00151

Chargé, S.B.P., Rudnicki, M., 2004. Cellular and molecular regulation of muscle regeneration. Physiol. Rev. 84, 209–238. https://doi.org/10.1152/physrev.00019.2003

Charville, G.W., Cheung, T.H., Yoo, B., Santos, P.J., Lee, G.K., Shrager, J.B., Rando, T.A., 2015. Ex vivo expansion and in vivo self-renewal of human muscle stem cells. Stem Cell Reports 5, 621–632. https://doi.org/10.1016/j.stemcr.2015.08.004

Chaturvedi, V., Dye, D.E., Kinnear, B.F., Van Kuppevelt, T.H., Grounds, M.D., Coombe, D.R., 2015. Interactions between skeletal muscle myoblasts and their extracellular matrix revealed by a serum free culture system. PLoS One 10, 1–27. https://doi.org/10.1371/journal.pone.0127675

Cheng, T.C., Wallace, M.C., Merlie, J.P., Olson, E.N., 1993. Separable regulatory elements governing myogenin transcription in mouse embryogenesis. Science (80). 261, 215–218. https://doi.org/10.1126/science.8392225

Colaluca, I.N., Basile, A., Freiburger, L., Uva, V.D., Disalvatore, D., Vecchi, M., Confalonieri, S., Tosoni, D., Cecatiello, V., Malabarba, M.G., Yang, C.J., Kainosho, M., Sattler, M., Mapelli, M., Pece, S., Paolo, P., Fiore, D., 2013. A Numb – Mdm2 fuzzy complex reveals an isoform- specific involvement of Numb in breast cancer. JCB 1–18.

Collins, C.A., Olsen, I., Zammit, P.S., Heslop, L., Petrie, A., Partridge, T.A., Morgan, J.E., 2005. Stem cell function, self-renewal, and behavioral heterogeneity of cells from the adult muscle satellite cell niche. Cell 122, 289–301. https://doi.org/10.1016/j.cell.2005.05.010

Collinsworth, A.M., Zhang, S., Kraus, W.E., Truskey, G. a, 2002. Apparent elastic modulus and hysteresis of skeletal muscle cells throughout differentiation. Am. J. Physiol. Cell Physiol. 283, C1219–C1227. https://doi.org/10.1152/ajpcell.00502.2001

Conboy, I.M., Rando, T.A., 2002. The regulation of Notch signaling controls satellite cell activation and cell fate determination in postnatal myogenesis. Dev. Cell 3, 397–409. https://doi.org/10.1016/S1534-5807(02)00254-X

Cornelison, D.D.W., 2018. "Known Unknowns": Current Questions in Muscle Satellite Cell Biology, 1st ed, Current Topics in Developmental Biology. Elsevier Inc. https://doi.org/10.1016/bs.ctdb.2017.08.006

Corradini, E., Meynard, D., Wu, Q., Chen, S., Ventura, P., Pietrangelo, A., Babitt, J.L., 2011. Serum and liver iron differently regulate the bone morphogenetic protein 6 (BMP6)-SMAD signaling pathway in mice. Hepatology 54, 273–284. https://doi.org/10.1002/hep.24359

Darehzereshki, A., Rubin, N., Gamba, L., Kim, J., Fraser, J., Huang, Y., Billings, J., Mohammadzadeh, R., Wood, J., Warburton, D., Kaartinen, V., Lien, C.L., 2015. Differential regenerative capacity of neonatal mouse hearts after cryoinjury. Dev. Biol. 399, 91–99. https://doi.org/10.1016/j.ydbio.2014.12.018

Denker, A.E., Haas, A.R., Nicoll, S.B., Tuan, R.S., 1999. Chondrogenic differentiation of murine C3H10T1/2 multipotential mesenchymal cells: I. Stimulation by bone morphogenetic protein-2 in high-density micromass cultures. Differentiation 64, 67–76. https://doi.org/10.1046/j.1432-0436.1999.6420067.x

Dho, S.E., French, M.B., Woods, S. a, McGlade, C.J., 1999. Characterization of Four Mammalian Numb Protein Isoforms. J. Biol. Chem. 274, 33097–33104.

Di Marcotullio, L., Ferretti, E., Greco, A., De Smaele, E., Po, A., Sico, M.A., Alimandi, M., Giannini, G., Maroder, M., Screpanti, I., Gulino, A., 2006. Numb is a suppressor of Hedgehog signalling and targets Gli1 for Itch-dependent ubiquitination. Nat. Cell Biol. 8, 1415–1423. https://doi.org/10.1038/ncb1510

Di Marcotullio, L., Greco, A., Mazzà, D., Canettieri, G., Pietrosanti, L., Infante, P., Coni, S., Moretti, M., De Smaele, E., Ferretti, E., Screpanti, I., Gulino, A., 2011. Numb activates the E3 ligase Itch to control Gli1 function through a novel degradation signal. Oncogene 30, 65–76. https://doi.org/10.1038/onc.2010.394

Diel, P., Baadners, D., Schlüpmann, K., Velders, M., Schwarz, J.P., 2008. C2C12 myoblastoma cell differentiation and proliferation is stimulated by androgens and associated with a modulation of myostatin and Pax7 expression. J. Mol. Endocrinol. 40, 231–241. https://doi.org/10.1677/JME-07-0175

Ding, K., Yang, Z., Xu, J.Z., Liu, W.Y., Zeng, Q., Hou, F., Lin, S., 2015. Elastic hydrogel substrate supports robust expansion of murine myoblasts and enhances their engraftment. Exp. Cell Res. 337, 111–119. https://doi.org/10.1016/j.yexcr.2015.07.021

Djordjevic, D., Kusumi, K., Ho, J.W.K., 2016. XGSA: A statistical method for cross-species gene set analysis. Bioinformatics 32, i620–i628. https://doi.org/10.1093/bioinformatics/btw428

Dominique, J.E., Gérard, C., 2006. Myostatin regulation of muscle development: Molecular basis, natural mutations, physiopathological aspects. Exp. Cell Res. 312, 2401–2414. https://doi.org/10.1016/j.yexcr.2006.04.012

Dooley, C.M., James, J., McGlade, C.J., Ahmad, I., 2002. Involvement of Numb in Vertebrate Retinal Development : Evidence for Multiple Roles of Numb in Neural Differentiation and Maturation ABSTRACT : 313–325. https://doi.org/10.1002/neu.10176

Dumont, N.A., Bentzinger, C.F., Sincennes, M.C., Rudnicki, M.A., 2015a. Satellite cells and skeletal muscle regeneration. Compr. Physiol. 5, 1027–1059. https://doi.org/10.1002/cphy.c140068

Dumont, N.A., Wang, Y.X., Von Maltzahn, J., Pasut, A., Bentzinger, C.F., Brun, C.E., Rudnicki, M.A., 2015b. Dystrophin expression in muscle stem cells regulates their polarity and asymmetric division. Nat. Med. 21, 1455–1463. https://doi.org/10.1038/nm.3990

Dunn, A., Talovic, M., Patel, K., Patel, A., Marcinczyk, M., Garg, K., 2019. Biomaterial and stem cell-based strategies for skeletal muscle regeneration. J. Orthop. Res. 37, 1246–1262. https://doi.org/10.1002/jor.24212

Echeverri, K., Tanaka, E.M., 2002. Mechanisms of muscle dedifferentiation during regeneration. Semin. Cell Dev. Biol. 13, 353–360. https://doi.org/10.1016/S1084

Echeverri, K., Zayas, R.M., 2018. Regeneration: From cells to tissues to organisms. Dev. Biol. 433, 109–110. https://doi.org/10.1016/j.ydbio.2017.12.005

Eckalbar, W.L., Lasku, E., Infante, C.R., Elsey, R.M., Markov, G.J., Allen, A.N., Corneveaux, J.J., Losos, J.B., DeNardo, D.F., Huentelman, M.J., Wilson-Rawls, J., Rawls, A., Kusumi, K., 2012. Somitogenesis in the anole lizard and alligator reveals evolutionary convergence and divergence in the amniote segmentation clock. Dev. Biol. 363, 308–319. https://doi.org/10.1016/j.ydbio.2011.11.021

Engler, A.J., Griffin, M.A., Sen, S., Bennemann, C.G., Sweeney, H.L., Discher, D.E., 2004. Myotubes differentiate optimally on substrates with tissue-like stiffness: Pathological implications for soft or stiff microenvironments. J. Cell Biol. 166, 877–887. https://doi.org/10.1083/jcb.200405004

Feige, P., Brun, C.E., Ritso, M., Rudnicki, M., 2018. Orienting Muscle Stem Cells for Regeneration in Homeostasis, Aging, and Disease. Cell Stem Cell 23, 653–664. https://doi.org/10.1016/j.stem.2018.10.006

Fisher, R.E., Geiger, L.A., Stroik, L.K., Hutchins, E.D., George, R.M., Denardo, D.F., Kusumi, K., Rawls, J.A., Wilson-Rawls, J., 2012. A Histological Comparison of the Original and Regenerated Tail in the Green Anole, Anolis carolinensis. Anat. Rec. 295, 1609–1619. https://doi.org/10.1002/ar.22537

Friedrichs, M., Wirsdöerfer, F., Flohé, S.B., Schneider, S., Wuelling, M., Vortkamp, A., 2011. BMP signaling balances proliferation and differentiation of muscle satellite cell descendants. BMC Cell Biol. 12, 7–10. https://doi.org/10.1186/1471-2121-12-26

Fujita, T., Azuma, Y., Fukuyama, R., Hattori, Y., Yoshida, C., Koida, M., Ogita, K., Komori, T., 2004. Runx2 induces osteoblast and chondrocyte differentiation and enhances their migration by coupling with PI3K-Akt signaling. J. Cell Biol. 166, 85–95. https://doi.org/10.1083/jcb.200401138

Gao, G., Zhang, X.F., Hubbell, K., Cui, X., 2017. NR2F2 regulates chondrogenesis of

human mesenchymal stem cells in bioprinted cartilage. Biotechnol. Bioeng. 114, 208–216. https://doi.org/10.1002/bit.26042

George, R.M., Biressi, S., Beres, B.J., Rogers, E., Mulia, A.K., Allen, R.E., Rawls, A., Rando, T. a, Wilson-Rawls, J., 2013. Numb-deficient satellite cells have regeneration and proliferation defects. Proc. Natl. Acad. Sci. U. S. A. 110, 18549–54. https://doi.org/10.1073/pnas.1311628110

Gilbert, E.A.B., Payne, S.L., Vickaryous, M.K., 2013. The anatomy and histology of caudal autotomy and regeneration in lizards. Physiol. Biochem. Zool. 86, 631–644. https://doi.org/10.1086/673889

Gilbert, P.M., Havenstrite, K.L., Magnusson, K.E.G., Sacco, A., Leonardi, N.A., Kraft, P., Nguyen, N.K., Thrun, S., Lutolf, M.P., Blau, H.M., 2010. Substrate elasticity regulates skeletal muscle stem cell self-renewal in culture. Science 329, 1078–81. https://doi.org/10.1126/science.1191035

Gill, R., Hitchins, L., Fletcher, F., Dhoot, G.K., 2010. Sulf1A and HGF regulate satellite-cell growth. J. Cell Sci. 123, 1873–1883. https://doi.org/10.1242/jcs.061242

Gilson, H., Schakman, O., Kalista, S., Lause, P., Tsuchida, K., Thissen, J.-P., 2009. Follistatin induces muscle hypertrophy through satellite cell proliferation and inhibition of both myostatin and activin. AJP Endocrinol. Metab. 297, E157–E164. https://doi.org/10.1152/ajpendo.00193.2009

Girardi, F., Le Grand, F., 2018. Wnt Signaling in Skeletal Muscle Development and Regeneration, Progress in Molecular Biology and Translational Science. Elsevier Inc. https://doi.org/10.1016/bs.pmbts.2017.11.026

Goel, A.J., Rieder, M.K., Arnold, H.H., Radice, G.L., Krauss, R.S., 2017. Niche Cadherins Control the Quiescence-to-Activation Transition in Muscle Stem Cells. Cell Rep. 21, 2236–2250. https://doi.org/10.1016/j.celrep.2017.10.102

Grant, B.D., Donaldson, J.G., 2009. Pathways and mechanisms of endocytic recycling. Nat. Rev. Mol. Cell Biol. 10, 597–608. https://doi.org/10.1038/nrm2755

Grefte, S., Adjobo-Hermans, M.J.W., Versteeg, E.M.M., Koopman, W.J.H., Daamen, W.F., 2016. Impaired primary mouse myotube formation on crosslinked type i collagen films is enhanced by laminin and entactin. Acta Biomater. 30, 265–276. https://doi.org/10.1016/j.actbio.2015.11.009

Grefte, S., Vullinghs, S., Kuijpers-Jagtman, A.M., Torensma, R., Von Den Hoff, J.W., 2012. Matrigel, but not collagen I, maintains the differentiation capacity of muscle derived cells in vitro. Biomed. Mater. 7. https://doi.org/10.1088/1748-6041/7/5/055004

Gulino, A., Di Marcotullio, L., Screpanti, I., 2010. The multiple functions of Numb. Exp. Cell Res. 316, 900–906. https://doi.org/10.1016/j.yexcr.2009.11.017

Haas, A.R., Tuan, R.S., 1999. Chondrogenic differentiation of murine C3H10T1/2 multipotential mesenchymal cells: II. Stimulation by bone morphogenetic protein-2 requires modulation of N-cadherin expression and function. Differentiation 64, 77–89. https://doi.org/10.1046/j.1432-0436.1999.6420077.x

Hashimoto, N., Kiyono, T., Wada, M.R., Umeda, R., Goto, Y. ichi, Nonaka, I., Shimizu, S., Yasumoto, S., Inagawa-Ogashiwa, M., 2008. Osteogenic properties of human myogenic progenitor cells. Mech. Dev. 125, 257–269. https://doi.org/10.1016/j.mod.2007.11.004

Hawke, T.J., Garry, D.J., 2001. Myogenic satellite cells Physiology to molecular biology. J. Appl. Physiol. 91, 534–551. https://doi.org/10.1063/1.3603452

Hirai, Maretoshi, Arita, Y., McGlade, C.J., Lee, K.-F., Chen, Ju, Evans, 2017. Adaptor proteins NUMB and NUMBL promote cell cycle withdrawal by targeting ERBB2 for degradation. J. Clin. Invest. 127, 386–390. https://doi.org/10.1172/JCI91081

Hirsinger, E., Duprez, D., Jouve, C., Malapert, P., Cooke, J., Pourquié, O., 1997. Noggin acts downstream of Wnt and Sonic Hedgehog to antagonize BMP4 in avian somite patterning. Development 124, 4605–4614.

Holterman, C.E., Le Grand, F., Kuang, S., Seale, P., Rudnicki, M., 2007. Megf10 regulates the progression of the satellite cell myogenic program. J. Cell Biol. 179, 911–922. https://doi.org/10.1083/jcb.200709083

Huang, Z., Chen, X., Chen, D., 2011. Myostatin: A novel insight into its role in metabolism, signal pathways, and expression regulation. Cell. Signal. 23, 1441–1446. https://doi.org/10.1016/j.cellsig.2011.05.003

Hughes, C.S., Postovit, L.M., Lajoie, G.A., 2010. Matrigel: a complex protein mixture required for optimal growth of cell culture. Proteomics 10, 1886–1890. https://doi.org/10.1002/pmic.200900758

Hutchins, E.D., Markov, G.J., Eckalbar, W.L., George, R.M., King, J.M., Tokuyama, M.A., Geiger, L.A., Emmert, N., Ammar, M.J., Allen, A.N., Siniard, A.L., Corneveaux, J.J., Fisher, R.E., Wade, J., DeNardo, D.F., Rawls, J.A., Huentelman, M.J., Wilson-Rawls, J., Kusumi, K., 2014. Transcriptomic analysis of tail regeneration in the lizard Anolis carolinensis reveals activation of conserved vertebrate developmental and repair mechanisms. PLoS One 9. https://doi.org/10.1371/journal.pone.0105004

Inada, M., Yasui, T., Nomura, S., Miyake, S., Deguchi, K., Himeno, M., Sato, M., Yamagiwa, H., Kimura, T., Yasui, N., Ochi, T., Endo, N., Kitamura, Y., Kishimoto, T., Komori, T., 1999. Maturational disturbance of chondrocytes in Cbfa1-deficient mice. Dev. Dyn. 214, 279–290. https://doi.org/10.1002/(SICI)1097-0177(199904)214:4<279::AID-AJA1>3.0.CO;2-W

Ishii, M., Han, J., Yen, H.Y., Sucov, H.M., Chai, Y., Maxson, R.E., 2005. Combined deficiencies of Msx1 and Msx2 cause impaired patterning and survival of the cranial neural crest. Development 132, 4937–4950. https://doi.org/10.1242/dev.02072

King, J.A., Marker, P.C., Seung, K.J., 1994. BMP5 and the Molecular, Skeletal, and Soft-Tissue Alterations in short ear Mice. Dev. Comp. Immunol. 166, 112–122.

Jopling, C., Boue, S., Belmonte, J.C.I., 2011. Dedifferentiation, transdifferentiation and reprogramming: Three routes to regeneration. Nat. Rev. Mol. Cell Biol. 12, 79–89. https://doi.org/10.1038/nrm3043

Jory, A., Le Roux, I., Gayraud-Morel, B., Rocheteau, P., Cohen-Tannoudji, M., Cumano,

A., Tajbakhsh, S., 2009. Numb promotes an increase in skeletal muscle progenitor cells in the embryonic somite. Stem Cells 27, 2769–2780. https://doi.org/10.1002/stem.220

Haimes, J., Kelley, M., 2010. Demonstration of a ΔΔCq Calculation Method to Compute Relative Gene Expression from qPCR Data, Tech note. https://doi.org/10.1007/978-3-319-41018-0_3

Kahn, E.B., Simpson, S.B., 1974. Satellite cells in mature, uninjured skeletal muscle of the lizard tail. Dev. Biol. 37, 219–223. https://doi.org/10.1016/0012-1606(74)90181-X

Katagiri, T., Yamaguchi, A., Komaki, M., Abe, E., Takahashi, N., Ikeda, T., Rosen, V., Wozney, J.M., Fujisawa-Sehara, A., Suda, T., 1994. Bone morphogenetic protein-2 converts the differentiation pathway of C2C12 myoblasts into the osteoblast lineage. J. Cell Biol. 127, 1755–1766. https://doi.org/10.1083/jcb.127.6.1755

Kawaguchi, K., Yoshida, S., Hatano, R., Asano, S., 2017. Pathophysiological roles of ezrin/radixin/moesin proteins. Biol. Pharm. Bull. 40, 381–390. https://doi.org/10.1248/bpb.b16-01011

Khodabukus, A., Baar, K., 2009. Regulating fibrinolysis to engineer skeletal muscle from the C2C12 cell line. Tissue Eng. - Part C Methods 15, 501–511. https://doi.org/10.1089/ten.tec.2008.0286

Kim, D., Langmead, B., Salzberg, S.L., 2015. HISAT: A fast spliced aligner with low memory requirements. Nat. Methods 12, 357–360. https://doi.org/10.1038/nmeth.3317

Knippenberg, M., Helder, M.N., Zandieh Doulabi, B., Wuisman, P.I.J.M., Klein-Nulend, J., 2006. Osteogenesis versus chondrogenesis by BMP-2 and BMP-7 in adipose stem cells. Biochem. Biophys. Res. Commun. 342, 902–908. https://doi.org/10.1016/j.bbrc.2006.02.052

Koshiba-Takeuchi, K., Mori, A.D., Kaynak, B.L., Cebra-Thomas, J., Sukonnik, T., Georges, R.O., Latham, S., Beck, L., Henkelman, R.M., Black, B.L., Olson, E.N., Wade, J., Takeuchi, J.K., Nemer, M., Gilbert, S.F., Bruneau, B.G., 2009. Reptilian heart development and the molecular basis of cardiac chamber evolution. Nature 461, 95–98. https://doi.org/10.1038/nature08324

Kragl, M., Knapp, D., Nacu, E., Khattak, S., Maden, M., Epperlein, H.H., Tanaka, E.M., 2009. Cells keep a memory of their tissue origin during axolotl limb regeneration. Nature 460, 60–65. https://doi.org/10.1038/nature08152

Krieger, J.R., Taylor, P., Gajadhar, A.S., Guha, A., Moran, M.F., McGlade, C.J., 2013. Identification and selected reaction monitoring (SRM) quantification of endocytosis factors associated with Numb. Mol. Cell. Proteomics 12, 499–514. https://doi.org/10.1074/mcp.M112.020768

Krieger, J.R., Taylor, P., Moran, M.F., Mcglade, C.J., 2015. Comprehensive identification of phosphorylation sites on the Numb endocytic adaptor protein. Proteomics 15, 434–446. https://doi.org/10.1002/pmic.201400232

Kumar, A., Velloso, C.P., Imokawa, Y., Brockes, J.P., 2004. The regenerative plasticity of

isolated urodele myofibers and its dependence on Msx1. PLoS Biol. 2. https://doi.org/10.1371/journal.pbio.0020218

Kwon, S.H., Lee, T.J., Park, J., Hwang, J.E., Jin, M., Jang, H.K., Hwang, N.S., Kim, B.S., 2013. Modulation of BMP-2-Induced chondrogenic versus osteogenic differentiation of human mesenchymal stem cells by cell-specific extracellular matrices. Tissue Eng. - Part A 19, 49–58. https://doi.org/10.1089/ten.tea.2012.0245

L'Honoré, A., Coulon, V., Marcil, A., Lebel, M., Lafrance-Vanasse, J., Gage, P., Camper, S., Drouin, J., 2007. Sequential expression and redundancy of Pitx2 and Pitx3 genes during muscle development. Dev. Biol. 307, 421–433. https://doi.org/10.1016/j.ydbio.2007.04.034

Lacraz, G., Rouleau, A.J., Couture, V., Söllrald, T., Drouin, G., Veillette, N., Grandbois, M., Grenier, G., 2015. Increased stiffness in aged skeletal muscle impairs muscle progenitor cell proliferative activity. PLoS One 10, 1–13. https://doi.org/10.1371/journal.pone.0136217

Lauing, K.L., Cortes, M., Domowicz, M.S., Henry, J.G., Baria, A.T., Schwartz, N.B., 2014. Aggrecan is required for growth plate cytoarchitecture and differentiation. Dev. Biol. 396, 224–236. https://doi.org/10.1016/j.ydbio.2014.10.005

Le Roux, I., Konge, J., Le Cam, L., Flamant, P., Tajbakhsh, S., 2015. Numb is required to prevent p53-dependent senescence following skeletal muscle injury. Nat. Commun. 6, 8528. https://doi.org/10.1038/ncomms9528

Lee, A.S.J., Harris, J., Bate, M., Vijayraghavan, K., Fisher, L., Tajbakhsh, S., Duxson, M., 2013. Initiation of primary myogenesis in amniote limb muscles. Dev. Dyn. 242, 1043–1055. https://doi.org/10.1002/dvdy.23998

Lee, H.-J., Goring, W., Ochs, M., Muhlfeld, C., Steding, G., Paprotta, I., Engel, W., Adham, I.M., 2004. Sox15 Is Required for Skeletal Muscle Regeneration. Mol. Cell. Biol. 24, 8428–8436. https://doi.org/10.1128/mcb.24.19.8428-8436.2004

Lepper, C., Partridge, T.A., Fan, C., 2011. An absolute requirement for Pax7-positive satellite cells in acute injury-induced skeletal muscle regeneration 3646, 3639–3646. https://doi.org/10.1242/dev.067595

Leung, V.Y.L., Gao, B., Leung, K.K.H., Melhado, I.G., Wynn, S.L., Au, T.Y.K., Dung, N.W.F., Lau, J.Y.B., Mak, A.C.Y., Chan, D., Cheah, K.S.E., 2011. SOX9 governs differentiation stage-specific gene expression in growth plate chondrocytes via direct concomitant transactivation and repression. PLoS Genet. 7, 1–16. https://doi.org/10.1371/journal.pgen.1002356

Li, X., Mcfarland, D.C., Velleman, S.G., 2008. Extracellular matrix proteoglycan decorin-mediated myogenic satellite cell responsiveness to transforming growth factor- b 1 during cell proliferation and differentiation Decorin and transforming growth factor- b 1 in satellite cells 35, 263–273. https://doi.org/10.1016/j.domaniend.2008.06.002

Li, Y., Li, J., Zhu, J., Sun, B., Branca, M., Tang, Y., Foster, W., Xiao, X., Huard, J., 2007. Decorin gene transfer promotes muscle cell differentiation and muscle

regeneration. Mol. Ther. 15, 1616–1622. https://doi.org/10.1038/sj.mt.6300250

Liao, J., Hu, N., Zhou, N., Lin, L., Zhao, C., Yi, S., Fan, T., Bao, W., Liang, X., Chen, H., Xu, W., Chen, C., Cheng, Q., Zeng, Y., Si, W., Yang, Z., Huang, W., 2014. Sox9 potentiates BMP2-induced chondrogenic differentiation and inhibits BMP2-induced osteogenic differentiation. PLoS One 9. https://doi.org/10.1371/journal.pone.0089025

Lim, J., Tu, X., Choi, K., Akiyama, H., Mishina, Y., Long, F., 2015. BMP-Smad4 signaling is required for precartilaginous mesenchymal condensation independent of Sox9 in the mouse. Dev. Biol. 400, 132–138. https://doi.org/10.1016/j.ydbio.2015.01.022

Liu, L., Lanner, F., Lendahl, U., Das, D., 2011. Numblike and Numb differentially affect p53 and Sonic Hedgehog signaling. Biochem. Biophys. Res. Commun. 413, 426–431. https://doi.org/10.1016/j.bbrc.2011.08.108

Liu, Z., Lavine, K.J., Hung, I.H., Ornitz, D.M., 2007. FGF18 is required for early chondrocyte proliferation, hypertrophy and vascular invasion of the growth plate. Dev. Biol. 302, 80–91. https://doi.org/10.1016/j.ydbio.2006.08.071

Lozano-Velasco, E., Contreras, A., Crist, C., Hernández-Torres, F., Franco, D., Aránega, A.E., 2011. Pitx2c modulates Pax3+/Pax7+ cell populations and regulates Pax3 expression by repressing miR27 expression during myogenesis. Dev. Biol. 357, 165–178. https://doi.org/10.1016/j.ydbio.2011.06.039

Luo, D., Renault, V.M., Rando, T.A., 2005. The regulation of Notch signaling in muscle stem cell activation and postnatal myogenesis. Semin. Cell Dev. Biol. 16, 612–622. https://doi.org/10.1016/j.semcdb.2005.07.002

Luo, X., Luo, Z., Zhang, Z., Yang, H., Lai, B., Yao, Q., Xiao, L., Wang, N., 2016. Homocysteine upregulates hepcidin expression through BMP6/SMAD signaling pathway in hepatocytes. Biochem. Biophys. Res. Commun. 471, 303–308. https://doi.org/10.1016/j.bbrc.2016.02.001

Mashinchian, O., Pisconti, A., Le Moal, E., Bentzinger, C.F., 2018. The Muscle Stem Cell Niche in Health and Disease, 1st ed, Current Topics in Developmental Biology. Elsevier Inc. https://doi.org/10.1016/bs.ctdb.2017.08.003

Mathur, A.B., Collinsworth, A.M., Reichert, W.M., Kraus, W.E., Truskey, G.A., 2001. Endothelial, cardiac muscle and skeletal muscle exhibit different viscous and elastic properties as determined by atomic force microscopy. J. Biomech. 34, 1545–1553. https://doi.org/10.1016/S0021-9290(01)00149-X

Mauro, A., 1961. Satellite cell of skeletal muscle fibers. J. Biophys. Biochem. Cytol. 9, 493–495. https://doi.org/10.1083/jcb.9.2.493

McCroskery, S., Thomas, M., Maxwell, L., Sharma, M., Kambadur, R., 2003. Myostatin negatively regulates satellite cell activation and self-renewal. J. Cell Biol. 162, 1135–1147. https://doi.org/10.1083/jcb.200207056

McCroskery, S., Thomas, M., Platt, L., Hennebry, A., Nishimura, T., McLeay, L., Sharma, M., Kambadur, R., 2005. Improved muscle healing through enhanced regeneration and reduced fibrosis in myostatin-null mice. J. Cell Sci. 118, 3531–3541. https://doi.org/10.1242/jcs.02482

McFarlane, C., Hui, G.Z., Amanda, W.Z.W., Lau, H.Y., Lokireddy, S., Xiaojia, G., Mouly, V., Butler-Browne, G., Gluckman, P.D., Sharma, M., Kambadur, R., 2011. Human myostatin negatively regulates human myoblast growth and differentiation. Am. J. Physiol. - Cell Physiol. 301, 195–203. https://doi.org/10.1152/ajpcell.00012.2011

McGill, M.A., McGlade, C.J., 2003. Mammalian Numb proteins promote Notch1 receptor ubiquitination and degradation of the Notch1 intracellular domain. J. Biol. Chem. 278, 23196–23203. https://doi.org/10.1074/jbc.M302827200

Meeson, A.P., Shi, X., Alexander, M.S., Williams, R.S., Allen, R.E., Jiang, N., Adham, I.M., Goetsch, S.C., Hammer, R.E., Garry, D.J., 2007. Sox15 and Fhl3 transcriptionally coactivate Foxk1 and regulate myogenic progenitor cells. EMBO J. 26, 1902–1912. https://doi.org/10.1038/sj.emboj.7601635

Michie, K.A., Bermeister, A., Robertson, N.O., Goodchild, S.C., Curmi, P.M.G., 2019. Two Sides of the Coin: Ezrin/Radixin/Moesin and Merlin Control Membrane Structure and Contact Inhibition. Int. J. Mol. Sci. 20. https://doi.org/10.3390/ijms20081996

Mihailovskaa, E., Raitha, M., Valenciaa, R.G., Fischera, I., Banchaabouchib, M. Al, Herbstc, R., Wiche, G., 2014. Neuromuscular synapse integrity requires linkage of acetylcholine receptors to postsynaptic intermediate filament networks via rapsyn-plectin 1f complexes. Mol. Biol. Cell 25, 4130–4149. https://doi.org/10.1091/mbc.E14-06-1174

Miron-Mendoza, M., Seemann, J., Grinnell, F., 2010. The differential regulation of cell motile activity through matrix stiffness and porosity in three dimensional collagen matrices. Biomaterials 31, 6425–6435. https://doi.org/10.1016/j.biomaterials.2010.04.064

Montarras, D., Morgan, J., Collins, C., Relaix, F., Zaffran, S., Cumano, A., Partridge, T., Buckingham, M., 2005. Direct Isolation of Satellite Cells for Skeletal Muscle Regeneration. Science (80-.). 309, 2064–2067. https://doi.org/10.1126/science.1114758

Morrison, J.I., Lööf, S., He, P., Simon, A., 2006. Salamander limb regeneration involves the activation of a multipotent skeletal muscle satellite cell population. J. Cell Biol. 172, 433–440. https://doi.org/10.1083/jcb.200509011

Nishimura, T., Fukata, Y., Kato, K., Yamaguchi, T., Matsuura, Y., Kamiguchi, H., Kaibuchi, K., 2003. CRMP-2 regulates polarized Numb-mediated endocytosis for axon growth. Nat. Cell Biol. 5, 819–826. https://doi.org/10.1038/ncb1039

Nishimura, T., Kaibuchi, K., 2007. Numb Controls Integrin Endocytosis for Directional Cell Migration with aPKC and PAR-3. Dev. Cell 13, 15–28. https://doi.org/10.1016/j.devcel.2007.05.003

Öcalan, M., Goodman, S.L., Kühl, U., Hauschka, S.D., von der Mark, K., 1988. Laminin alters cell shape and stimulates motility and proliferation of murine skeletal myoblasts. Dev. Biol. 125, 158–167. https://doi.org/10.1016/0012-1606(88)90068-1

Odelberg, S.J., Kollhoff, A., Keating, M.T., 2000. Dedifferentiation of Mammalian Myotubes Induced by msx1 Generation of C2C12 Clones Containing. Cell 103,

1099–1109.

Ono, Y., Boldrin, L., Knopp, P., Morgan, J.E., Zammit, P.S., 2010. Muscle satellite cells are a functionally heterogeneous population in both somite-derived and branchiomeric muscles. Dev. Biol. 337, 29–41. https://doi.org/10.1016/j.ydbio.2009.10.005

Osses, N., Brandan, E., 2002. ECM is required for skeletal muscle differentiation independently of muscle regulatory factor expression. Am. J. Physiol. - Cell Physiol. 282. https://doi.org/10.1152/ajpcell.00322.2001

Ozeki, N., Jethanandani, P., Nakamura, H., Ziober, B.L., Kramer, R.H., 2007. Modulation of satellite cell adhesion and motility following BMP2-induced differentiation to osteoblast lineage. Biochem. Biophys. Res. Commun. 353, 54–59. https://doi.org/10.1016/j.bbrc.2006.11.110

Padilla, C., Ramos, A., González, N., Isaacs, M., Zacconi, F., Olguín, H.C., Valenzuela, L.M., 2017. Chitosan/poly-octanoic acid 2-thiophen-3-yl-ethyl ester blends as a scaffold to maintain myoblasts regeneration potential in vitro. J. Biomed. Mater. Res. - Part A 105, 118–130. https://doi.org/10.1002/jbm.a.35889

Pagel, C.N., Wasgewatte Wijesinghe, D.K., Taghavi Esfandouni, N., Mackie, E.J., 2014. Osteopontin, inflammation and myogenesis: Influencing regeneration, fibrosis and size of skeletal muscle. J. Cell Commun. Signal. 8, 95–103. https://doi.org/10.1007/s12079-013-0217-3

Park, J., Kim, Y., Lee, S., Park, J.J., Park, Z.Y., Sun, W., Kim, H., Chang, S., 2010. SNX18 shares a redundant role with SNX9 and modulates endocytic trafficking at the plasma membrane. J. Cell Sci. 123, 1742–1750. https://doi.org/10.1242/jcs.064170

Parker, S.B., Eichele, G., Zhang, P., Rawls, A., Sands, A.T., Bradley, A., Olson, E.N., Harper, J.W., Elledge, S.J., 1995. p53-independent expression of p21Cip1 in muscle and other terminally differentiating cells. Science (80-.). 267, 1024–1027. https://doi.org/10.1126/science.7863329

Partridge, T.A., Grounds, M., Sloper, J.C., 1978. Evidence of fusion between host and donor myoblasts in skeletal muscle grafts. Nature 273, 306–308. https://doi.org/10.1038/273306a0

Péault, B., Rudnicki, M., Torrente, Y., Cossu, G., Tremblay, J.P., Partridge, T., Gussoni, E., Kunkel, L.M., Huard, J., 2007. Stem and progenitor cells in skeletal muscle development, maintenance, and therapy. Mol. Ther. 15, 867–877. https://doi.org/10.1038/mt.sj.6300145

Pece, S., Confalonieri, S., R. Romano, P., Di Fiore, P.P., 2011. NUMB-ing down cancer by more than just a NOTCH. Biochim. Biophys. Acta - Rev. Cancer 1815, 26–43. https://doi.org/10.1016/j.bbcan.2010.10.001

Perniconi, B., Coletti, D., Aulino, P., Costa, A., Aprile, P., Santacroce, L., Chiaravalloti, E., Coquelin, L., Chevallier, N., Teodori, L., Adamo, S., Marrelli, M., Tatullo, M., 2014. Muscle acellular scaffold as a biomaterial: Effects on C2C12 cell differentiation and interaction with the murine host environment. Front. Physiol. 5, 1–13. https://doi.org/10.3389/fphys.2014.00354

Plumb, D.A., Ferrara, L., Torbica, T., Knowles, L., Mironov, A., Kadler, K.E., Briggs, M.D., Boot-Handford, R.P., 2011. Collagen XXVII organises the pericellular matrix in the growth plate. PLoS One 6. https://doi.org/10.1371/journal.pone.0029422

Porrello, E.R., Mahmoud, A.I., Simpson, E., Hill, J.A., Richardson, J.A., Olson, E.N., Sadek, H.A., 2011. Transient regenerative potential of the neonatal mouse heart. Science (80-.). 331, 1078–1080. https://doi.org/10.1126/science.1200708

Pumberger, M., Qazi, T.H., Ehrentraut, M.C., Textor, M., Kueper, J., Stoltenburg-Didinger, G., Winkler, T., von Roth, P., Reinke, S., Borselli, C., Perka, C., Mooney, D.J., Duda, G.N., Geißler, S., 2016. Synthetic niche to modulate regenerative potential of MSCs and enhance skeletal muscle regeneration. Biomaterials 99, 95–108. https://doi.org/10.1016/j.biomaterials.2016.05.009

Qazi, T.H., Mooney, D.J., Pumberger, M., Gei??ler, S., Duda, G.N., 2015. Biomaterials based strategies for skeletal muscle tissue engineering: Existing technologies and future trends. Biomaterials 53, 502–521. https://doi.org/10.1016/j.biomaterials.2015.02.110

Qu-Petersen, Z., Deasy, B., Jankowski, R., Ikezawa, M., Cummins, J., Pruchnic, R., Mytinger, J., Cao, B., Gates, C., Wernig, A., Huard, J., 2002. Identification of a novel population of muscle stem cells in mice: Potential for muscle regeneration. J. Cell Biol. 157, 851–864. https://doi.org/10.1083/jcb.200108150

Quarta, M., Brett, J.O., DiMarco, R., De Morree, A., Boutet, S.C., Chacon, R., Gibbons, M.C., Garcia, V.A., Su, J., Shrager, J.B., Heilshorn, S., Rando, T.A., 2016. An artificial niche preserves the quiescence of muscle stem cells and enhances their therapeutic efficacy. Nat. Biotechnol. 34, 752–759. https://doi.org/10.1038/nbt.3576

Raines, A.M., Magella, B., Adam, M., Potter, S.S., 2015. Key pathways regulated by HoxA9,10,11/HoxD9,10,11 during limb development. BMC Dev. Biol. 15, 1–15. https://doi.org/10.1186/s12861-015-0078-5

Rajendran, D., Zhang, Y., Berry, D.M., McGlade, C.J., 2016. Regulation of Numb isoform expression by activated ERK signaling. Oncogene 1–12. https://doi.org/10.1038/onc.2016.69

Re'em-Kalma, Y., Lamb, T., Frank, D., 1995. Competition between noggin and bone morphogenetic protein 4 activities may regulate dorsalization during Xenopus development. Proc. Natl. Acad. Sci. U. S. A. 92, 12141–12145. https://doi.org/10.1073/pnas.92.26.12141

Reddi, A.H., Gay, R., Gay, S., Miller, E.J., 1977. Transitions in collagen types during matrix-induced cartilage, bone, and bone marrow formation. Proc. Natl. Acad. Sci. U. S. A. 74, 5589–5592. https://doi.org/10.1073/pnas.74.12.5589

Relaix, F., Zammit, P.S., 2012. Satellite cells are essential for skeletal muscle regeneration: the cell on the edge returns centre stage. Development 139, 2845–2856. https://doi.org/10.1242/dev.069088

Reshef, R., Maroto, M., Lassar, A.B., 1998. Regulation of dorsal somitic cell fates: BMPs and Noggin control the timing and pattern of myogenic regulator expression. Genes

Dev. 12, 290–303. https://doi.org/10.1101/gad.12.3.290

Rezniczek, G.A., Winter, L., Walko, G., Wiche, G., 2016. Functional and Genetic Analysis of Plectin in Skin and Muscle. Methods Enzymol. 569, 235–259. https://doi.org/10.1016/bs.mie.2015.05.003

Rhyu, M.S., Jan, L.Y., Jan, Y.N., 1994. Asymmetric distribution of numb protein during division of the sensory organ precursor cell confers distinct fates to daughter cells. Cell 76, 477–491. https://doi.org/10.1016/0092-8674(94)90112-0

Robinson, M.D., McCarthy, D.J., Smyth, G.K., 2009. edgeR: A Bioconductor package for differential expression analysis of digital gene expression data. Bioinformatics 26, 139–140. https://doi.org/10.1093/bioinformatics/btp616

Rodgers, J.T., King, K.Y., Brett, J.O., Cromie, M.J., Charville, G.W., Maguire, K.K., Brunson, C., Mastey, N., Liu, L., Tsai, C.R., Goodell, M.A., Rando, T.A., 2014. MTORC1 controls the adaptive transition of quiescent stem cells from G 0 to GAlert. Nature 510, 393–396. https://doi.org/10.1038/nature13255

Rodgers, J.T., Schroeder, M.D., Ma, C., Rando, T.A., 2017. HGFA Is an Injury-Regulated Systemic Factor that Induces the Transition of Stem Cells into GAlert. Cell Rep. 19, 479–486. https://doi.org/10.1016/j.celrep.2017.03.066

Rudnicki, M., Chang, N., 2014. Satellite Cells: The Architects of Skeletal Muscle, in: Current Topics in Dev Bio.

Rudnicki, M., Williams, B.O., 2015. Wnt signaling in bone and muscle. Bone 80, 60–66. https://doi.org/10.1016/j.bone.2015.02.009

Ryall, J.G., Dell'Orso, S., Derfoul, A., Juan, A., Zare, H., Feng, X., Clermont, D., Koulnis, M., Gutierrez-Cruz, G., Fulco, M., Sartorelli, V., 2015. The NAD+-dependent sirt1 deacetylase translates a metabolic switch into regulatory epigenetics in skeletal muscle stem cells. Cell Stem Cell 16, 171–183. https://doi.org/10.1016/j.stem.2014.12.004

Sacco, A., Doyonnas, R., Kraft, P., Vitorovic, S., Blau, H.M., 2008. Self-renewal and expansion of single transplanted muscle stem cells. Nature 456, 502–506. https://doi.org/10.1038/nature07384

Sambasivan, R., Yao, R., Kissenpfennig, A., Wittenberghe, L. Van, Paldi, A., Gayraud-morel, B., Guenou, H., Malissen, B., Tajbakhsh, S., Galy, A., Sambasivan, R., Yao, R., Kissenpfennig, A., Wittenberghe, L. Van, 2011. Erratum to Pax7-expressing satellite cells are indispensable for adult skeletal muscle regeneration (Development (2011), 138 (3647-3656)). Development 138, 4333. https://doi.org/10.1242/dev.073601

Sandoval-Guzmán, T., Wang, H., Khattak, S., Schuez, M., Roensch, K., Nacu, E., Tazaki, A., Joven, A., Tanaka, E.M., Simon, A., 2014. Fundamental differences in dedifferentiation and stem cell recruitment during skeletal muscle regeneration in two salamander species. Cell Stem Cell 14, 174–187. https://doi.org/10.1016/j.stem.2013.11.007

Sanes, J.R., 2003. The basement membrane/basal lamina of skeletal muscle. J. Biol. Chem. 278, 12601–12604. https://doi.org/10.1074/jbc.R200027200

Santolini, E., Puri, C., Salcini, A.E., Gagliani, M.C., Pelicci, P.G., Tacchetti, C., Di Fiore, P.P., 2000. Numb is an endocytic protein. J. Cell Biol. 151, 1345–1351. https://doi.org/10.1083/jcb.151.6.1345

Sartori, R., Gregorevic, P., Sandri, M., 2014. TGF?? and BMP signaling in skeletal muscle: Potential significance for muscle-related disease. Trends Endocrinol. Metab. 25, 464–471. https://doi.org/10.1016/j.tem.2014.06.002

Satokata, I., Ma, L., Ohshima, H., Bei, M., Ian, W., Nishizawa, K., Maeda, T., Takano, Y., Uchiyama, M., Heaney, S., Peters, H., Tang, Z., Maxson, R., Maas, R., 2000. Msx2 deficiency in mice causes pleiotropic defects in bone growth and ectodermal organ formation. Nat. Genet. 24, 391–395. https://doi.org/10.1038/74231

Scarda, A., Franzin, C., Milan, G., Sanna, M., Dal Pr, C., Pagano, C., Boldrin, L., Piccoli, M., Trevellin, E., Granzotto, M., Gamba, P., Federspil, G., De Coppi, P., Vettor, R., 2010. Increased adipogenic conversion of muscle satellite cells in obese Zucker rats. Int. J. Obes. 34, 1319–1327. https://doi.org/10.1038/ijo.2010.47

Schmitt, B., Ringe, J., Häupl, T., Notter, M., Manz, R., Burmester, G.R., Sittinger, M., Kaps, C., 2003. BMP2 initiates chondrogenic lineage development of adult human mesenchymal stem cells in high-density culture. Differentiation 71, 567–577. https://doi.org/10.1111/j.1432-0436.2003.07109003.x

Sciorati, C., Clementi, E., Manfredi, A.A., Rovere-Querini, P., 2015. Fat deposition and accumulation in the damaged and inflamed skeletal muscle: Cellular and molecular players. Cell. Mol. Life Sci. 72, 2135–2156. https://doi.org/10.1007/s00018-015-1857-7

Seale, P., Bjork, B., Yang, W., Kajimura, S., Chin, S., Kuang, S., Scimè, A., Devarakonda, S., Conroe, H.M., Erdjument-Bromage, H., Tempst, P., Rudnicki, M.A., Beier, D.R., Spiegelman, B.M., 2008. PRDM16 controls a brown fat/skeletal muscle switch. Nature 454, 961–967. https://doi.org/10.1038/nature07182

Seale, P., Sabourin, L.A., Girgis-Gabardo, A., Mansouri, A., Gruss, P., Rudnicki, M., 2000. Pax7 is required for the specification of myogenic satellite cells. Cell 102, 777–786. https://doi.org/10.1016/S0092-8674(00)00066-0

Sengupta, D., Gilbert, P.M., Johnson, K.J., Blau, H.M., Heilshorn, S.C., 2012. Protein-Engineered Biomaterials to Generate Human Skeletal Muscle Mimics. Adv. Healthc. Mater. 1, 785–789. https://doi.org/10.1002/adhm.201200195

Shea, C.M., Edgar, C.M., Einhorn, T.A., Gerstenfeld, L.C., 2003. BMP Treatment of C3H10T1/2 Mesenchymal Stem Cells Induces Both Chondrogenesis and Osteogenesis. J. Cell. Biochem. 90, 1112–1127. https://doi.org/10.1002/jcb.10734

Shefer, G., Wleklinski-Lee, M., Yablonka-Reuveni, Z., 2004. Skeletal muscle satellite cells can spontaneously enter an alternative mesenchymal pathway. J. Cell Sci. 117, 5393–5404. https://doi.org/10.1242/jcs.01419

Shefer, G., Yablonka-Reuveni, Z., 2007. Reflections on lineage potential of skeletal muscle satellite cells: Do they sometimes go MAD? Crit. Rev. Eukaryot. Gene Expr. 17, 13–29. https://doi.org/10.1615/critreveukargeneexpr.v17.i1.20

Shen, B., Wei, A., Whittaker, S., Williams, L.A., Tao, H., Ma, D.D.F., Diwan, A.D., 2010.

The role of BMP-7 in chondrogenic and osteogenic differentiation of human bone marrow multipotent mesenchymal stromal cells in vitro. J. Cell. Biochem. 109, 406–416. https://doi.org/10.1002/jcb.22412

Shen, Q., Zhong, W., Jan, Y.N., Temple, S., 2002. Asymmetric Numb distribution is critical for asymmetric cell division of mouse cerebral cortical stem cells and neuroblasts. Development 129, 4843–4853.

Shenje, L.T., Andersen, P., Uosaki, H., Fernandez, L., Rainer, P.P., Cho, G.S., Lee, D.I., Zhong, W., Harvey, R.P., Kass, D.A., Kwon, C., 2014. Precardiac deletion of Numb and Numblike reveals renewal of cardiac progenitors. Elife 3, e02164. https://doi.org/10.7554/eLife.02164

Shu, B., Zhang, M., Xie, R., Wang, M., Jin, H., Hou, W., Tang, D., Harris, S.E., Mishina, Y., O'Keefe, R.J., Hilton, M.J., Wang, Y., Chen, D., 2011. BMP2, but not BMP4, is crucial for chondrocyte proliferation and maturation during endochondral bone development. J. Cell Sci. 124, 3428–3440. https://doi.org/10.1242/jcs.083659

Singh, M., Dalal, S., Singh, K., 2014. Osteopontin: At the cross-roads of myocyte survival and myocardial function. Life Sci. 118, 1–6. https://doi.org/10.1016/j.lfs.2014.09.014

Smith, C.A., Dho, S.E., Donaldson, J., Tepass, U., McGlade, C.J., 2004. The Cell Fate Determinant Numb Interacts with EHD/ Rme-1 Family Proteins and Has a Role in Endocytic Recycling. Mol Biol Cell 15, 5318–5328. https://doi.org/10.1091/mbc.E04

Song, Y., Lu, B., 2012. Interaction of notch signaling modulator numb with alpha-adaptin regulates endocytosis of notch pathway components and cell fate determination of neural stem cells. J. Biol. Chem. 287, 17716–17728. https://doi.org/10.1074/jbc.M112.360719

Soofi, S.S., Last, J.A., Liliensiek, S.J., Nealey, P.F., Murphy, C.J., 2009. The elastic modulus of Matrigel™ as determined by atomic force microscopy. J. Struct. Biol. 167, 216–219. https://doi.org/10.1016/j.jsb.2009.05.005

Yi, S.E., Daluiski, A., Pederson, R., Rosen, V., 2000. The type i BMP receptor ACVR1/ALK2 is required for chondrogenesis during development. Development 127, 621–630. https://doi.org/10.1002/jbmr.2385

T. Komori, H. Yagi, S. Nomura, A. Yamaguchi, K. Sasaki, K. Deguchi, Y. Shimizu, R. T. Bronson, Y. H. Gao, M. Inada, M. Sato, R. Okamoto, Y. Kitamura, S. Yoshiki, T.K., 1997. Targeted disruption of Cbfa1 Results in a Complete Lack of Bone Formation owning to Maturational Arrest of Osteoblasts. Cell 89, 755–764.

Takács, R., Matta, C., Somogyi, C., Juhász, T., Zákány, R., 2013. Comparative analysis of osteogenic/chondrogenic differentiation potential in primary limb bud-derived and C3H10T1/2 cell line-based mouse micromass cultures. Int. J. Mol. Sci. 14, 16141–16167. https://doi.org/10.3390/ijms140816141

Takarada, T., Hinoi, E., Nakazato, R., Ochi, H., Xu, C., Tsuchikane, A., Takeda, S., Karsenty, G., Abe, T., Kiyonari, H., Yoneda, Y., 2013. An analysis of skeletal development in osteoblast-specific and chondrocyte-specific runt-related

transcription factor-2 (Runx2) knockout mice. J. Bone Miner. Res. 28, 2064–2069. https://doi.org/10.1002/jbmr.1945

Tokumitsu, H., Hatano, N., Inuzuka, H., Sueyoshi, Y., Yokokura, S., Ichimura, T., Nozaki, N., Kobayashi, R., 2005. Phosphorylation of Numb family proteins. Possible involvement of Ca2+/calmodulin-dependent protein kinases. J. Biol. Chem. 280, 35108–35118. https://doi.org/10.1074/jbc.M503912200

Toriya, M., Tokunaga, A., Sawamoto, K., Nakao, K., Okano, H., 2006. Distinct functions of human numb isoforms revealed by misexpression in the neural stem cell lineage in the Drosophila larval brain. Dev. Neurosci. 28, 142–155. https://doi.org/10.1159/000090760

Trapnell, C., Pachter, L., Salzberg, S.L., 2009. TopHat: Discovering splice junctions with RNA-Seq. Bioinformatics 25, 1105–1111. https://doi.org/10.1093/bioinformatics/btp120

Trapnell, C., Williams, B.A., Pertea, G., Mortazavi, A., Kwan, G., Van Baren, M.J., Salzberg, S.L., Wold, B.J., Pachter, L., 2010. Transcript assembly and quantification by RNA-Seq reveals unannotated transcripts and isoform switching during cell differentiation. Nat. Biotechnol. 28, 511–515. https://doi.org/10.1038/nbt.1621

Tsuji, K., Bandyopadhyay, A., Harfe, B.D., Cox, K., Kakar, S., Gerstenfeld, L., Einhorn, T., Tabin, C.J., Rosen, V., 2006. BMP2 activity, although dispensable for bone formation, is required for the initiation of fracture healing. Nat. Genet. 38, 1424–1429. https://doi.org/10.1038/ng1916

Umansky, K.B., Gruenbaum-Cohen, Y., Tsoory, M., Feldmesser, E., Goldenberg, D., Brenner, O., Groner, Y., 2015. Runx1 Transcription Factor Is Required for Myoblasts Proliferation during Muscle Regeneration. PLoS Genet. 11, 1–31. https://doi.org/10.1371/journal.pgen.1005457

Urciuolo, A., Quarta, M., Morbidoni, V., Gattazzo, F., Molon, S., Grumati, P., Montemurro, F., Tedesco, F.S., Blaauw, B., Cossu, G., Vozzi, G., Rando, T.A., Bonaldo, P., 2013. Collagen VI regulates satellite cell self-renewal and muscle regeneration. Nat. Commun. 4. https://doi.org/10.1038/ncomms2964

Verdi, J.M., Bashirullah, a, Goldhawk, D.E., Kubu, C.J., Jamali, M., Meakin, S.O., Lipshitz, H.D., 1999. Distinct human NUMB isoforms regulate differentiation vs. proliferation in the neuronal lineage. Proc. Natl. Acad. Sci. U. S. A. 96, 10472–10476. https://doi.org/10.1073/pnas.96.18.10472

Vettor, R., Milan, G., Franzin, C., Sanna, M., De Coppi, P., Rizzuto, R., Federspil, G., 2009. The origin of intermuscular adipose tissue and its pathophysiological implications. Am. J. Physiol. - Endocrinol. Metab. 297. https://doi.org/10.1152/ajpendo.00229.2009

Wada, M.R., Inagawa-Ogashiwa, M., Shimizu, S., Yasumoto, S., Hashimoto, N., 2002. Generation of different fates from multipotent muscle stem cells. Development 129, 2987–2995.

Wang, H., Noulet, F., Edom-Vovard, F., Le Grand, F., Duprez, D., 2010. Bmp Signaling at the Tips of Skeletal Muscles Regulates the Number of Fetal Muscle Progenitors and

Satellite Cells during Development. Dev. Cell 18, 643–654. https://doi.org/10.1016/j.devcel.2010.02.008

Wang, L., Cao, L., Shansky, J., Wang, Z., Mooney, D.J., Vandenburgh, H., 2014. Minimally Invasive Approach to the Repair of Injured Skeletal Muscle With a Shape-memory Scaffold. Mol. Ther. 22, 1441–9. https://doi.org/10.1038/mt.2014.78

Wang, Z., Sandiford, S., Wu, C., Li, S.S.C., 2009. Numb regulates cell-cell adhesion and polarity in response to tyrosine kinase signalling. EMBO J. 28, 2360–2373. https://doi.org/10.1038/emboj.2009.190

Wen, Y., Bi, P., Liu, W., Asakura, A., Keller, C., Kuang, S., 2012. Constitutive Notch Activation Upregulates Pax7 and Promotes the Self-Renewal of Skeletal Muscle Satellite Cells. Mol. Cell. Biol. 32, 2300–2311. https://doi.org/10.1128/mcb.06753-11

Wilson, A., Ardiet, D., Saner, C., Vilain, N., Beermann, F., Aguet, M., Macdonald, H.R., Zilian, O., 2007. Normal hemopoiesis and lymphopoiesis in the combined absence of numb and numblike. J. Immunol. 178, 6746–51. https://doi.org/178/11/6746 [pii]

Wilson, D.G., Phamluong, K., Lin, W.Y., Barck, K., Carano, R.A.D., Diehl, L., Peterson, A.S., Martin, F., Solloway, M.J., 2012. Chondroitin sulfate synthase 1 (Chsy1) is required for bone development and digit patterning. Dev. Biol. 363, 413–425. https://doi.org/10.1016/j.ydbio.2012.01.005

Winbanks, C.E., Chen, J.L., Qian, H., Liu, Y., Bernardo, B.C., Beyer, C., Watt, K.I., Thomson, R.E., Connor, T., Turner, B.J., McMullen, J.R., Larsson, L., McGee, S.L., Harrison, C.A., Gregorevic, P., 2013. The bone morphogenetic protein axis is a positive regulator of skeletal muscle mass. J. Cell Biol. 203, 345–357. https://doi.org/10.1083/jcb.201211134

Wright, E., Hargrave, M.R., Christiansen, J., Cooper, L., Kun, J., Evans, T., Gangadharan, U., Greenfield, A., Koopman, P., 1995. The Sry-related gene Sox9 is expressed during chondrogenesis in mouse embryos. Nature 9, 15–20.

Fan, X., Cui, L., Zeng, Y., Song, W., Gaur, U., Yang, M., 2019. 14-3-3 Proteins Are on the Crossroads of Cancer, Aging, and Age-Related Neurodegenerative Disease. Int. J. Mol. Sci. 20. https://doi.org/10.18632/oncotarget.3896

Yang, H.S., Ieronimakis, N., Tsui, J.H., Kim, H.N., Suh, K.Y., Reyes, M., Kim, D.H., 2014. Nanopatterned muscle cell patches for enhanced myogenesis and dystrophin expression in a mouse model of muscular dystrophy. Biomaterials 35, 1478–1486. https://doi.org/10.1016/j.biomaterials.2013.10.067

Yang, J., Bücker, S., Jungblut, B., Böttger, T., Cinnamon, Y., Tchorz, J., Müller, M., Bettler, B., Harvey, R., Sun, Q.Y., Schneider, A., Braun, T., 2012. Inhibition of Notch2 by Numb/Numblike controls myocardial compaction in the heart. Cardiovasc. Res. 96, 276–285. https://doi.org/10.1093/cvr/cvs250

Yilmaz, A., Engeler, R., Constantinescu, S., Kokkaliaris, K.D., Dimitrakopoulos, C., Schroeder, T., Beerenwinkel, N., Paro, R., 2015. Ectopic expression of Msx2 in

mammalian myotubes recapitulates aspects of amphibian muscle dedifferentiation. Stem Cell Res. 15, 542–553. https://doi.org/10.1016/j.scr.2015.09.012

Yin, H., Price, F., Rudnicki, M., 2013. Satellite cells and the muscle stem cell niche. Physiol. Rev. 93, 23–67. https://doi.org/10.1152/physrev.00043.2011

Yoon, B.S., Ovchinnikov, D.A., Yoshii, I., Mishina, Y., Behringer, R.R., Lyons, K.M., 2005. Bmpr1a and Bmpr1b have overlapping functions and are essential for chondrogenesis in vivo. Proc. Natl. Acad. Sci. U. S. A. 102, 5062–5067. https://doi.org/10.1073/pnas.0500031102

Yoshida, T., Tokunaga, A., Nakao, K., Okano, H., 2003. Distinct expression patterns of splicing isoforms of mNumb in the endocrine lineage of developing pancreas. Differentiation 71, 486–495. https://doi.org/10.1046/j.1432-0436.2003.7108006.x

Yu, L., Han, M., Yan, M., Lee, E.C., Lee, J., Muneoka, K., 2010. BMP signaling induces digit regeneration in neonatal mice. Development 137, 551–559. https://doi.org/10.1242/dev.042424

Yue, F., Cheng, Y., Breschi, A., Vierstra, J., Wu, W., Ryba, T., Sandstrom, R., Ma, Z., Davis, C., Pope, B.D., Shen, Y., Pervouchine, D.D., Djebali, S., Thurman, R.E., Kaul, R., Rynes, E., Kirilusha, A., Marinov, G.K., Williams, B.A., Trout, D., Amrhein, H., Fisher-Aylor, K., Antoshechkin, I., DeSalvo, G., See, L.H., Fastuca, M., Drenkow, J., Zaleski, C., Dobin, A., Prieto, P., Lagarde, J., Bussotti, G., Tanzer, A., Denas, O., Li, K., Bender, M.A., Zhang, M., Byron, R., Groudine, M.T., McCleary, D., Pham, L., Ye, Z., Kuan, S., Edsall, L., Wu, Y.C., Rasmussen, M.D., Bansal, M.S., Kellis, M., Keller, C.A., Morrissey, C.S., Mishra, T., Jain, D., Dogan, N., Harris, R.S., Cayting, P., Kawli, T., Boyle, A.P., Euskirchen, G., Kundaje, A., Lin, S., Lin, Y., Jansen, C., Malladi, V.S., Cline, M.S., Erickson, D.T., Kirkup, V.M., Learned, K., Sloan, C.A., Rosenbloom, K.R., De Sousa, B.L., Beal, K., Pignatelli, M., Flicek, P., Lian, J., Kahveci, T., Lee, D., Kent, W.J., Santos, M.R., Herrero, J., Notredame, C., Johnson, A., Vong, S., Lee, K., Bates, D., Neri, F., Diegel, M., Canfield, T., Sabo, P.J., Wilken, M.S., Reh, T.A., Giste, E., Shafer, A., Kutyavin, T., Haugen, E., Dunn, D., Reynolds, A.P., Neph, S., Humbert, R., Hansen, R.S., De Bruijn, M., Selleri, L., Rudensky, A., Josefowicz, S., Samstein, R., Eichler, E.E., Orkin, S.H., Levasseur, D., Papayannopoulou, T., Chang, K.H., Skoultchi, A., Gosh, S., Disteche, C., Treuting, P., Wang, Y., Weiss, M.J., Blobel, G.A., Cao, X., Zhong, S., Wang, T., Good, P.J., Lowdon, R.F., Adams, L.B., Zhou, X.Q., Pazin, M.J., Feingold, E.A., Wold, B., Taylor, J., Mortazavi, A., Weissman, S.M., Stamatoyannopoulos, J.A., Snyder, M.P., Guigo, R., Gingeras, T.R., Gilbert, D.M., Hardison, R.C., Beer, M.A., Ren, B., 2014. A comparative encyclopedia of DNA elements in the mouse genome. Nature 515, 355–364. https://doi.org/10.1038/nature13992

Zammit, P.S., Relaix, F., Nagata, Y., Ruiz, A.P., Collins, C.A., Partridge, T.A., Beauchamp, J.R., 2006. Pax7 and myogenic progression in skeletal muscle satellite cells. J. Cell Sci. 119, 1824–1832. https://doi.org/10.1242/jcs.02908

Zhang, J.L., Patterson, L.J., Qiu, L.Y., Graziussi, D., Sebald, W., Matthias, H., 2010. Binding between crossveinless-2 and chordin von willebrand factor type c domains promotes bmp signaling by blocking chordin activity. PLoS One 5, 1–12. https://doi.org/10.1371/journal.pone.0012846

Zhao, M., Harris, S.E., Horn, D., Geng, Z., Nishimura, R., Mundy, G.R., Chen, D., 2002. Bone morphogenetic protein receptor signaling is necessary for normal murine postnatal bone formation. J. Cell Biol. 157, 1049–1060. https://doi.org/10.1083/jcb.200109012

Zhao, P., Hoffman, E.P., 2004. Embryonic Myogenesis Pathways in Muscle Regeneration. Dev. Dyn. 229, 380–392. https://doi.org/10.1002/dvdy.10457

Zhong, W., Jiang, M.M., Weinmaster, G., Jan, Y.N., 1997. Differential expression of mammalian Numb, Numblike and Notch1 suggests distinct roles during mouse cortical neurogenesis. Development 124, 1887–1897.

Zhou, N., Li, Q., Lin, X., Hu, N., Liao, J.Y., Lin, L.B., Zhao, C., Hu, Z.M., Liang, X., Xu, W., Chen, H., Huang, W., 2016. BMP2 induces chondrogenic differentiation, osteogenic differentiation and endochondral ossification in stem cells. Cell Tissue Res. 366, 101–111. https://doi.org/10.1007/s00441-016-2403-0

Zhu, N., Wang, H., Wang, B., Wei, J., Shan, W., Feng, J., Huang, H., 2016. A Member of the Nuclear Receptor Superfamily, Designated as NR2F2, Supports the Self-Renewal Capacity and Pluripotency of Human Bone Marrow-Derived Mesenchymal Stem Cells. Stem Cells Int. 2016. https://doi.org/10.1155/2016/5687589

Zong, F.Y., Fu, X., Wei, W.J., Luo, Y.G., Heiner, M., Cao, L.J., Fang, Z., Fang, R., Lu, D., Ji, H., Hui, J., 2014. The RNA-Binding Protein QKI Suppresses Cancer-Associated Aberrant Splicing. PLoS Genet. 10. https://doi.org/10.1371/journal.pgen.1004289

APPENDIX A

PREVIOUSLY PUBLISHED WORK

This appendix describes publication status of chapters included in this body of work. Chapter 2, IDENTIFICATION OF SATELLITE CELLS FROM ANOLE LIZARD SKELETAL MUSCLE AND DEMONSTRATION OF EXPANDED MUSCULOSKELETAL POTENTIAL, was published in the journal Developmental Biology. The article was sent for publication May 2017, revised June-July 2017, and finally accepted for publication August 2017. The article was made available online December 2017. The authors listed on the publication are Joanna Palade, Djordje Djordjevic, Elizabeth D. Hutchins, Rajani M. George, John A. Cornelius, Alan Rawls, Joshua W.K. Ho, Kenro Kusumi, and Jeanne Wilson-Rawls. The first two mentions are co-first authors.

Chapter 3, MOLECULAR ANALYSIS OF MUSCLE PROGENITOR CELLS ON EXTRACELLULAR MATRIX COATINGS AND HYDROGELS, was published in the journal Acta Biomaterialia. The article was sent for publication May 2019, and after revisions, accepted and made available online August 2019. The authors listed on the publication are Joanna Palade, Amrita Pal, Alan Rawls, Sarah Stabenfeldt and Jeanne Wilson-Rawls, with the first mention as sole first-author.

The remaining chapters in this work are not published.

APPENDIX B

AUTHOR STATEMENT

Chapter 2 of this body of work constitutes a previously published article co-authored with Djordje Djordjevic, a student in the laboratory of Dr. Joshua Ho at the Victor Chang Cardiac Research Institute. The co-author has granted permission for the article to be used as a chapter.